# Characterization of the Interaction between Amyloid-β Peptide and Membrane Models with the Use of Supercritical Angle Microscopy Technique

---

**Dissertation**

**zur**

**Erlangung der naturwissenschaftlichen Doktorwürde**

**(Dr. sc. nat.)**

**Vorgelegt der**

**Mathematisch-naturwissenschaftlich Fakultät**

**der**

**Universität Zürich**

**von**

Valentin Dubois

**aus**

Belgien

**Promotionskommission**

Prof. Dr. Stefan Seeger (Vorsitz)

Prof. Dr. Benjamin Schuler

Prof. Dr. Christian Baumann

Zürich, 2020

# 失败是成功之母

"Failure is the mother of success" - Chinese idiom

## ABSTRACT

Alzheimer disease, like many neurodegenerative diseases, has become a tremendously important subject of research in our over-ageing society. People suffering from Alzheimer experience loss of memory and basic cognitive functions. The main hallmark of Alzheimer disease is the post-mortem observation of amyloid plaque composed of aggregated amyloid-β (Aβ peptides surrounding dead neuron cells). The reasons why Aβ, which is naturally produced from a transmembrane protein in healthy individuals, become triggered to aggregated and promote the death of neuron cells are currently investigated. Aβ is also known to interact with the membrane of neurons before and during the aggregation phase, probably causing its toxicity. The effects of such toxic interaction on the cell membrane are also under debate among the scientific community.
The purpose of this Ph.D. thesis was to improve the understanding of the abnormal effects promoted by the interaction of two types of Aβ (40 and 42) with an artificial membrane model, a supported lipid bilayer (SLB). Supercritical angle spectroscopy, a spectroscopic technique developed in our lab, provided a selective detection of the sample molecules of interest at the very level of the SLB. This technique was combined with both fluorescence and Raman signal, providing a broad insight in many aspects of the interaction between Aβ and the SLB.

At first, Fluorescence experiments were performed to elaborate a model for the adsorption of Aβ on the SLB. In this hypothetical model, Aβ adsorbs weakly and reversibly on the surface of the SLB but can undergo a transition of state or structure which strengthens the adsorption of the peptide. Peptides durably adsorbed act as a seed for the cooperative adsorption of more peptides in their vicinity, hence promoting aggregation and oligomerization if the local concentration in Aβ is high enough.
It was also found out that Aβ(1-42) was more prone than Aβ(1-40) to form aggregates, supposing it also undergoes the structure transition faster than its counterpart.

Then, the impacts of this adsorption on the membrane model were investigated. Fluorescent SLBs were incubated with an increasing concentration of Aβ and their integrity

as well as their intrinsic mobility were measured. It was observed that Aβ promoted a concentration-dependent extraction of lipid molecules from the bilayer. At low concentration, this effect was just observed as a decrease of fluorescence. But as the concentration of peptides increased, lipid clusters were observed above the surface of the SLB and the bilayer could event present signs of disruption.
The average mobility of the lipids within the SLB was only decreased by high concentration of Aβ(1-42) while Aβ(1-40) only hindered the diffusion of lipids locally, around the membrane damages.

Finally, Raman spectroscopy was performed to analyse the structure of Aβ responsible for the above-mentioned effects. Comparison between surface selective and classical Raman signal permitted to sort the secondary structure exhibited by the peptides in function of their proximity with the SLB. Aβ(1-42) situated directly on the surface of the SLB preferably adopted an α-helix structure, while peptides situated further away from the lipids folded as a great amount of β-sheet structure. On the other side, Aβ(1-40) exhibited almost exclusively a β-sheet structure. The presence of α-helix structure in the first Aβ can explain why its adsorption and aggregation seemed more durable and faster than its shorter version, since this structure is more stable in non-aqueous environment. It is smoothly combined with previous data to explain the hypothesis elaborated so far.

In conclusion, the experiments performed during this Ph.D. project allowed to design a detailed model for the adsorption of Aβ on membrane and its impact on the lipids. Aβ potentially fold into α-helix once inserted within the bilayer, which can act as a nucleus for the aggregation of the peptide into β-sheet oligomers. If the aggregation process is severe enough because of the local concentration in Aβ, lipid molecules might be extracted from the bilayer by the motion of aggregating peptides, hence causing various impairments due to the modified membrane integrity.
While this pathway is theoretical and based on an *in vitro* simplified model, it brings a good amount of details in the usual description of the mechanism of Aβ and could be of help in the general understanding of the disease correlated with this peptide.

# PUBLICATIONS

Some ideas and figures have appeared previously in the following publications:

*Supercritical angle fluorescence as a tool to study the interaction between lipid bilayer and peptides.* V. Dubois, D. Serrano, S. Seeger. SPIE digital library. Proceedings Volume 10231, Optical Sensors (2017).

*Reduced Bacterial Colonisation on Surfaces Coated with Silicone Nanostructures.* M. Meier, V. Dubois, S. Seeger. Applied Surface Science 459 (2018).

*Amyloid-Beta Peptide-Lipid Bilayer Interaction investigated by Supercritical Angle Fluorescence.* V. Dubois, D. Serrano, S. Seeger. ACS Chem. Neurosci. (2019).

*Structure Analysis of amyloid aggregates at lipid bilayers by Supercritical Angle Raman Microscopy.* V. Dubois, D. Serrano, X. Zhang, S. Seeger - *in submission*

# CONTENTS

# LIST OF FIGURES

# LIST OF TABLES

# ACRONYMS

AFM atomic force microscopy

APP amyloid precursor protein

BSA bovine albumin serum

DOPC 1,2-dioleoyl-sn-glycero-3-phosphocholine

DOPE-Atto647 1,2-dioleoyl-sn-glycero-3-phosphoethanolamine-Atto647

DOPS 1,2-Dioleoyl-sn-glycero-3-phospho-L-serine

PBS phosphate buffer saline

PUFAs Poly-unsaturated fatty acids

SLB supported lipid bilayer

SM brain porcine sphingomyelin

SAF supercritical angle fluorescence

UAF undercritical angle fluorescence

SAR supercritical angle Raman

SESAR surface-enhanced supercritical angle Raman

UAR undercritical angle Raman

# Part I

# INTRODUCTION AND METHODS

# 1

# INTRODUCTION

## 1.1 ALZHEIMER DISEASE AND AMYLOID-$\beta$

### 1.1.1 *Presentation of Alzheimer disease and symptoms*

Alzheimer disease was first described in the early 20th century by Alois Alzheimer, who acknowledged and presented the case of a 51-years-old woman suffering of a "peculiar disease of the cerebral cortex"[1]. Among the symptoms exhibited by Alzheimer patients, progressive memory and language impairment, disorientation, behavioural symptoms (hallucinations, delusions, paranoia), and psychosocial impairment are the most widely known. Alzheimer is therefore sorted as an illness of dementia - characterized by multiple cognitive troubles - but distinguishable from other form of dementia by the predominance of memory loss in the symptoms, and the absence of any motor symptoms (unlike i.e. Parkison's disease) except for excessively late stages of the disease[2]. Among irreversible dementia diseases, Alzheimer is dominant since it gather approximately 70% of all dementia cases in the United States[3]. Several risk factors are associated with Alzheimer disease (i.e. abnormal blood pressure, diabetes, traumatic brain injury, etc) but the major non-genetic risk factor remains the age[4]. The likelihood of developing Alzheimer increases exponentially with age beyond 65 years old and reaches more than 6% probability every year after 85 years old[5]. People suffering from Alzheimer disease after 65 years old are said to exhibit a "late-onset" or "sporadic" form of the disease and represent the majority (> 95%) of Alzheimer patients. People can also bear the symptoms of Alzheimer before the age of 65, then known as "early-onset" or "familial" disease. People with familial forms of Alzheimer have an autosomal dominant mutation in one of the presenilin genes located on chromosomes 1 and 14 or in the amyloid precursor protein (APP - cfr. Section 1.1.2) gene located on chromosome 21. In addition, people suffering from Down's syndrome (trisomy 21) have an increased risk of developing the early-onset disease[6]. All the symptoms encountered by patients suffering from any form of Alzheimer are due to a progressive damaging of brain normal structure and functions. At cellular level, Alzheimer is characterized by a loss

of cortical neurons, especially pyramidal cells, and synaptic dysfunction which hinders the communication in neuronal circuits necessary for cognitive functions[7, 8]. Degeneration starts in the medial temporal lobe, more accurately in the entorhinal cortex and hippocampus[9]. These damages yield the deficits in memory observed in the early-stage of the disease. Damaging then progresses throughout the temporal association cortex towards parietal areas. Eventually, degeneration is observed in the frontal cortex, neocortex and within the limbic system[10].

### 1.1.2 *Correlation between Alzheimer disease and Amyloid-β peptide*

The neuron degeneration mentioned in the previous section is thought to be the consequence of abnormal intra and extracellular deposition of protein aggregates. These depositions constitute the hallmark pathological lesions of Alzheimer, known as "tangles" and "plaques". "Neurofibrillary tangles" are deposited inside the neuron cells and constituted of aggregated, abnormally hyper-phosphorylated, protein tau. Proteins tau in normal form serve as stabilizing microtubules and help intracellular transport along the axon[11]. "Senile plaques", on the other hand, are extracellular accumulation of amyloid proteins and mainly composed of a small peptide called Amyloid-β (Aβ ). These two forms of aggregates are thought to interfere with the normal neuron functions and metabolism, eventually causing the cells to die. Some works have attested that the amyloid deposition of aggregated Aβ is one of the earliest stages in the progression of Alzheimer disease within the brain, and can precede the cognitive impairments by more than 10 years[6]. Aβ is released outside the neurons by the cleavage of a transmembrane protein, the amyloid precursor protein (APP). However, production of Aβ peptide occurs normally in healthy people as well as Alzheimer patients, therefore its production itself cannot be considered as the main cause of Alzheimer[12].

### 1.1.3 *Remedies and therapeutic approach against Alzheimer disease*

Medicine is currently unable to reverse or even prevent the progression of Alzheimer disease. Therapeutic drugs are used nowadays essentially for symptomatic relief. For example, cholinesterase inhibitors prevent the degradation of acetylcholine, a molecule improving the communication between neurons, hence slowing down or stabilizing the cognitive im-

pairments of the disease by maintaining the levels of acetylcholine. Blocking the damaging effect of glutamate against neurons by the use of NMDA-receptor antagonist (memantine) is another strategy[13]. However, the increasing number of patients suffering from Alzheimer, in parallel with the increasing lifetime, makes an urgent need for the elaboration of an efficient treatment. Strategies acting on the different proteins (Aβ , protein tau) have been developed and reached the clinical test phase but with small success. The options currently exploited to act on Aβ are focused either on the production and release of the peptide, preventing its aggregation or reducing its deposition on the neurons[14]. Preventing the release of Aβ is done by up-regulating the activity of the enzyme cleaving the APP (cfr. Section 1.1.2). There are, however, several drawbacks about this strategy. The first one is that the alternative product of APP cleaving, although considered non-amyloidogenic, is highly hydrophobic and has been reported to be also present in senile plaque (see Section 1.1.4.3)[15]. Another problem is the difficulty to specifically target, and with the proper dosage, the enzymes responsible for the cleavage of APP[16, 17]. Moreover, reduction of the release of Aβ could also induce side effects since some scientists argue that the peptide performs essential functions, although no definite one has been found out yet[18]. Inhibition of the enzyme generating Aβ is also problematic because of collateral clearance of other important molecules produced with the same enzyme[19], although specificity toward one bio-product can be tuned due to the variability of the enzyme-complex[20]. Another option is to prevent the aggregation of Aβ and the formation of toxic species. Synthetic glycosaminoglycan 3-amino-1-propaneosulfonic acid (3APS) has been evaluated in clinical trial, with a decreased level of the more toxic Aβ (1-42) but no cognitive improvements[21]. Aggregation of Aβ is also inhibited *in vitro* by metal chelators, therefore trial was made with zinc and copper binding drugs, with significant reduced plasma Aβ levels for patients bearing mild disease but no influence on severe cases[22]. A third option is directed toward the prevention of senile plaque deposition by the use of immunotherapy. Promising results were obtained with Aβ -vaccination in animal studies, but despite a significant reduction of plaque load, no cognitive improvements nor delay for the progression of the disease were obtained in clinical trial[23]. As mentioned previously, Aβ is produced naturally in healthy people therefore there is a natural regulation of production and clearance of the peptide, accomplished by several enzymes. Abnormal accumulation of Aβ can be the consequence of enhanced production or hindered clearance. Degradation of the peptide has been reported *in vitro* by various enzyme such as insulin degrading enzyme, angiotensin-converting enzyme, neprilysin and cathepsin D[24].

Alzheimer patients have been reported to suffer from defective clearance of the peptide. Upregulation of Aβ clearance instead of its production could be an alternative approach for therapeutics. In addition to the focus on Aβ, drugs promoting neuroprotection are being explored. Compounds inhibiting or reducing oxidative stress, neuroinflammation or mitochondrial dysfunction in neurons could prevent neuronal damage and help to protect cognitive function[25].

### 1.1.4 *Amyloid-β peptide*

#### 1.1.4.1 *General structure and functions of proteins*

Proteins are synthesized from the information contained in the DNA of the cell nucleus. Transcription into messenger RNA and exploitation of the nucleotides sequence in the ribosomal machinery of the cell ends up with the production of a corresponding chain of amino acids. The succession of amino acid residues is thoroughly optimized to permit the proteins to adopt a structure specific to their function (catalysis, transporter, etc). The ability of a given protein to fulfil its function is often represented by the scheme of a lock exactly shaped for the proper key, the protein being the lock and the co-factor of the protein being the key. The three-dimensional structure - or conformation - exhibited by the protein determines whether or not the protein is able to interact with and only with its co-factor[26]. The forces which guide a newly synthesized protein toward its proper structure are mainly entropy (favourable/unfavourable interaction of residues with water) and Van der Waals interactions. The information about the structure of proteins is sorted between different levels of organization: the primary structure refers to the number, the type of residues and the exact sequence of amino acids in a given protein. Hydrogen bonding between specific amino acids (more precisely between the amide and the carbonyl group of the protein backbone) forms local three-dimensional structures that help the protein to reach its proper conformation in a decent span of time. Such local structures are called secondary structures. The different secondary structures, although specific of every protein and localization, have two most represented shapes: α-helix and β-sheet. The global three-dimensional structure of a protein, obtained by combination of all local structures and orientations, is defined as tertiary structure. Tertiary structure is generally considered as the global conformation of the protein and determinant for its function. When the tertiary structure of a protein is suited for the execution of its biological function, such structure or

conformation is called "native". Some proteins gather into complexes which are required for their function, the structure of such assembled complexes being considered as a quaternary structure. The conformation of protein is a dynamic feature: proteins start to shape or reshape toward their native structure when they are synthesized (phenomenon known as "folding") and the structure evolves according to the necessity of a given function to be fulfilled or not. However, this dynamism *per se* can lead to mistakes during the folding or functional pathway of proteins, especially when considering the concentration of various molecules of the medium in which the proteins are to be fold. Part of the proteostasis (the pathways processed in living organisms to control the network of their proteins) consists to prevent such erratic misfolding by the use of chaperone proteins which help to reach the native conformation, or by degradation of these misfolded proteins by proteases[27]. Misfolding of proteins often causes toxicity for the organism, either by loss of important biological functions or through the gain of toxic properties. In addition, misfolded proteins can also expose hydrophobic residues or patches to the cell medium, sometimes interacting with the hydrophobic patches of other proteins. These interactions result in the clustering of the proteins, a process known as aggregation. Protein aggregates adopt various structures which stabilize the misfolded molecules by lowering its energy and might become too stable to be properly refolded by chaperones[28]. Among the conformations observed for protein clusters, fibrillar aggregates composed of a common structure received great interest and were named as "amyloid" fibrils[29, 30].

#### 1.1.4.2 *Overview of amyloid fibrils*

Electron microscopy and atomic force microscopy (AFM) were used to characterize these amyloid fibrils and reported results described them as long, twisted structures with a diameter of 7-13 nanometers. They are formed from the combination of aligned smaller protofilaments of 2-5 nanometers diameter each[31]. Protofilaments themselves are shaped as cross-β structures (β -sheet, turn, β -sheet) with the β -strands stacked perpendicular to the filament axis. Consecutive strands are spaced by 4.7 Å and the distance between opposite β -sheet is 10 Å (Figure 1)[32]. Different proteins without homology in their sequence can reach this fibrillar structure, therefore the main interactions of the amyloid core come from the common protein backbone[33]. However, variations can be observed in the number of strands, their length and orientation, or in the structure of the intermittent loops in the protein chain. The tendency of a protein to aggregate and form amyloid fibril is dependent of its electrical charge, hydrophobicity and propensity to adopt β -sheet struc-

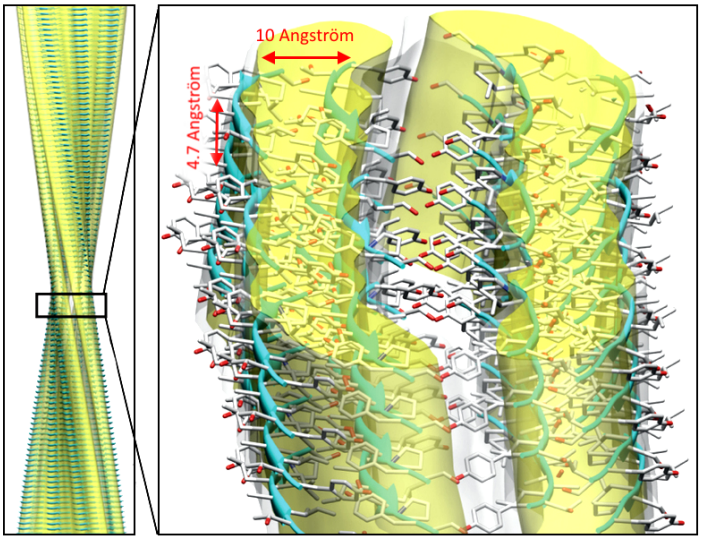


Figure 1: Representation of the structure of amyloid fibrils.

ture. Sequences with high hydrophobicity, and neutral or low net charge are more prone to cluster into fibrils[34]. Aggregation can occur at almost any stage of protein folding: unfolded, partially folded and even native structures can evolve into various aggregate states and fluctuate until the ordered amyloid structure is reached[35]. The formation of these structures is highly sensitive to the protein environment and concentration. Variation of pH, temperature or the presence of salts can affect the interactions between molecules and hence determine whether amyloid or amorphous aggregates are formed[36, 37].

The fibrillation of various proteins has been studied to elucidate the mechanism of aggregation. The models elaborated through these studies share the common condition of a critical protein concentration to exceed in order to form a nucleus of aggregation before the elongation of the fibril takes place[38, 39]. Before nucleation of the protein, the addition of monomers/oligomers is thermodynamically unfavourable. Nucleation requires a minimum protein concentration but when this ordered-aggregated state is formed, further addition of proteins becomes favourable. Therefore, nucleation is the rate-limiting step. Elongation of the fibril upon nucleation proceeds by addition of monomers or oligomers. Two models describe the elongation with monomers, with a one-step or two-step mechanism. The one-step model assumes that the conformation of the monomers fluctuates and eventually adopt a structure prone to aggregation which adsorbs directly on the growing filament[40]. The two-steps model rather suggest that monomers first adsorb at the end of the filament, then undergo conformational changes which stabilize and lock the new monomers on the aggregate[41]. According to recent theories, the small oligomers formed

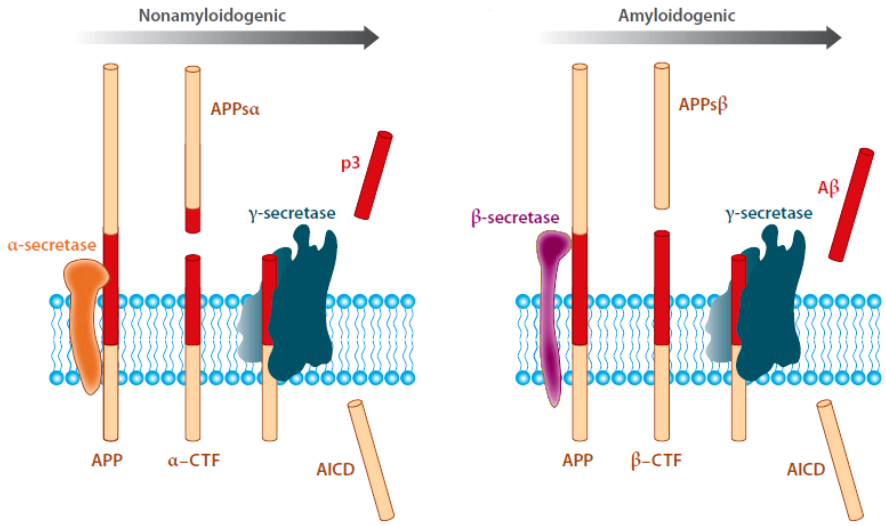


Figure 2: The two proteolytic cleavages of APP. Non-amyloidogenic pathway starts with α-secretase and finally generates a specific p3 fragment. Amyloidogenic pathway is started by β-secretase and generates the Aβ peptide (Figure from [43]).

in the early stage of aggregation are supposed to be more harmful for the neurons than the late fibrillar aggregates, although this assumption still has to be proven[42]. Experiments have been designed and still have to be performed in order to understand the cause of the toxicity arising from the smaller oligomeric species.

#### 1.1.4.3 *Generation and structure of Amyloid-β peptide*

Aβ seems to be a key factor of Alzheimer disease and the main target of many studies. However, it was previously mentioned that this peptide was also produced in the brain of healthy people[12]. The role of this peptide when normally produced is still elusive. Several functions were hypothesized without being confirmed: reduction of metal ions which would be either a protection against oxidative damage[44] or conversely a potential cause of toxicity[45]; signaling function in secretase activity[46]; implication in cholesterol transport[47] or transcription factor[48]. The Aβ peptide is generated from APP by two successive proteolytic cleavages. Two pathways can occur during the cleavages of this transmembrane protein (Figure 2). Both pathways release an extracellular soluble fragment (APPs) and a second membrane-spanning C-terminal fragment (CTF)[43]. The non-amyloidogenic pathway is determined during the first cleavage when subjected by α-secretase, releasing $APPs_{\alpha}$ and α-CTF (or CTF83). This pathway prevents the generation of Aβ since the α-secretase cleavage site is located within the Aβ sequence. The amyloidogenic pathway occurs when the first cleavage is produced by β-secretase instead, at the N-terminus of

Aβ sequence, releasing $APPs_\beta$ and β-CTF (or CTF99). Both $APPs_\alpha$ and $APPs_\beta$ are then cleaved a second time by γ-secretase, generating p3 fragment and Aβ peptide respectively, as well as an APP intracellular domain (AICD). The p3 fragment is generally defined as non-amyloidogenic although it has been reported as highly hydrophobic and found in amyloid plaque[15]. Aβ fragments undergo a succession of proteolytic cleavages by γ-secretase which release a 38, 40 or 42 amino acids-long peptide (Aβ(1-38), Aβ(1-40) and Aβ(1-42)), depending on the initial length of the Aβ fragments[49]. These different peptides represent approximately 90% of the content in Aβ with minor amount in Aβ(1-42). Further heterogeneity of Aβ is introduced at the N-terminus during or after release by modifications such as oxidation, isomerization or racemization which can modify its hydrophobicity or resistance to degradation, with consequences on Alzheimer disease progression[50]. Predominant Aβ(1-40) and Aβ(1-42) peptides were intensively studied since they were identified as the main components of senile plaque, with higher proportion of Aβ(1-42) and smaller amount of the other peptides and other molecules[51]. The 42 amino acids-version of Aβ only contains an additional isoleucine and alanine but was found to polymerize more rapidly into fibrils than Aβ(1-40), which exhibits a nucleation lag phase before aggregation[52]. Not only are their pathways of aggregation different, but they are also mutually dependent when the two peptides are mixed. Aβ(1-40) moderates the aggregation process of Aβ(1-42) and reciprocally Aβ (1-42) enhances the aggregation of Aβ(1-40)[53, 54]. Aβ(1-40) was found to be protective against plaque formation *in vivo*, hence the higher proportion of the longer Aβ in the fibrillar aggregates[55]. Fibrils composed of Aβ adopt the common structure of amyloid fibrils described in Section 1.1.4.2, characterized by a stack of β-sheets perpendicular to the fibril axis. Each peptide adopt a "hair pin" shape of β-strand, turn, β-strand with the N-terminus side of the peptide taking no part in the structure, as it is thought to be unstructured (and more hydrophilic due to the number a charged residues)[56, 57].

Both Aβ(1-40) and Aβ(1-42) can adopt this aggregated structure. Residues 25 to 29 compose the turn of the hairpin, while residues 23 and 28 stabilize the structure by formation of a salt-bridge. discrepancies occur between the two peptides considering the stabilizing interactions between two β-strand. Aβ(1-40) makes intramolecular interactions between the two strands of the same peptide separated by the turn, while Aβ(1-42) makes intermolecular interactions between the shifted strands of two peptides[57, 58]. However, the suspicions against the toxicity of Aβ shifted from fibrillar aggregates toward smaller oligomeric species. As an example, studies showed that the progression of Alzheimer disease was not

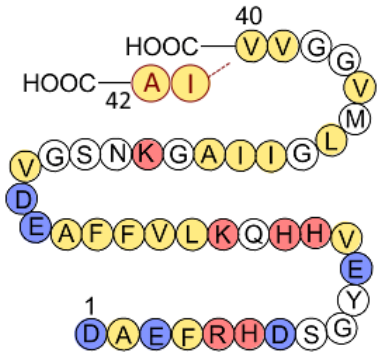


Figure 3: Primary structure of Aβ (1-40) and Aβ (1-42). Negatively charged residues are highlighted in blue, positively charged residues in red and hydrophobic residues in yellow.

necessarily correlated with the plaque load[59]. On the other side, experiments showed that the aggregation of synthetic monomeric Aβ into oligomers was required for the peptides to exert neurotoxicity, hence suggesting that the monomers are in fact innocuous[60]. Additionally, studies with various amount of oligomers correlated well with the level of dementia[61], and memory impairment could be observed for transgenic mice before plaque deposition[62]. Another evidence came from anti-Aβ treatment which reversed memory loss in mice, but had no impact on the plaque burden[63]. Various toxic soluble species have been identified for Aβ such as protofibrils[64], Aβ-derived diffusible ligands (ADDLs - or oligomeric species formed with clusterin)[65], a 56 kDa species (Aβ*56)[66] and amylospheroids (or spherical aggregates)[67]. Heterogeneity of these oligomeric species conduct to think that the global toxicity of Aβ is related to more than one assembly, or that a common key feature between all these structures is yet to be identified. It must be mentioned though, that the toxic oligomers formed by different polypeptides (i.e. Aβ, α-synuclein, insulin or prion protein) are all recognized by a single oligomer-specific antibody (A11). This result indicates a correlation between a structural feature and toxicity[68].

## 1.2 MEMBRANES

### 1.2.1 *Composition and function of natural membranes*

Apart from fulfilling functions of energy storage, lipids are the major component of natural membranes which defines the border of a biological cell with its surrounding, crucial for sustainability of life. Membranes are formed spontaneously by the natural tendency

of amphipathic polar lipids to self-aggregate in a defined lipid bilayer structure: the hydrophobic parts of the molecules associate together, entropically driven by water, while the hydrophilic part interacts with water molecules. This principle allows the cell to separate its constituents from external environment. The same process is recapitulated inside the cell to segregate multiple compartments and organelles for specific functions[69]. This compartmentalization increases the efficiency of biochemical reactions to a specific organelle and limits the dispersion of reactants and products. In addition to segregation properties, lipid membranes are subject to tubulation, fission and fusion, all these processes being determinant for cell division, reproduction and trafficking of molecules within the cells. Lipids also render some proteins able to interact with the membrane, by adsorbing, aggregating, dispersing or going through the bilayer. Membrane proteins are present with approximately the same mass than the lipids, meaning one protein for 50 - 100 lipids considering the discrepancy in molecular weight[70]. The major lipids which constitute eukaryotic membrane are the glycerophospholipids such as phosphatidylcholine (PtdCho - PC) and phosphatidylethanolamine (PtdEtn - PE). In neurons, phospholipids account for more than 50% of the total mass of lipids, with approximately 27/29% of PtdCho and 16.5 to 22% of PtdEtn in neuron bodies and dendrites respectively[71]. PtdCho molecules have a nearly cylindrical shape and assemble into a planar bilayer with hydrophobic tails facing each other. Additionally, most of PtdCho molecules have one cis-unsaturated fatty acyl chain, which renders them fluid at room temperature. In contrast, PtdEtn exhibits a more conical shape due to its small polar head group, and its insertion in the membrane induces curvature stress for budding, fusion and fission[72]. Sphingolipids such as sphingomyelin (SM) and glycosphyngolipids (GSLs), more precisely gangliosides (GSLs terminated with a sialic acid), are also important compounds of the neuron membrane. Sphingolipids have saturated (or trans-unsaturated) chains and exhibit narrower cylinder shapes than PtdCho of the same chain length, hence they pack more tightly. This tight association forms what is called "solid-gel" (or $S_o$, see below) phase within the membrane. These phases are fluidized by the insertion of sterols. The sterols are non-polar lipids, among which cholesterol is the most common in mammals. Sterols are preferentially mixed with sphingolipids because of a shielding of these non-polar lipids with the sphingolipids headgroup, called "umbrella" model[73].

Membranes are in most cases represented by a rather simple structure, first proposed in 1972 and still valid today : the fluid-mosaic membrane model (F-MMM, Figure 4)[74, 75]. this model describes membrane as a fluid bilayer of phospholipids with mobile glob-

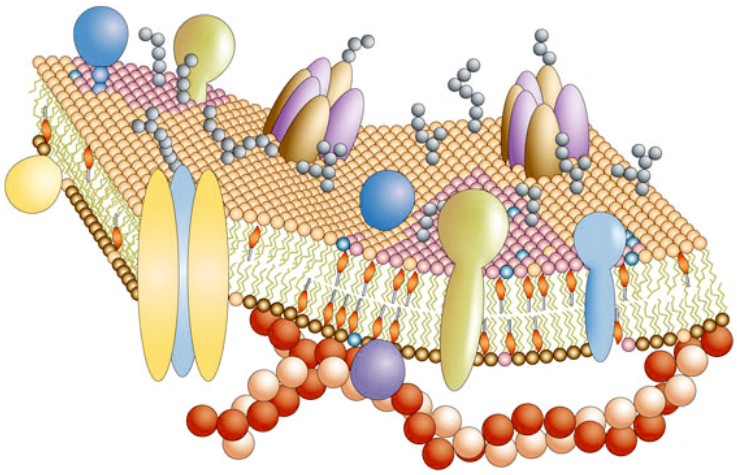

Figure 4: The fluid-mosaic membrane model (F-MMM) proposed by Singer and Nicholson. Proteins are integrated within the bilayer formed by phospholipids. According to the F-MM model, the bilayer is a dynamic structure whose topology is stabilized by an internal cytoskeleton.

ular integral membrane proteins and glycoproteins that are intercalated into the bilayer. However, this model suffers from limitations and criticism made up decades after its elaboration - including the description of recently discovered "lipid-raft"[76] or the dynamics of some membrane components - and has been refined over years. It must be included in the representation of membranes that there is an asymmetry of lipid and protein distribution between the two leaflets of the bilayer[77, 78]. This asymmetry is necessary to maintain the proper display of receptors and adhesion molecules on one side of the membrane, and other molecules on opposite membrane surface. The basic phospholipids constituents of the membrane are also asymmetrically distributed[79]. For example, amine and serine-containing phospholipids are found essentially on the cytoplasmic side of the membrane while choline-containing phospholipids and sphingomyelin (consequently enhancing the insertion of cholesterol) are concentrated within the outer bilayer leaflet. This might be simply considered as a mechanism to improve enzymatic activities or association of membrane proteins but there is also a critical need for maintaining this asymmetry. Indeed, the loss of membrane asymmetry is generally associated with cell activation (activation of cell adhesion, aggregation, apoptosis, etc.), and with pathologic conditions[79]. The asymmetry of the membrane is also a guide for its curvature[80]. Composition of the leaflets indicates that the outer layer exhibits a rather neutral curvature, whereas the cytoplasmic layer tends toward negative curvature, because the inner phospholipids have a small polar head compared with the hydrocarbon chain. This feature induces a net curvature to mini-

mize the total curvature energy of the bilayer[81]. Since the asymmetry of the membrane is so important, various molecules defined as lipid transporters have the function to displace lipids from one leaflet of the membrane to the other. These transporters can be monodirectional transporter, bidirectional transporter, ATP-dependent or independent[82]. Not only are the lipids asymmetrically distributed in bilayers but they are also heterogeneously and dynamically distributed in the membrane plane[83]. The heterogeneity and preferential association of some lipids yields the appearance of different "phases" within the membrane. Each phase features a specific behaviour which is defined by its order and its diffusion velocity. The two extremes are the solid-gel phase ($S_o$) and liquid-disordered phase ($L_d$). Solid-gel phase is characterized by a high ordering between long, saturated hydrocarbon chains (i.e. sphingomyelin) and a slow diffusion. Liquid-disordered phase, on the contrary, are formed of low-ordered, unsaturated lipids (i.e. PtdCho) and fast diffusion. Some lipids such as cholesterol change the fluidity, the dynamics and the lateral diffusion of some areas of the membrane. The association of cholesterol with sphingomyelin or PtdCho allows the formation of liquid-ordered phase which combine a higher ordering of lipid chains with a faster diffusion[84]. Moreover, cholesterol also influence the partitioning of transmembrane proteins by modifying the core thickness of the bilayer, hence the hydrophobic matching between the bilayer and the size of inserted proteins[85]. These local modifications of the membrane brought the elaboration of the membrane domain and lipid-raft hypotheses. Basically, the interactions between the lipids (hydrogen bonding, hydrophobic entropic forces, charge pairing and van der Waals forces) can lead to the formation of dynamic and reversible nano-scale domains (mostly 10–200 nm)[86, 87]. When specific lipids belong to transient membrane meso-sized domains in cell membranes, the structures that are formed are called lipid rafts. Rafts containing specific lipids, integral proteins or peripheral proteins can constitute compartmentalized signaling platforms for cellular functions like apoptosis and intracellular lipid transport[88].

### 1.2.2 *Neuronal cell membranes*

The main function of neuron cells is the transduction of nervous signal and their membrane is adapted to fulfill the propagation of this electric signal. The neurons membrane contains a higher amount of lipids and carbohydrate to account for the need of high electrical resistance, and to prevent propagation of random electrical impulse[89]. Besides,

the ratio of cholesterol/phospholipids is also increased as the formation of lipid rafts is enhanced[90]. This outstanding amount of lipid rafts is necessary for the multiple functions of the neuron membrane. These ordered domains act as anchor points for signaling molecules like GPI-receptors or lipid second messengers[91]. Rafts also account for the presence of adhesion molecules permitting contact of the neuron cell with its surrounding, required for guidance and transmission of the nerve impulses between neurons[92]. Protein channels involved in the propagation of neurotransmitters are also located in the rafts domains[93]. As stated in Section 1.1.1 the age is a critical factor for the development of Alzheimer disease. Experiments in mouse models have shown that aging is not just a chronological delay for the illness to manifest itself but that the effects of equivalent A$\beta$ injections strongly depend on the age[94]. Therefore, the impact of aging on the neurons and neuron membrane have been studied extensively.

Electrical properties of the neurons membrane evolve with aging. This is critical since the very objective of neurons is to transmit nerve impulse upon the excitation, transduction and release of neurotransmitters, each of them relying on variation of the membrane potential. Aged mollusc neurons have been showed to be less reactive than young neurons, with an increase of the threshold current needed to trigger an action potential[95]. Electrical properties of the membrane are linked to the lipid composition of the brain, subject to change with aging and dependent of the region of the brain which is studied. Most of the lipid levels are reduced but some specific lipids are increased with age[96, 97]. Special attention is accorded to cholesterol, linked to important lipid rafts. They are contradictory results concerning the change in cholesterol levels in the brain, some studies reporting increased levels[98] while others indicate a decreased amount of this lipid[99], or even the absence of notable change in certain brain areas[100]. These discrepancies in results suggest a specificity of the evolution of the cholesterol content, depending on the region of the brain which is studied. However, a consensus is found describing how aging actually affects the asymmetry of cholesterol which tends to enrich the outer leaflet of the membrane compared with younger subjects[100]. Sphingomyelin content also evolves with age, with an increase of the general SM levels and a higher ratio of unsaturated (monoenoic) aliphatic chains compared with saturated chains[101]. Gangliosides, also playing important role in cell functions, are subject to alteration over aging. Not only does their content decline beyond 70 years of age[102], but the proportion of C20-lenght to C18-lenght aliphatic chain gangliosides is greatly increased[97]. Poly-unsaturated fatty acids (PUFAs), including linoleic and alpha-linoleic acids, exhibit a decreased level in the brain of aged

rats[103]. In parallel, a decline of saturated fatty acid and reciprocal increase of mono-unsaturated fatty acids is observed[104], with the ratio between saturated and unsaturated fatty acids being one of the key factors influencing the cell membrane fluidity[105]. The ability to change the strength of a synaptic connection is called synaptic plasticity and is correlated to memory and learning processes. The decline of synaptic plasticity is therefore correlated with neuro-cognitive impairments[106]. On molecular scale, the plasticity of neurons relies on various factor such as the probability of neurotransmitters release and response during the fusion of synaptic vesicles. Fusion occurs when two bilayers merge together and is highly dependent on the curvature and fluidity of the membrane[107]. In the previous section, these two parameters have been correlated with the lipid composition and their physical properties, which is subjected to change upon aging. Cholesterol, when asymmetrically distributed, induces an intrinsic negative curvature which support fusion between membranes[108]. Depletion of Cholesterol or reduced asymmetry would both result in an inhibition of the rate and kinetic of fusion[109]. The subsequent reduction of membrane fluidity also hinders the mobility of neurotransmitter receptors[110]. Similarly, the enrichment of membranes in sphingomyelin also reduces the efficiency of vesicles fusion through a modified organization and integrity of lipid rafts. SM-enriched membranes also exhibit a lower curvature[111, 112]. Gangliosides influence the synaptic plasticity due to their concentration on the outer leaflet and the bulky structure of their sugar headgroup. These features confer a positive curvature to membrane rafts which facilitates membrane fusion. Therefore, the decrease of ganglioside content reported previously diminishes membrane curvature and fusion ability[113]. A specific increase of C20-GM1 is observed in aged brain[114]. The large oligosaccharide of C20-GM1 promotes their clustering in lipid rafts and attenuates the positive curvature gangliosides normally provide[115]. Furthermore, C20-ganglioside species tends to reduce the membrane fluidity compared with C18 species[97], hence disturbing the function of neurotransmitter receptors which require dynamic clustering within the membrane[116].

Counterintuitively, aged brain without specific pathologies exhibits but few dead neurons, yet the function of remaining neurons explicitly decline over aging[117]. Results of *in vitro* and *in vivo* experiments point at reactive oxygen species (ROS) produced by respiration as main culprits for this dysfunction. Cells control the amount of ROS through detoxification pathways involving antioxidants, and adapt themselves and their function when the level of ROS exceeds their detoxification capacity. These adaptation processes in neurons have different consequences influencing cognitive functions (i.e. reduced dendritic remodeling),

reducing their efficiency as a price for improving neuronal survival[118]. The alteration of lipid levels, such as the ratio between cholesterol and sphingomyelin, modifies the organization of lipid rafts and triggers the activity of survival receptors[119, 120]. Oxidative stress also favours the lipid peroxidation in cell membrane, especially in the brain where not less than 20% of the oxygen intake is used[121]. Lipid peroxidation occurs through the high amount of PUFAs, easily damaged by oxidation[122]. Intermediate peroxidation products, which include radical species, stabilize themselves by abstracting hydrogen atoms from neighbouring PUFAs, hence perpetuating the oxidation damages[123]. One of the effects of lipid peroxidation is to promote "flip-flop" motion between the leaflets of the membrane, hence perturbing the asymmetry of lipids whose synaptic plasticity is dependent[124]. A loss of membrane fluidity, influenced by unsaturated lipids, is another consequence of oxidation damage. A higher activity of lipoxygenases, the enzymes which catalyse the oxidation of unsaturated fatty acids, is associated with neurodegenerative diseases such as Alzheimer[125] while it has been showed that oxidized lipids increase the adsorption of Aβ peptide on the membrane[126]. In animal models, this higher activity of lipoxygenases is correlated with the vulnerability of neurons to excitotoxicity, namely the toxicity arising from excessive stimulation by neurotransmitters[127]. Therefore, the decrease of PUFAs level with age that was reported above could be a protection mechanism against peroxidation, by limiting the amount of available oxidation sites and products. Similarly, the reduced efficiency of neuronal main functions could be a protection against the excitotoxicity associated with the activity of lipoxygenases.

## 1.3 INVESTIGATION TECHNIQUES FOR THE INTERACTION BETWEEN Aβ AND MEMBRANES

### 1.3.1 *Description of the models used to mimic natural membranes*

Several models exist to mimic the natural membrane, though bypassing the complexity of living cells. Some of these models are notably used to study lipid-protein adsorption processes and they differ in their properties or relevancy, or are more or less suitable for specific experiments.

One of the easiest model to assess the binding of proteins onto lipids is to use an overlay-assay, namely to incubate proteins on spots of lipid molecules immobilized on various

supports (nitrocellulose, polyvinylidene difluoride (PVDF), or streptavidin solid-support for biotonylated lipids)[128, 129]. While this has the advantage of simplicity and relative high throughput to collect great amount of data on various interactions, it suffers many disadvantages. Lipids are not presented in the physiological context of the lipid membrane and little information can be gained about the impact of protein adsorption on lipid molecules. In addition, homogeneity between the spots of lipids is difficult to reach due to the deposition method and the different solubility of different lipid headgroups[130]. After an overlay-assay, further tests on membrane mimetic models are often required.

A lipid monolayer is a film of one single molecule thickness formed at the interface between air and water, with the hydrophobic tails directed toward the air and the polar headgroups immersed in water. It mimics a single leaflet of a membrane and exhibit the same thermodynamic properties than a bilayer at the "monolayer–bilayer equivalent pressure" (i.e. the force that balances the internal lateral pressure between lipid components, and allows the hydrophobic chains escaped from water to reach an equilibrium)[131]. Briefly, this system allows the detection et quantification of proteins through the change in surface pressure provoked by their insertion within the monolayer. The surface pressure is monitored and associated first with the initial lipid composition, then with the amount of adsorbed proteins[132]. Additionally, the initial surface pressure of the monolayer can be tuned and correlated to the capability of proteins to insert afterwards. Such measurement allows to determine if a protein is peripheral (its function depends on membrane penetration) or not[131]. The main disadvantages of this model are that the leaflets coupling effects of a bilayer are absent from this configuration, and it is suitable to form planar monolayers only hence prohibiting the study of curvature-related effects. following the so-called "Blodgett" deposition approach - a slow vertical lift of the slide from the solvent phase to air at constant surface pressure - the monolayer can be transferred onto a solid support. By doing so, the sample can be subjected to scanning technique (AFM, electron microscopy, ...) and permits to characterize the morphology or the organization of adsorbed proteins as a function of surface pressure[133].

Lipid bilayer models mainly regroup two configurations. The first is the hybrid bilayer or hemi-lipid layer, composed of a monolayer of phospholipids deposited onto a sensor surface which is previously coupled with another monolayer of organic, hydrophobic molecules[134]. Often composed of a self-assembled monolayer of alkanethiol, the choice of base components (i.e. different chain length or ethylene oxide spacer units) can tune the biophysical properties of the phospholipids layer. The advantage and limitation of this

model are both correlated to the interaction of the phospholipids with a monolayer fixed on the substrate. This feature renders the hybrid bilayer model more stable than a supported lipid bilayer, but at the same time decreases its fluidity and increases its packing density. Supported lipid bilayers (SLBs) are more commonly used, and formed by the absorption and fusion of small or large unilamellar vesicles (SUVs or LUVs, respectively) onto a hydrophilic substrate[135]. Compared with the hybrid bilayer, a real lipid bilayer is obtained. Its physical properties strongly depend on ionic interactions between lipids and the support substrate, although a water gap of 10-20 Å is reported between the substrate and the bilayer[135]. This gap is sufficient to increase the membrane fluidity, although some residual frictional coupling with the support still hinders the diffusion of the lower leaflet. Combination with Langmuir technique permits the addition of a monolayer or vesicles of given composition on a pre-deposited phospholipid monolayer. This process allows formation of a lipid bilayer with asymmetric leaflets[136]. SLB are suitable for a great variety of measurements (AFM[137], total internal reflection fluorescence microscopy[138], surface plasmon resonance[139], etc...) providing information about the kinetic of protein binding[140] but also various structural data about the proteins or the lipids[141, 142]. Recently, protocols using micro-beads as substrate yielded the formation of SLBs exhibiting uniform curvature for the study of proteins involved in curvature-sensing mechanisms[143]. Although this is an interesting way of using the substrate, it should be emphasized that the support will always have some influence on the SLBs, sometimes undesirable. Another disadvantage of SLBs is the relatively poor membrane integrity due to the frequent defects in the bilayer.

Pore-suspending membrane is another model where the equivalent of a lipid bilayer is formed on a substrate presenting an open aperture, hence cancelling the influence of the support on the membrane within this aperture area[144]. They are generally formed through Langmuir–Blodgett transfer of lipid monolayers on a grid, or by painting of the lipid solution on a pierced hydrophobic material[145]. The free-standing part of the membrane has both leaflets in contact with the buffer, sometimes different on each side, and can be used to study transport phenomenon or ion-channel activity with electrodes. However, in parallel with the independence from the support comes a lower stability of the model. Some alternative influence on lipid diffusion can also arise from residual organic solvent used to cover the grid[146].

Another model freed from the influence of support is the liposome. Liposomes are aqueous filled vesicles formed from bilayer-thick lamellae resulting from the dispersion of phospholipids in buffer (Unilamellar (UVs) and multilamellar vesicles both exist, depending on the

lipids) [147]. The hydration of a dry lipid film is used to generate heterogeneous vesicles, whose diameter size can be decreased by further sonication, and are then sorted between small (SUVs, d < 100 nm) and large (LUVs, d > 100 nm) vesicles. Concerns about the size of the liposomes come from the constraints it imposes on protein-lipid interactions[148]. However, the remaining of stable small vesicles unaffected by sonication or extrusion and the consequent heterogeneity of the liposome sample may have an undesired influence on experimental results[149].
Finally, giant unilamellar vesicles (GUVs) is a model similar to the liposomes, the main difference being the cell-sized diameter of the vesicles (10-100 μm). This large diameter makes GUVs local structure comparable to SLBs, although completely free of any support and hindrance of the lipid diffusion [150]. Formation of these GUVs requires the use of charged phospholipids or electroformation to promote the swelling and curvature of a bilayer[151]. The disadvantage of this model is the poor control on the lipid composition of individual vesicles. The discrepancies between individual vesicles have repercussions on the interaction of proteins with a given population of GUVs. However, it has been used to study membrane partitioning, lipid phases and the preferential association of proteins with these domains[152].

### 1.3.2 *Techniques for the investigation of protein-lipid interactions*

Several techniques exist to detect, measure or characterize the interaction of proteins with a membrane model. They differ by their method of detection, the amount of information that can be gained and the necessity - or not - to chemically modify the sample (label and label-free techniques).

Surface plasmon resonance spectroscopy (SPR) is a label-free technique which allows the detection of membrane-protein interactions and to characterize their affinity and kinetic of binding[153]. The principle is to detect the adsorption of the target near a surface coated with metal (typically gold) through the change in refractive index of the surrounding medium. This change in refractive index induces a shift of the angle at which an incident light excites the electron in the upper layer of metal. This excitation is called plasmon resonance and by measuring the shift in the angle of maximum excitation, quantitative data about the adsorption of the analyte can be collected. The plasmon generates an electric

field whose extending range is about 300 nm from the metal surface and limits the region susceptible to influence the plasmon resonance, hence making SPR a surface-sensitive technique[154]. The layer of metal can be functionalized with proper receptors for the target and the limit of detection of SPR biosensors can go as low as 10 pg/mL. SPR can also be used to detect a conformational change among the adsorbed proteins, although the technique can merely correlates a structural transition with a change of affinity and/or refractive index[155]. However, the technique does not possess the capability to characterize the structure on its own.

Quartz crystal microbalance (QCM) is another label-free detection technique. A piezoelectric crystal is sandwiched between two electrodes and the alteration of the crystal natural oscillation frequency in response to small changes of mass is measured[156]. First designed to work in gaseous or vacuum media, QCM measurements were successfully extended to biosensing in aqueous media[157] with the oscillation frequency shift incorporating a combined effect of mass, temperature and viscosity changes. As for SPR, the QCM biosensor can be functionalized to detect specifically one adsorbate (i.e. proteins). QCM was notably used to correlate the progressive increase in mass deposited with the kinetic of aggregation and growth of Aβ [158].

Like the two previous techniques, X-ray reflectometry is a surface sensitive method of observation since X-rays possess a very small penetration depth. The specular reflection of a X-ray beam from the sample surface is analyzed, with the reflectivity influenced by the electron density gradient normal to the surface[159]. This allows to measure the electron density profile of a SLB and the insertion of proteins within the bilayer[160]. However, the use of X-rays induces severe degradation on biological samples like membranes[161]. This effect can be countered by the use of neutrons beam instead of photons, but at the cost of a lower beam flux and spatial resolution.

However, the three techniques described above present the disadvantage to yield information about the whole average surface of the sample. No lateral differentiation is possible and therefore the exact localization of protein adsorbate on the surface plan remains unknown.

Atomic force microscopy (AFM) can fulfil the need for lateral resolution down to the nanometer scale. The principle is to scan the surface of the sample with a micro-machined cantilever probe and a sharp tip. The deflection of the tip while scanning the surface at a constant force, or constant height, is monitored by a beam reflected on the cantilever hence

establishing a height profile of the sample. Different mode of scanning are used, such as non-contact mode to probe electric, magnetic or atomic attractive forces acting at short distance (50-150 Å)[162]. Tapping mode alternates between contact and contactless scanning by oscillating the cantilever tip at or near its natural resonance frequency. Changes in the frequency of oscillation due to interaction with the sample are detected to construct the surface topography[163]. AFM has been used extensively to study the progression of amyloid-related diseases and notably the morphology of Aβ 's fibrils[164]. Alternatively, the interaction between a single molecule attached to the tip and the substrate can be measured in force spectroscopy mode via scanning tunneling microscopy (STM)[165]. Current can flow between the single molecule and the substrate without direct contact because of the tunneling effect. Measurement of this current in function of the oscillations of the cantilever is used to quantify the forces of interaction between the tip and the substrate. Force-distance profile gives information about the elasticity and stability of the substrate, i.e. conformational changes of a protein layer[166]. The disadvantage of AFM is that despite being considered as a label-free technique, measurements rely on the perturbation of the sample with the tip and bring additional interactions on the sample.

Another label-free technique is circular dichroism spectroscopy (CD), which is used to characterize the secondary structure of proteins. The technique consists to measure the difference of absorption of a sample between left and right circularly polarized light[167]. Active sample such as proteins have different absorption coefficient for each of these polarized light. The amide band of proteins is the most prominent chromophore group observed by CD spectroscopy. Electronic transitions promoted by far UV excitation beam are dependent on the hydrogen bonds and specific absorption profiles are obtained for the main secondary structures of the protein backbone. However, CD spectra only display the average of all structural contributions and can correspond to a mixture of the secondary structures adopted by the protein. This drawback is sometimes avoided by using a combination of shorter synthetic peptides composing the full-length protein[168].
Polyacrylamide gel electrophoresis (PAGE) is a method to gain insight about the structure of proteins (but provides no information on membrane). The method consists to force protein diffusion through a polyacrylamide gel by application of an electrical current. The diffusion through the gel, called electrophoretic mobility, is influenced by intrinsic properties of the proteins such as the mass, the charge or the conformation[169]. The influence of the global charge and shape of the molecule can be cancelled by the use of denatur-

ing buffer (i.e. containing sodium dodecyl sulfate, SDS) hence sorting the proteins only by their mass. Blue native (BN) PAGE is used to separate proteins while conserving their mutual interactions and structure. Coomassie dyes are introduced to induce a charge shift on the proteins which are not separated according to the charge/mass ratio but according to size[170]. However, BN-PAGE suffers from a poor resolution compared with denaturing electrophoresis. SDS-PAGE is still one of the most used technique to characterize rapidly the oligomers of various proteins, although the method is blamed for introducing some artefacts in the results[171].

Nuclear magnetic resonance (NMR) can also be used to characterize the structure of proteins. The resonance of atom nuclei aligned according to a magnetic field and subjected to an electromagnetic excitation pulse is correlated with the chemical environment of these nuclei[172]. Atoms abundant in proteins or added by labelling, such as hydrogen and isotopes of carbon and nitrogen, possess a nuclear spin that allows them to interact with a magnetic field. Interactions between nuclei, such as dipole and scalar coupling, chemical environment (hydrogen bonding) and a massive set of techniques to interpret these pieces of information (2D and 3D spectra, NOE, COSY) allow to construct a 3-dimensional structure of proteins. A rather limiting factor is the insensitivity of NMR technique, hence the need of high concentration of proteins. Required concentration can lead to aggregation of the proteins in the sample. NMR can also be used to investigate the effect of protein interaction on a membrane model, although this technique considers membranes as in solid state due to the anisotropic dynamic motion of the lipids. The so-called "solid-state NMR" requires the use of the magic angle spinning (MAS) technique - namely to rotate the sample at specific orientation with the magnetic field - to obtain good resolution on NMR spectra[173]. The relative alignment of lipid molecules as well as the thinning of the membrane or pore formation could be resolved with NMR[174].

Apart from isotope labelling for NMR, the other most common technique using labels to investigate protein-lipid interactions is fluorescence microscopy.
On the other hand, Raman spectroscopy is another label-free method, that allows to gain precious information about the structure of studied molecules, including the local conformation of proteins. However, due to their use in this thesis, these last two techniques will be described more extensively in the following sections.

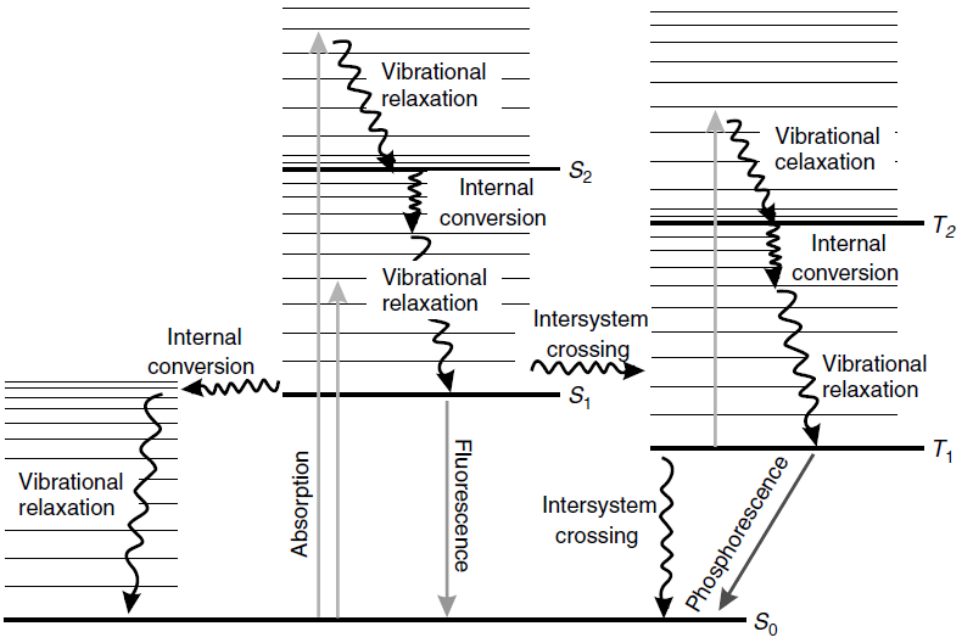


Figure 5: Jablonski diagram describing the electronic levels of a fluorophore and the possible transitions between different electronic states (from [175]).

### 1.3.3 *Fluorescence microscopy*

Fluorescence is a phenomenon used extensively for research purpose in order to locate and observe a target. Fluorescence occurs when a chromophore absorbs light at specific wavelength and undergoes an excitation toward a higher energy electronic state ($S_1$), then relaxes to the ground electronic state ($S_0$) by re-emission of light at another specific wavelength[175]. Fluorescence is then one of the many mechanisms by which a molecule can release the excess of energy following the absorption of light. Those mechanisms are represented on the Jablonski diagram and fluorescence is generally in competition with other radiationless or phosphorescence processes (Figure 5). Many commercial chromophores are available and usually optimized to favour the fluorescence process with good yield, stability over excitation and often straightforward labelling protocols. The high sensitivity of fluorescence microscopy is a major advantage of the technique, in addition to a good signal-to-noise ratio due to the difference of wavelength between excitation and emission photons[176]. The diffraction limit imposes physical constraint to the maximum resolution of fluorescence (200-300 nm), typically too low to differentiate two biomolecules interacting together or simply too close. Several techniques have been developed to overcome this limit, such as structured illumination microscopy (SIM)[177], stimulated emission deple-

tion (STED)[178], saturated structured illumination microscopy (SSIM)[179] and the indirect stochastic optical reconstruction microscopy (STORM)[180] allowed to reach a resolution between 50 and 20 nm.

However, other adaptations of fluorescence microscopy are available to gain specific information about protein-lipid interactions, without the need to increase the resolution. An option is to adapt fluorescence in a surface-sensitive technique where lipids are deposited on the surface. These techniques provide a selective excitation of the fluorophores near the interface, hence gathering information mostly from proteins interacting with the lipids while discarding the influence of non-interacting molecules.

One of these surface-sensitive techniques is the total internal reflection fluorescence (TIRF) microscopy. TIRF exploits the difference of refractive index between two media (the sample and the substrate, generally water and glass respectively) and its influence on the refraction/reflection properties of light[181]. Due to the different refractive indexes, a light beam directed toward the interface between the two media above a specific angle (called critical angle) will be totally reflected. The critical angle ($\theta$) is determined by the refractive index of the sample ($n_1$) and the substrate ($n_2$):

$$\theta = \arcsin(\frac{n_1}{n_2}) \tag{1}$$

For classic water/glass sample, this critical angle is 61° from the normal of the surface. However, the reflected light generates a thin electromagnetic field (the evanescent wave) beyond the interface with the same frequency than the incident light and the ability to excite fluorophores within the field range. The depth of this field is dependent of the incident illumination angle, wavelength, and refractive index differences but generally, only molecules within a range up to 100-200 nm from the surface are efficiently excited. The disadvantage of TIRF is the inconvenient to provide high angle of illumination. This is achieved by the use of a prism-configuration and/or by high numerical aperture objectives[182].

Another surface-sensitive technique based of the critical angle is the supercritical angle fluorescence (SAF), developed in the group of Prof. Seeger[183]. When an excited fluorophore is situated near an interface, a substantial part of the emitted fluorescence will be directed toward the medium of higher refractive index, above the critical angle. SAF uses a specific objective with high numerical aperture and parabolic mirrors to collect this light emitted above the critical angle (Figure 6 a,b). One of the advantage of SAF is that its selec-

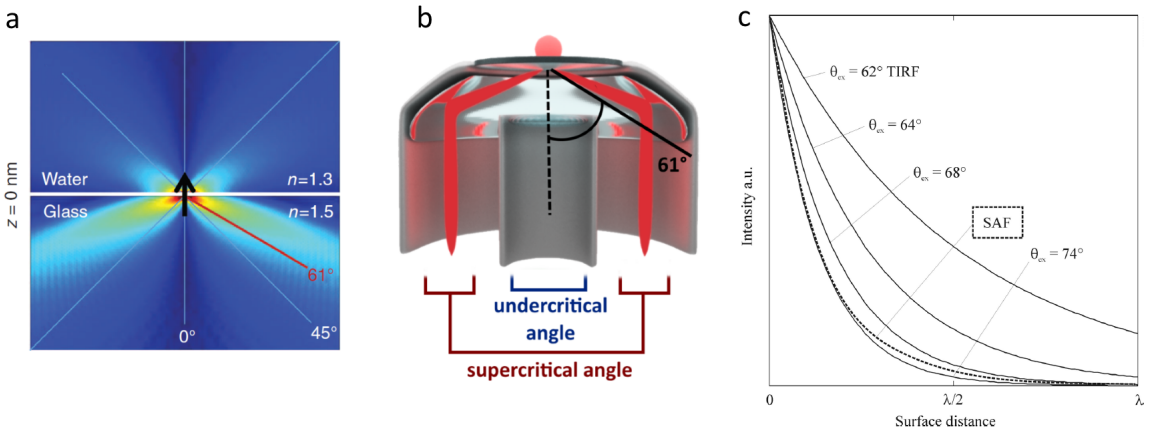


Figure 6: (a) Plot of the emission of a fluorophore directly adsorbed on a glass/water interface. (b) Scheme of the SAF objective collecting light from a surface-bound emitting fluorophore. (c) Comparison of the penetration depths of the observation volumes between SAF and TIRF with different angles of illumination (from [183]).

tivity for surface-bound fluorophores depends on their own features of emission related to their position, and is independent of the largeness of the illumination angle as long as the fluorescence is collected above the critical angle. Accomplishing similar selectivity with TIRF requires to decrease the depth of exciting field, by illuminating the sample at angles largely exceeding the critical angle (Figure 6 c). On the other side, since the selectivity of SAF does not depend on the illumination angle, the sample can be illuminated below the critical angle. In this way, fluorophores within the bulk solution can be excited and detected through their emission below the critical angle while fluorescence emitted above the critical angle is still collected selectively and simultaneously. Therefore, both the selective detection of surface-bound emitters and the observation of fluorophores in the bulk solution are accomplished.

SAF is not only used as independent fluorescence microscopy but its selectivity can also be combined with other techniques relying on the signal of labelled targets. Förster resonance energy transfer (FRET) is one of them. The technique relies on the radiationless transfer of energy from a first excited fluorophore (donor) toward a second fluorophore (acceptor) whose emission and excitation spectra partially overlap. This transfer occurs beyond interatomic distance, typically between 10-100Å, and the separated collection of donor and acceptor signal yields information about the interaction and the distance between the two molecules[184]. FRET has been notably used to study the folding of protein[185] or combined with SAF to monitor the aggregation of α -synuclein near a SLB[186].

Fluorescence correlation spectroscopy (FCS) was also used in conjunction with SAF. The

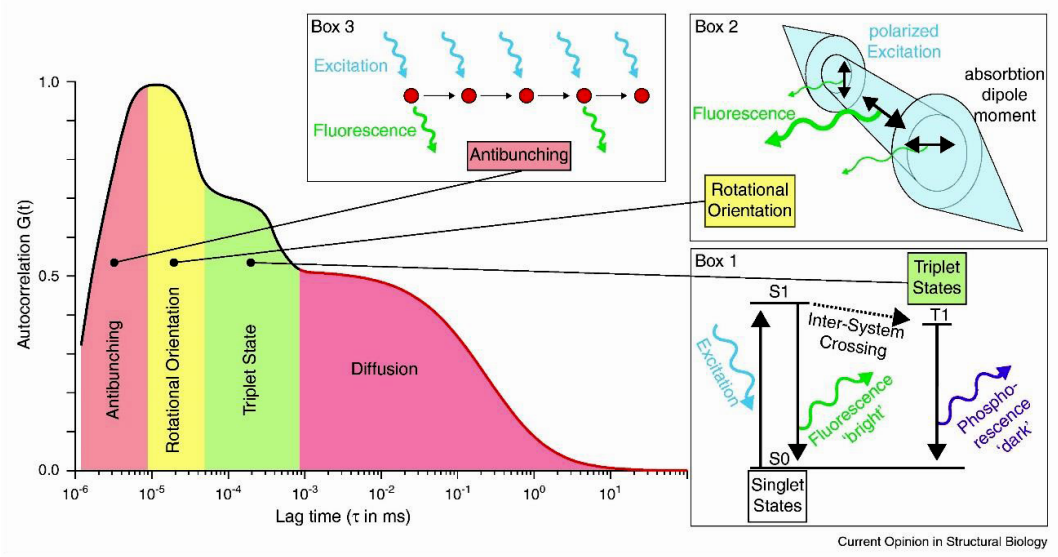


Figure 7: Depiction of the processes observed by FCS according to the time delay of the autocorrelation procedure.

basic principle of FCS is to monitor the fluctuations of fluorescence signal - generally of a highly diluted solution - during a fixed amount of time, then to mathematically correlate the signal with itself in function of an increasing time delay. This correlation output is associated with the persistence of the signal over time, hence with the speed of diffusion of the fluorophores in and out of the detection volume. The faster the fluorophores diffuse, the more the signal will fluctuate and the faster the autocorrelation value will decrease with delay. Therefore, the average mobility and amount of fluorescent molecules within this volume can derived from the autocorrelation process[187]. FCS can also be used to monitor other events, since the diffusion of fluorophores out of detection is actually the slowest way to alter fluorescence signal. Hence, interpretation of the autocorrelation function with shorter time delays can cover the effects of photon antibunching (impossibility for a fluorophore to emit more than a single photon at any given time)[188], rotational diffusion (polarization differences between absorption and emission dipoles)[189] and triplet states (Figure 7).

SAF-FCS is a direct application of the autocorrelation procedure to the signal collected from SAF detection. The fluctuations of the signal coming from the interface are monitored and interpreted selectively, with an increased effect of the fluorophore's remoteness from the surface due to exponential decrease of the detection efficiency (described more extensively in the next Chapter).

### 1.3.4 *Raman spectroscopy*

Raman spectroscopy is a label-free and non-destructive technique whose main result is to characterize the molecular bonds within a molecule, hence helping its identification. Raman Spectroscopy is based on the inelastic scattering of an incident monochromatic red or (near) infra-red light upon interaction with the sample. This occurs when the beam promotes transitions of the molecular bonds from lower to higher energy vibrational levels[190], but unlike fluorescence there is not requirement for matching the energy gap between the vibrational levels. From the shifts in frequencies between the incident and the diffracted light, a spectrum of the sample is extracted and the type of chemical groups constituting the molecule can be elucidated. Compared with the incident light, the energy of the scattered photons can either be identical (elastic scattering forms the "Rayleigh" peak of Raman spectrum), smaller (Stokes shift resulting from transition toward higher vibrational level) or even bigger (due to the depopulation of excited states toward the lowest vibrational level). However, inelastic scattering is a rare event as approximately one photon out of $10^8$ is inelastically scattered. Furthermore, the condition for a vibration to be visible on Raman spectrum is to induce change in polarizability during molecular vibration (by contrast with infra-red spectroscopy for which the molecule must undergo a change of dipole moment during vibration). When applied to the study of proteins or polypeptides, the analysis of specific peaks of the Raman spectra (i.e. the peaks of amide bonds) allows to characterize the secondary structures present in the conformation of the molecule[191]. Indeed, the chemical environment (such as hydrogen-bonding) relative to the secondary structure of proteins has an influence on the energy required to promote vibration of the amide bond, yielding recognizable shifts for each structure. However, the detection of proteins by Raman spectroscopy is limited by the small cross-sections of the chemical groups present in such biomolecules.

There are different ways to improve the low signal of Raman spectroscopy. One of them is the use of resonance Raman spectroscopy (RRS). In RRS experiment, the sample is still subjected to a monochromatic light but the laser wavelength is tuned to be as close as possible of an electronic absorption band (resonance). This feature enhances the light scattering by a factor of $10^4$. However, the very principle of using resonant light makes the sample subject to fluorescence as well[192]. Another consequence is that the specificity of the wavelength, optimized for one transition, renders the other non-enhanced vibrations

hard or even impossible to characterize. This could be considered either as a drawback for identification, or as an advantage when aiming for specific chemical bounds in a crowded environment. Rejection of fluorescence background is often the critical step of RSS experiments. It is often achieved by exploiting the difference of time scale between "instant" scattering and longer (nanoseconds) fluorescence processes[193].

Another very common technique that improves Raman signal is called surface-enhanced Raman spectroscopy (SERS). When compared with RRS, SERS is effective with a wider range of target molecules and gives a bigger enhancement in sensitivity (factor of $10^6$). SERS is based on the interaction of the target molecule with the high local electromagnetic field generated from plasmon resonance (excitation of the electrons cloud) near the roughened surface or nanostructure of a noble metal, typically gold or silver[194]. The effectiveness of SERS is strongly dependent on the strength of the electromagnetic field, hence on the substrate producing plasmon resonance. Size, shape, and the spacing between the metal edges or particles strongly influence the electromagnetic enhancement[195]. Since the strongest part of the electromagnetic field arises in small gaps of 1-5 nm between metal edges (called "hot-spot")[196], only the molecules in the close vicinity of specific metal structures will be subjected to the enhancement, hence making SERS not only more sensitive but also surface selective.

SAR is the supercritical angle version of Raman spectroscopy, which was recently applied to Raman scattering as well. Characterization of polystyrene microspheres demonstrated the surface selectivity of supercritical angle detection applied to scattered photons instead of fluorescence signal[197]. SAR is an interesting alternative to SERS for the study of interfacial molecules. Despite the lack of signal enhancement compared to SERS, a discrimination between molecular vibrations occurring at the surface and vibrations taking place in the bulk of the sample is possible. In addition, SAR is as straightforward to prepare than classical Raman and eliminates the requirement of nanostructures which may influence the behaviour of targeted molecules.

# 2

# MATERIALS AND METHODS

## 2.1 HANDLING AND LABELLING OF THE PEPTIDES

Monomeric Aβ (1-40), Aβ (1-42), Aβ (1-40)-Hylite Fluor 647 and Aβ (1-42)-Hylite Fluor 647 (Anaspec) were reconstituted in a 1% $NH_4OH$ solution, then immediately diluted in PBS. Solution were centrifuged at 12,000 rpm during 10 min and any undissolved material was removed. Non-labelled peptides were aliquoted at a concentration of 1 mg/mL and kept at -20°C until use (before 6 months of aging). Labelled peptides were aliquoted at the desired concentration and kept frozen until use.

Monomeric Aβ was also subjected to labelling procedure for the first experiments. One of the most frequently used method for labelling proteins is to covalently bind a dye with N-hydroxysuccinimide-ester (NHS) function to the primary amino group of the polypeptide. Here, Atto647-NHS was used and dissolved in DMSO. For the first labelling procedure, Aβ was dissolved in PBS, stabilized at pH 8 with HCl and KOH. The dye was added to the peptide solution with a 5-fold molar excess. The mixture was let to steer at room temperature for 2 hours. A second labelling procedure was tested by repeating the previous protocol in a carbonate-bicarbonate buffer at pH 9.2.

Solution was purified with the same buffer through a superdex 75 10/300 GL column (GE, healthcare) at a flow rate of 0.5 mL/min. The protein concentration and the ratio of successful labelling of the protein fractions were measured by UV-Vis spectroscopy with the following equations :

$$DOL = \frac{C_{dye}}{C_{protein}} = \frac{A_{647} \times \varepsilon_{protein}}{(A_{280} - A_{647} \times CF_{280})\varepsilon_{dye}} \tag{2}$$

$$CF_{280} = \frac{\varepsilon_{dye,280}}{\varepsilon_{dye,647}} \tag{3}$$

Streptavidin (Lucerna Chem AG) was dissolved in deionized water just before Raman measurements, at a concentration of 60% (m/w) or 10 mg/20 µL. Streptavidin-Atto633 (Sigma-Aldrich) was dissolved in PBS at a concentration of 10 µg/mL. Bovine serum albu-

min powder (BSA, Sigma-Aldrich) was dissolved just before measurements in deionized water at the desired concentration.

## 2.2 PROTOCOL FOR NATIVE-PAGE AND GEL STAINING

A NuPAGE 12% bis-tris mini gel (Thermofisher) was used for the separation of peptides according to their mass and aggregation state. The separation protocol was adapted from the work of Itkin et al[198]. The samples were prepared to load 10 µg of peptides in each well. Each sample was composed of the peptide load, 0.5 µL of NuPAGE LDS (lithium dodecyl sulfate) sample buffer and deionized water up to 10 µL. Running buffer was composed of 25 mM Tris, 192 mM Glycine and deionized water. Migration of the peptides through the gel was done with a constant voltage of 100 V for 1h at room temperature.
In order to observe the bands of peptides, the gel was incubated into a Coomassie blue solution (Roti blue) for 2 h, then destained with an aqueous solution of 40% ethanol and 10% acetic acid for 15 min. The remaining coloured bands correspond to the protein bands of different mass.

## 2.3 PRE-TREATMENT OF GLASS SLIDES AND SAMPLE PLATE/CELLS

Glass coverslips (Menzel-Gläser, Thermo scientific) were cleaned with ethanol in ultrasonic bath during 15 min, rinsed with water and dried with nitrogen before being subjected to plasma activation. They were placed in an ozone plasma chamber (Femto plasma cleaner, Diener electronic) for 10 min at 100 W in order to make the glass surface hydrophilic. Plasma treatment let the glass slide hydrophilic for few hours but the coverslips were used immediately.
Measuring cells (steady-state and flow-cell) were both cleaned with a three washing-steps procedure in ultrasonic bath. Each washing lasted for 15 min in the following solutions : Deconex Cip7 (1% in $H_2O$), ethanol and deionized water. The cell were coated with a Plastik 70 spray (Kontaktchemie, CRC Industries) to protect them against corrosion and homogenize the surface. The spray was let to dry for 1 h.
The activated glass slide and the measuring cells were glued together with Loctite 3311 (Henkel corporation). The closed flow-cells were connected to a rotating pump through a

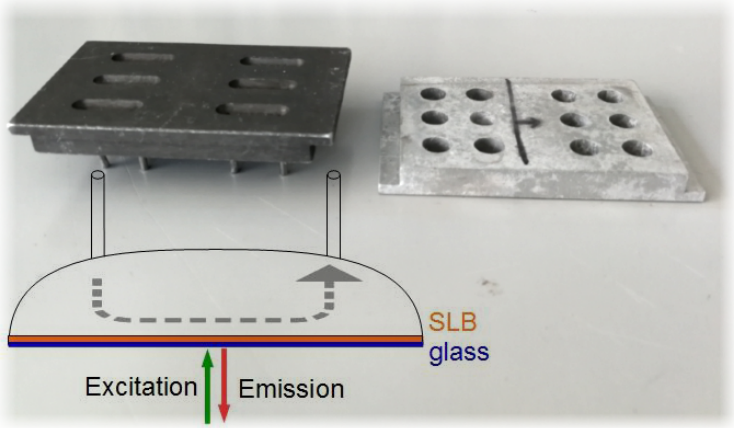


Figure 8: Picture and cross-section of the measuring cells. The left-one can be connected to a tubing and pump system for measurements including a flow of buffer. The right-one consisted of simple well-plate used for steady-state measurements.

tubing previously washed with a flow of Deconex Cip11 (10% in deionized water), then pure deionized water (3 mL/min during 30 min).

## 2.4 HANDLING OF LIPIDS AND FORMATION OF SLB

1,2-dioleoyl-sn-glycero-3-phosphocholine (DOPC); 1,2-Dioleoyl-sn-glycero-3-phospho-L-serine (DOPS) and brain porcine sphingomyelin (SM) in chloroform were used as received (Avanti Polar Lipids). Ganglioside GM1 (Ovine Brain) was received as a powder and diluted in chloroform (Scharlab S.L.). Fluorescently labelled 1,2-dioleoyl-sn-glycero-3-phosphoethanolamine powder (DOPE-Atto647; Atto-tec) was diluted in chloroform. When experiments required fluorescent SLB, DOPE-Atto647 was added to the lipids mixture to achieve a mass ratio of 1/62500. This amount was determined to give an optimum fluorescence signal with the SAF technique.

The following protocol was used to form both fluorescent and non-fluorescent SLB. The lipid solution was stirred under nitrogen then left under vacuum (10 mbar) overnight to remove any trace of solvent. Dried lipids were resuspended in degassed "membrane buffer" (NaCl (150 mM), $CaCl_2.3H_2O$ (5 mM), Tris (10 mM), pH 7.4; Sigma Aldrich) and extruded at least 20 times through a porous membrane (0.1 µm pore size) to yield unilamellar vesicles with homogeneous size distribution. For solutions of vesicles containing sphingomyelin, the extrusion was carried out at approximately 45°C (above the transition

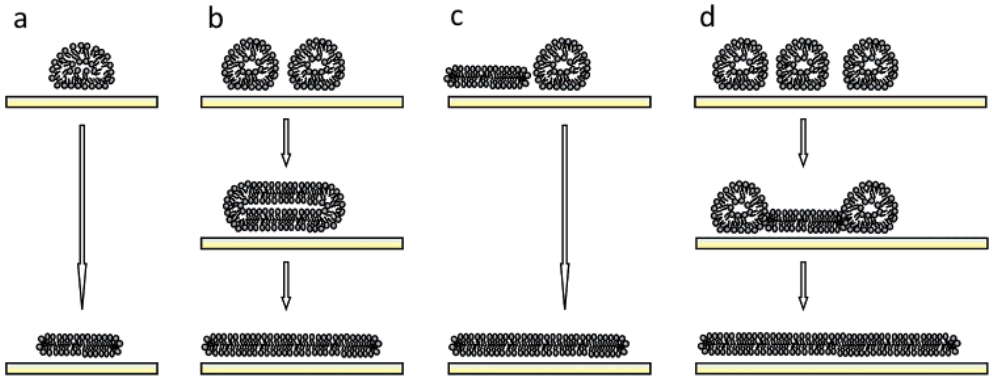


Figure 9: Different mechanisms of vesicles disruption and SLB formation. (a) Isolated vesicles disruption induced by the deformation upon adsorption on the substrate. (b) Fusion and disruption of neighboring vesicles. (c) Vesicles adjacent to a SLB patch disrupt under the influence of the patch active edges. (d) Collapsing of one vesicle under the pressure of neighbouring vesicles, turning into active SLB patch. Taken from [199].

temperature of SM, 37°C). The vesicles solution was then diluted in the membrane buffer to a concentration of 0.1 mg/mL. In constant-flow experiments, the vesicles solution was then passed through a circulating flow system (0.25 mL/min) connected to the flow-cell (see previous section). The solution circulating through the pump was changed following the protocol below (at constant flow-rate) :

- 10 min with the vesicles solution.
- 20-30 min rest with the pumping turned off.
- 15-30 min washing with "membrane buffer"
- (15 min with EDTA buffer (NaCl (133 mM), $Na_2EDTA.2H_2O$ (5 mM), Tris (10 mM), pH 7.4; Sigma Aldrich))

Variations of this protocol and their explanations are described in Section 3.2.1.

When a steady-state measurement was required, 50 µL of the lipid solution was poured in the well of the sample plate (see previous section).

In both case, when the lipid vesicles adsorbed on this coverslip reached a critical concentration, vesicles fused to form a SLB (Figure 9). Non-disrupted vesicles were removed by extensive washing with the membrane buffer, either by incoming flow of the pump or by pipetting. Finally, SLB was let to stabilize for at least one hour before any measurement.

## 2.5 PROTOCOL FOR BIOTINYLATION OF THE GLASS SLIDES

Glass microscope slides were first cleaned by immersion in piranha solution for 2 h, then thoroughly rinsed with deionized water.
Clean slides were immersed into freshly prepared 3-Aminopropyltriethoxysilane (APTES) solution (2% in toluene) at room temperature for 2 h. Following immersion, the glass slides were rinsed with toluene, methanol, and finally deionized water.
APTES-functionalized slides were incubated overnight in a solution of 10 mM biotin-NHS in DMF, then rinsed with deionized water.
The different steps of the functionalization were controlled by infra-red spectroscopy. Attenuated total reflectance (ATR) IR spectroscopy was performed using a Vertex 70 spectrometer (Bruker) with an ATR accessory. Samples were scanned from 500-4000 $cm^{-1}$ with 252 scans. Spectrum of uncoated glass substrate immersed in pure toluene was taken as background spectrum.

## 2.6 SUPERCRITICAL ANGLE SPECTROSCOPY SET-UP

All the spectroscopic measurements reported in this thesis (fluorescence and Raman) were accomplished using a special custom-built microscopy set-up developed in the group (Figure 10). This set-up included a home-made microscope objective composed of multiple lenses and parabolic mirrors to collect and transmit light coming from both above and under the critical angle of total internal reflection (cfr. Section 1.3.3) of a glass/water system (typically 61°). A power-tuneable diode laser at 633 nm (Toptica) provided the excitation beam. Two concentric collimated beams resulting from supercritical angle (SA) and undercritical angle (UA) collection were transmitted through the setup prepared for imaging and spectral analysis. These two concentric beams were separated by a 45° mirror mounted on a glass window before detection. Afterwards, each beam proceeded on a distinct path and could be focused into two identical single-photon avalanche diodes (SPADs) with an active area of 180 µm. These SPADs detectors were used for fluorescence measurements and imaging. For Raman measurements, the beams could instead be injected through fiber couplers into a 200 µm core multimode fiber. The fiber output was connected to a spectrometer equipped with a low-noise CCD camera cooled to −70°C (iHR320, Horiba). The choice of the spectroscopic method was applied by the means of flip mirrors. Fluorescence

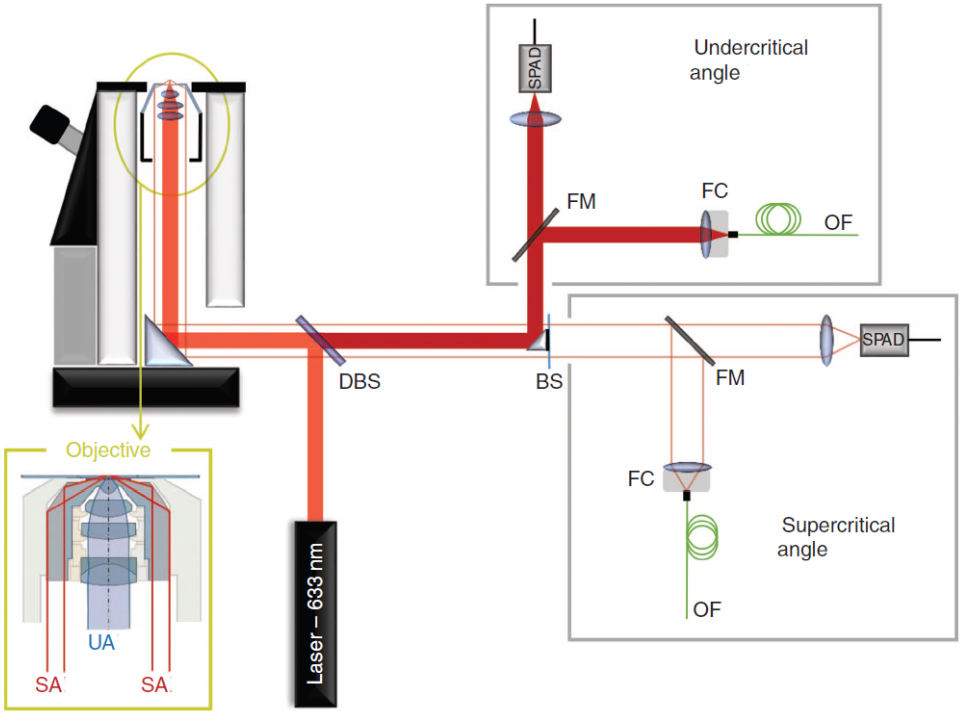


Figure 10: Experimental set-up scheme. Legend : DBS, dichroic beam splitter; FM, flip mirror; BS, beam splitter, referring to the 45° split mirror; FC, fibre coupler; OF, optical fibre; and SPAD, single-photon avalanche diode. The detailed view of the objective shows the multilens focusing and far-field collection system as well as the parabolic element for supercritical angle collection. Taken from [197].

images were recorded by using a custom-written Borland C++ program, whereas LabSpec (Horiba, Irvine, CA, USA) software was used for Raman measurements. The images and spectra were then processed in MATLAB and Origin.

## 2.7 SUPERCRITICAL ANGLE FLUORESCENCE (SAF) SCANS

When performing fluorescent measurements of the peptides, fluorescent Aβ represented 1% of the total amount of peptides. When monitoring fluorescent lipids, a mass ratio of 1/62500 (labelled/unlabelled) was used. The scanning images were obtained by scanning a square area of various edge size, commonly between 9.8 and 37.5 µm (whole scanning time of approximately 1 and 5 min respectively). Excitation light at 633 nm was cut by the use of spectral filter (616-646 nm effect). When measuring fluorescence signal, separate op-

tical path allowed for simultaneous collection of supercritical (SAF) and bulk/undercritical (UAF) fluorescence.

## 2.8 FLUORESCENCE CORRELATION SPECTROSCOPY (FCS)

FCS was used to investigate and quantify the mobility of fluorescent lipids and peptides. The principle is to monitor the fluctuation of fluorescence intensity within a defined detection volume during a finite amount of time, then to autocorrelate the signal in order to extract information about the speed of different processes (cfr. Section 1.3.3). The range of delay used for the autocorrelation function determines which parameter of the fluorescence fluctuation is analysed (cfr. Figure 7). Generally, several autocorrelation processes (at least 3) were measured at different points of the SLB and results were averaged. The signal was monitored during 1 minute for every FCS measurement. In addition, the resultant autocorrelation curves must be fitted with an appropriate model to quantify the parameters influencing fluorescence fluctuation. In this study, the translational diffusion (i.e. the diffusion of the molecule in space) is the only parameter that was investigated. The data within the biggest range of delay (from $10^{-3}$ to 1 sec) permitted to analyse this translational diffusion. Three different models were used to fit the FCS curves:

### 2.8.1 *2-dimensional diffusion with two diffusion coefficients*

This model is adapted for the study of a supported lipid bilayer (SLB) with components moving freely in the xy-direction. The following equations introduce two diffusion coefficients ($D_a$ and $D_b$), either to account for the two leaflets moving differently or for errors that occur at higher $\tau$ values. These errors arise when the measuring time is too short to compensate all irregularities. However, short measuring time can be necessary when targeting a specific fluorescent aggregate moving along the SLB.

$$G(\tau) = a \times G_0 \times \frac{1}{1+4D_a/\omega_0^2\tau} + (1-a) \times G_0 \times \frac{1}{1+4D_b/\omega_0^2\tau} \tag{4}$$

$$D_L = a \times D_a + (1-a) \times D_b \tag{5}$$

$$G_0 = \frac{1}{N} \tag{6}$$

Where G is the autocorrelation value, $G_0$ is the value at the y intercept, N is the average number of fluorescent molecules in the detection volume, $\tau$ is the time delay for the autocorrelation and $\omega_0$ is the radius of the detection volume.

### 2.8.2 *Anomalous diffusion*

Anomalous diffusion occurs when the diffusion of the lipids within the SLB is not free anymore, for example in the presence of lipid rafts. In this case, the time dependence of the mean square displace-ment (i.e. average translational diffusion along the surface) is no longer linear[200]. An anomaly factor or temporal factor ($0<\alpha<1$) is introduced to fit the displacement of the molecules and the equation for the model becomes :

$$G(\tau) = G_0 \times \frac{1}{1 + (4D/\omega_0^2\tau)^\alpha} \tag{7}$$

### 2.8.3 *3-dimensional diffusion (SAF)*

Fluorophores in bulk solution are expected to move freely in the three dimensions if there is no external perturbation. A 3D model was elaborated to fit the displacement of such type of sample[201]. However, the standard 3D model cannot be used when fitting the motion of fluorescent molecules in solution using the supercritical angle signal. The reason is that an exponential decay along the optical axis applies to the efficiency of detection of the supercritical angle spectroscopy (which is exactly what grants its surface selectivity) : $e^{-2\omega(\theta)z}$. Therefore, the fluorescence signal decreases even faster than with standard 3D model when the molecules recede from the surface. An appropriate 3D-SAF-FCS fitting was developed by Ries et al., taking the efficiency of detection into account. The complete set of formulas can be found in his paper[202].

## 2.9 SUPERCRITICAL ANGLE RAMAN (SAR) SCANS

For Raman measurement, a 200 µm core multimodes fiber was used to transmit the microscope set-up output to a separated spectrometer. Due to the optical set-up, the fiber needed to be connected to each coupler separately. Therefore, only one range of detection angle (supercritical angle or undercritical angle) could be transmitted at one time. The power of

the excitation beam was set between 10 and 70 mW to maximize the amount of scattered photons. The general configuration for the Raman detector was an opening slit of 50 to 100 µm, a grating of 300 grooves/mm and an accumulation of approximately 20-30 scans. The acquisition time depended on the sample, but was generally between 1 and 10 sec. Peptides required longer acquisition time than lipids.

## 2.10 MATERIALS

| | |
|---|---|
| 1,2-dioleoyl-sn-glycero-3-phosphocholine (DOPC) | Avanti Polar Lipids Inc., Alabama, USA |
| 1,2-Dioleoyl-sn-glycero-3-phospho-L-serine (DOPS) | Avanti Polar Lipids Inc., Alabama, USA |
| 1,2-dioleoyl-sn-glycero-3-phosphoethanolamine-Atto647 (DOPE-Atto647) | Atto-TEC GmbH, Siegen Germany |
| 3-Aminopropyltriethoxysilane (APTES) | TCI Europe, Boerenveldseweg, Belgium |
| Acetic acid | Merck and Co., Inc., New York, USA |
| Amyloid-β (1-40) human | Anaspec, California, USA |
| Amyloid-β (1-40)-Hylite$^{TM}$ Fluor 647 | Anaspec, California, USA |
| Amyloid-β (1-42) human | Anaspec, California, USA |
| Amyloid-β (1-42)-Hylite$^{TM}$ Fluor 647 | Anaspec, California, USA |
| Atto647, Atto 647N | Atto-TEC GmbH, Siegen Germany |
| Biotin-NHS | Lucerna Chem AG, Luzern, Switzerland |
| Bromophenolblue | Sigma-Aldrich Co. LLC, Buchs, Switzerland |
| Calcium chloride dihydrate | Sigma-Aldrich Co. LLC, St. Louis, USA |
| Chloroform | Scharlab S.L.; Barcelona, Spain |
| Coomassie blue (Roti-Blue) | Carl Roth GmbH + Co. KG, Germany |
| Deconex 11UNIVERSAL | Borer Chemie AG, Zuchwil, Switzerland |
| Deconex CIP seven | Borer Chemie AG, Zuchwil, Switzerland |
| Dimethyl sulfoxide (DMSO) | Sigma-Aldrich Co. LLC, Buchs, Switzerland |

| | |
|---|---|
| Ethanol | Reuss-Chemie AG, Tägerig, Switzerland |
| Ethylenediaminetetraacetic acid (EDTA) | Sigma-Aldrich Co. LLC, St. Louis, USA |
| Methanol | Merck and Co., Inc., New York, USA |
| Sodium azide | Sigma-Aldrich Co. LLC, St. Louis, USA |
| Phosphate buffered saline (PBS) | Sigma-Aldrich Co. LLC, St. Louis, USA |
| Protein Standard : SeeBlue Plus2 Pre-stained | Thermo Fisher Scientific, Carlsbad, USA |
| Sodium chloride | Sigma-Aldrich Co. LLC, Buchs, Switzerland |
| Streptavidin | Lucerna Chem AG, Luzern, Switzerland |
| Streptavidin-Atto633 | Sigma-Aldrich Co. LLC, St. Louis, USA |
| Toluene, anhydrous, 99.8% | Sigma-Aldrich Co. LLC), Buchs, Switzerland |
| Tris(hydroxymethyl)aminomethane (Tris) | Sigma-Aldrich Co. LLC, Buchs, Switzerland |

# Part II

# RESULTS AND DISCUSSION

The results presented in the following part are sorted between those obtained with the supercritical angle fluorescence and the supercritical angle Raman spectroscopy, but also between the results concerning the supported lipid bilayer and the Amyloid-β peptide. Since the project of this thesis consisted to monitor both lipid bilayer and Aβ in successive distinct experiments, special attention is accorded towards the observable target of each measurement. However, it is likely that discussions about the mechanism of interaction will spread beyond one single result. Relevant hypothesis regarding the adsorption and toxicity of the peptide require correlations between the behaviour of both molecules: Aβ *and* the lipid membrane.

# 3

# FLUORESCENCE MEASUREMENTS

## 3.1 FLUORESCENT PEPTIDES

### 3.1.1 *Fluorescent labelling of Amyloid-β*

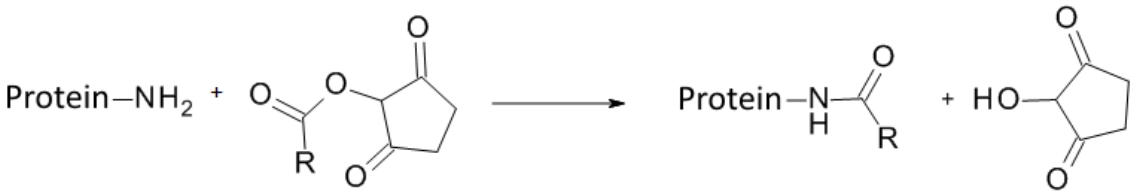


Figure 11: Reaction of NHS-ester function with the primary amine of proteins. The R-group is bound covalently with the protein through amide bond.

In order to detect Aβ peptides at the interface with the SAF technique, fluorescent labelling of the peptides was required. Atto647N is a rhodamine derived fluorophore which possesses outstanding quantum yield, photostability[203] (i.e., resistance to irreversible, light-induced reactions) and does not exhibit triplet blinking. A spectral analysis of this dye was conducted by Dempsey et al[204]. The structure of Atto647N reveals a positive charge which resonates between two structures. Among the commercially available Atto647N used for labelling, the N-hydroxysuccinimide-ester (NHS) dye-tag was selected for the simplicity of its functionalization procedure. NHS-ester chemical groups allow a convenient labelling of compounds with the dye through reaction with the primary amines of proteins to form a new and stable amide bound (Figure 11). All aliphatic amines can react with NHS-esters, therefore Aβ has three potential sites of binding available: the α-amino group at the N-terminus and two lysine residues ($Lys_{16}$, $Lys_{28}$). This could yield an over-labelling of the peptide with more than one fluorophore moiety. Such situation would be problematic since both the positive charge of several Atto647N's and their molecular size could hinder the natural functions of Aβ . However, the free base form of amino group is necessary to proceed the acylation reaction.

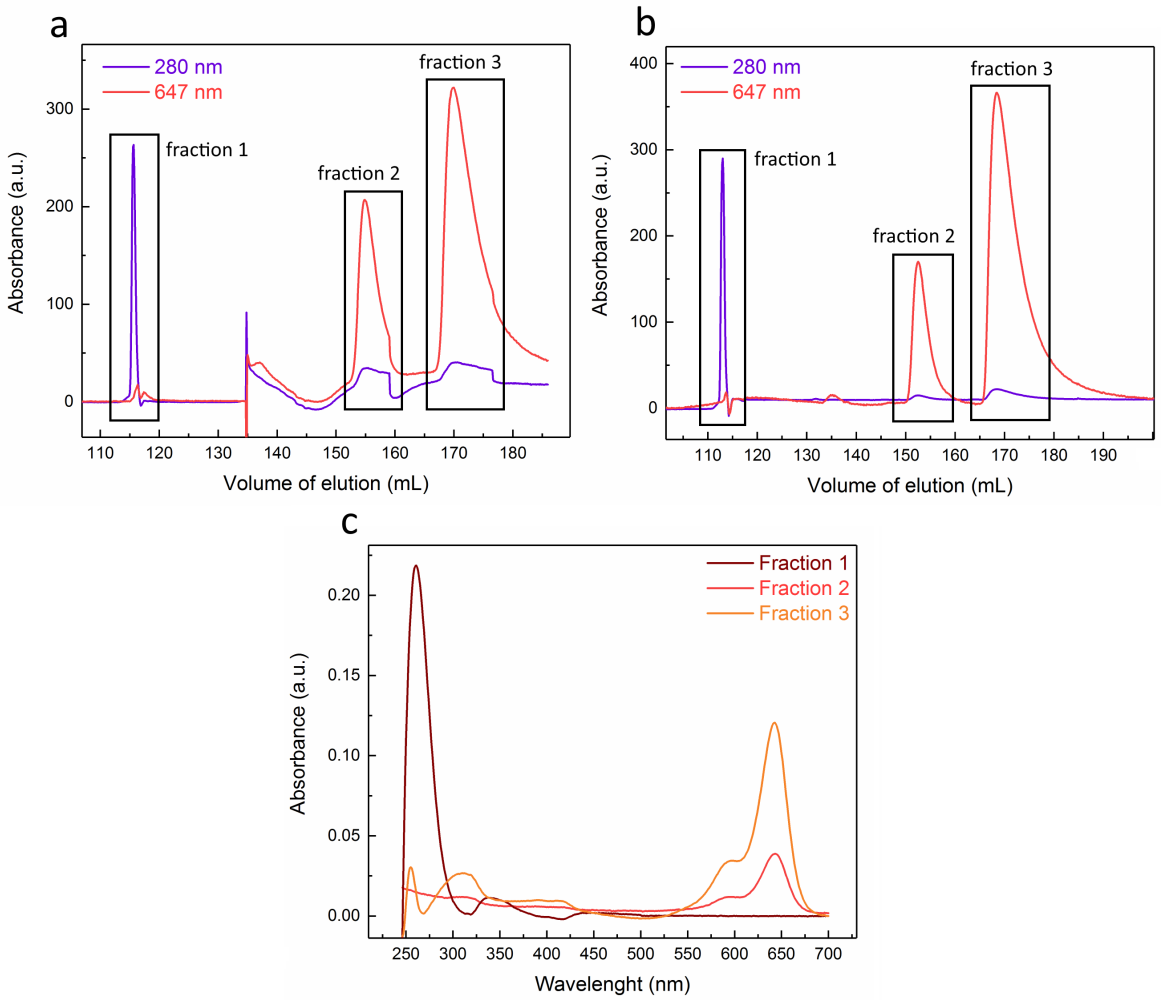


Figure 12: SEC elution spectra of the samples from the labelling procedure of Aβ with Atto647N-NHS-ester (a) at pH 8. (b) at pH 9. (c) UV-Vis spectra of the three fractions from labelling at pH 8.

The proportion of this free base form of amine is very low, i.e. below pH 8. Depending on their surroundings, ε-amino groups of lysine residues have a $pK_a$ range of 9.8 - 10.4 while α-amino groups have a $pK_a$ range of 8.0 - 9.0[26]. Therefore, the kinetic of functionalization with NHS-ester is highly pH dependent. It means that a neutral or slightly basic pH is optimum to proceed the acylation with α amino groups only, and avoid multi-labelling of one peptide. Additionally, working below pH 9 slows down the hydrolysis of the NHS-ester into an unreactive carboxylic acid[205]. Aβ (1-40) was subjected to labelling at pH 8 following the procedure described in Chapter 2. While the protocol provided by the Atto-company advised to use a 3-fold molar excess, here a 5-fold molar excess was used to compensate the hydrolysis side-reaction and the limited amount of available labelling sites. The sample was purified after reaction using a size exclusion chromatography (SEC). The

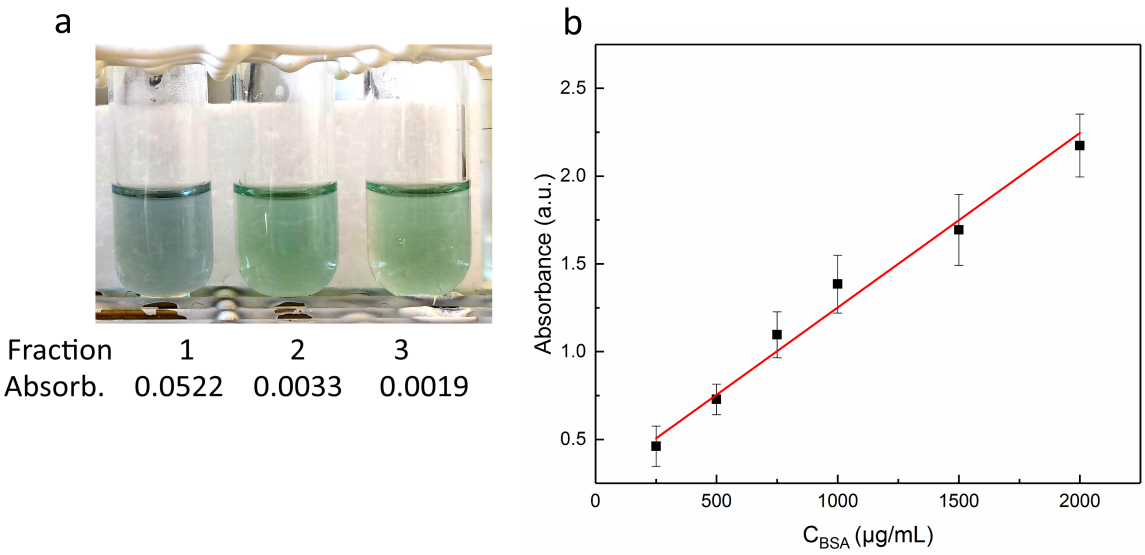


Figure 13: (a) BCA assay and absorbance at 562 nm of the fractions eluted from Aβ labelling procedure with Atto647N-NHS-ester at pH 9. (b) BCA assay standard curve with BSA.

elution spectrum displayed three peaks, collected and analyzed individually as fraction 1, 2 and 3 (Figure 12 a). The first peak was identified as the protein fraction. The second and third peaks were respectively attributed to Atto647N-NHS-ester and the smaller hydrolyzed Atto647N-COOH. From the elution spectra, the success of labelling of Aβ(1-40) was uncertain. This assumption came from the absence of overlapping between the absorption at 280 nm (characteristic of the peptide) and at 647 nm (characteristic of the fluorescent moiety). The concentration of protein and the labelling ratio of fraction 1 were calculated by UV-Vis absorbance (Figure 12 c) and with equation 2 and 3. Data are reported in Table 1. The extreme low values of the labelling ratio suggests that the functionalization of the peptide actually did not occur. To overcome this result, the reaction was repeated at pH 9 to increase the amount of free amine available. However, the elution spectra of this new attempt did not show a better labelling but the amount of hydrolyzed ester (fraction 3) increased, as expected at basic pH (Figure 12 b).

In addition to UV-Vis, a bicinchoninic acid (BCA) assay was carried out to calculate the protein concentration of every fraction. The reduction of $Cu^{2+}$ into $Cu^{+}$ by proteins and its chelation by BCA produces a purple colored compound. The intensity of the coloration and its adsorption at 562 nm was related to the amount of peptide in solution (Figure 13). The concentrations calculated from a standard curve using BSA protein are displayed in Table 1. Unlike the UV-Vis data, the amount of peptide obtained with the BCA assay was possible. Although it was slightly smaller than the total amount of peptide used for the

labelling, it suggested that the whole amount of peptide is concentrated in the unlabelled fraction 1.

| | |
|---|---|
| Molar amount of peptide used | 23 nmol |
| **Fraction 1 at pH 8 *(Figure 12 a)*** | |
| Average absorbance at 280 nm (a.u.) | $0.2185 \pm 0.0313$ |
| Average absorbance at 647 nm (a.u.) | $(1.104 \pm 0.841) \times 10^{-4}$ |
| Concentration of proteins (Mol) | $1.71 \times 10^{-4}$ |
| Labelling ration (DOL) | $4.29 \times 10^{-6}$ |
| Molar amount of proteins in 1 mL | 171 nmol |
| **Fraction 1 at pH 9 *(Figure 12 b)*** | |
| Average absorbance at 280 nm (a.u.) | $0.2881 \pm 0.0139$ |
| Average absorbance at 647 nm (a.u.) | $0.0182 \pm 0.0004$ |
| Concentration of proteins (Mol) | $2.25 \times 10^{-4}$ |
| Labelling ration (DOL) | $5.34 \times 10^{-4}$ |
| Molar amount of proteins in 1 mL | 225 nmol |
| **BCA assay of fractions at pH 9 *(Figure 13 a)*** | |
| Molar amount of peptides in fraction 1 | $(14.99 \pm 6.53)$nmol |
| Molar amount of peptides in fraction 2 | $(0.41 \pm 0.06)$nmol |
| Molar amount of peptides in fraction 3 | $(0.24 \pm 0.03)$nmol |

Table 1: Values obtained for the concentration and labelling ratio determined with UV-Vis spectroscopy, and the molar amount measured from BCA assay.

It is assumed that the amount of free amine was too limited to obtain an effective fluorescent labelling of the peptide with NHS-ester, when compared with other peptides or proteins. This labelling reaction depends of a competition between the acylation process and the fast hydrolysis of the ester moiety. Longer polypeptide chains highly influence

the success of the procedure by increasing the probability of reaction between the dye and a free amino group (i.e., α-Synuclein possesses 16 lysine residues and BSA has 59 lysine residues, among which 30-35 residues can react with linkers). Eventually, it was decided to use a commercially available fluorescent Aβ , selectively tagged on the α-amino group with HiLyte Fluor$^{TM}$647. Other studies were performed using Aβ labelled with analogue fluorophores, and showed that the tag moiety did not hinder the typical aggregation process of the peptide[206].

### 3.1.2 *Dependency of the adsorption of Amyloid-β on the composition of the lipid bilayer*

The SLB model is renowned for its simplicity of use and adaptation. The composition of the bilayer can be tuned following the need of a particular experiment with only slight modifications of the protocol of formation of the SLB (Chapter 2). When applied for the study of the interaction between Aβ and lipid membrane, various compositions were experimented. Cholesterol (Chol), sphingomyelin (SM), and gangliosides (especially GM1) have been reported to trigger the interaction between the peptide and the lipids by formation of micro-domains within the bilayer[207, 208]. Therefore, the adsorption of Aβ has been monitored on different SLBs as a preamble to the study of its toxic effects, and in order to select a proper SLB model. The different ratios of lipids were:

1. (DOPC:DOPS) with a lipid ratio of (65:35)
2. (DOPC:DOPS:Chol) with a lipid ratio of (50:25:25),(50:20:30),(50:15:35),(50:10:40) or (50:0:50 without DOPS)
3. (DOPC:DOPS:Chol:SM) with a lipid ratio of (40:10:25:25)
4. (DOPC:DOPS:Chol:SM:GM1) with a lipid ratio of (40:10:20:20:10)

The more complex SLBs are closer to the biological lipid composition of the neurons, either the soma or dendrites part of the cells[71]. They are not only more biologically relevant but were supposed to promote the interaction between the peptides and the SLB. 500 nM of fluorescent Aβ (1-40) have been incubated with each of these SLBs and the maximum of change in SAF intensity was measured after 2 hours of incubation and correlated to the amount of adsorbed peptides (Figure 14 a). Since the SAF technique only detects photons arising from the interface, its collection was assumed to be representative of the signal of Aβ adsorbed on the surface of the SLB. The background signal due to peptides

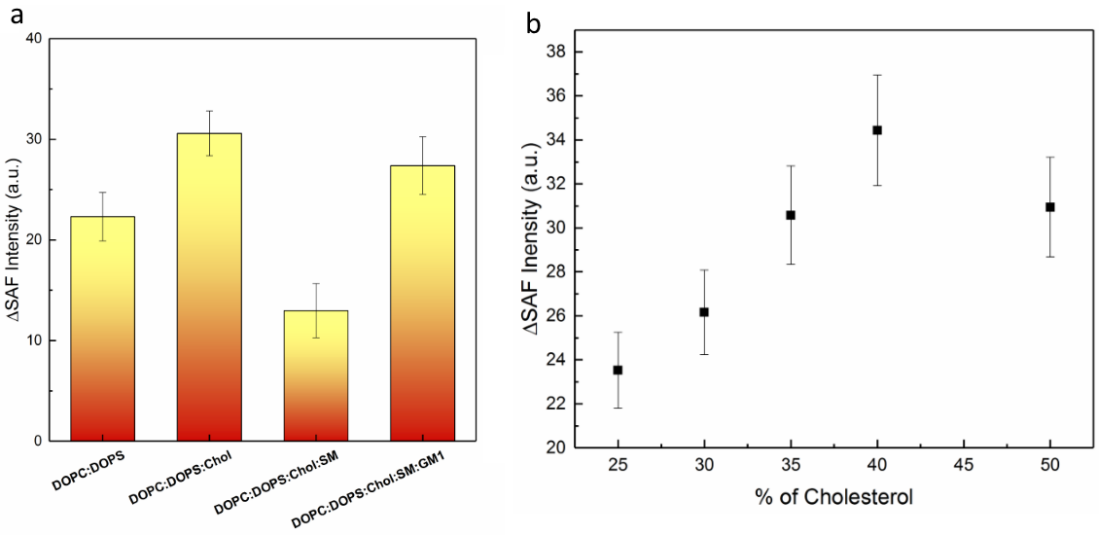


Figure 14: Maximum of change in SAF intensity after 2 hours of incubation of 500 nM Aβ (1-40) (a) on SLBs of different lipid compositions, (b) on SLBs **2** with different cholesterol content.

floating in the bulk of solution was not detected in SAF. Considering the deviation of the data, the values of adsorption on the SLB **1, 2** and **4** did not exhibit an important variation. It is obvious though, that the presence of cholesterol and GM1 molecules within the bilayer slightly enhanced the adsorption of Aβ. Other studies state that not only the presence but also the proportion of each lipid molecule is an important parameter in the enhancement factor of the interaction with the peptide. In the experiments performed by other scientists on a similar topic, cholesterol content varies from 20% to 40% of the total lipid amount, and yields an increase of the adsorption of Aβ within this range[209–211]. GM1 content varies from 3% to 50% while some groups affirm that 30% is required to obtain the association between the gangliosides and the peptides[211–213].

Among the four SLBs detailed above, the cholesterol content was systematically in the range required for an enhancement of the interaction with Aβ. The influence of the cholesterol was studied by comparing the SAF intensity of adsorbed Aβ (1-40) between SLBs **2** formed with different proportions of cholesterol (Figure 14 b). The amount of DOPS was inversely proportional to the amount of cholesterol. The membrane with the lowest cholesterol content barely yielded any enhancement compared with SLB **1**. When increasing the cholesterol content, the SAF intensity increased as well until a maximum value at 40% of cholesterol. When increasing this amount up to 50%, SAF intensity slightly decreased. This could be due to the absence of any charged lipid (DOPS) to drive the electronic interactions between the peptides and the bilayer, as a similar effect was observed with SLB **3** (see

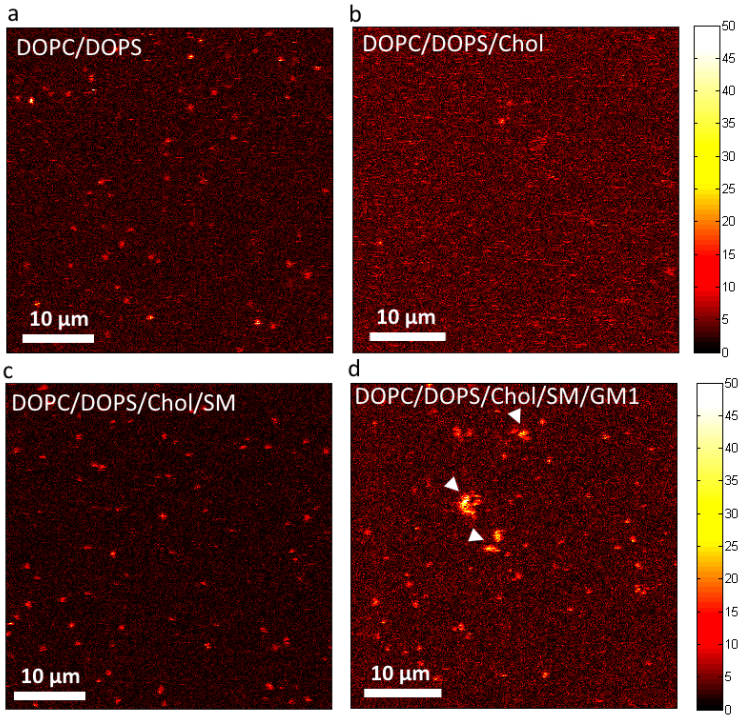


Figure 15: Maximum of change in SAF intensity after 2 hours of incubation of 500 nM Aβ (1-40) on SLBs of different lipid compositions.

below).

The adsorption of Aβ on SLB **3** was unexpectedly lower than on the other SLBs. Although the amount of cholesterol is lower than in SLBs **2**, its mixing with sphingomyelin was supposed to form lipid-raft domains which are known to favor the adsorption of Aβ. A possible explanation is based on the electrical charge of the bilayer and the great influence of electrostatic interactions regarding the adsorption of Aβ. Both cholesterol and zwitterionic lipids (DOPC, SM) exhibit a net zero charge, which left only 10% of net charged lipid (DOPS) in SLB**3**, limiting the electrostatic interactions. Although the incorporation of cholesterol is supposed to strengthen local electrostatic interactions with zwitterionic lipids, this effect is reported to arise only when cholesterol represents 40% of the lipids content[210]. These two simultaneous considerations based on electrostatic interactions could explain the low number of adsorbed peptides.

Since the amounts of both cholesterol and charged lipids are important, the efficiency of SLB **4** is likely related to the presence of GM1 which is also a trigger of interaction with the peptide. SLB **4** exhibits the same limiting factors as SLB **3** but the presence of only 10% of GM1 was sufficient to enhance the adsorption of the peptide.

In addition, these experiments showed that not only the amount of adsorbed peptide but also the mechanism of adsorption depended on the composition of the SLBs. SLB **1** and **3** showed some small fluorescent clusters, likely corresponding to small protein aggregates (Figure 15 a,c). On the other side, SLB **2** showed none of these clusters after 2 hours of incubation, but rather a homogeneous fluorescent layer (Figure 15 b). It seems that the cholesterol content of SLB **2** indeed enhanced the adsorption of fluorescent Aβ without promoting local aggregation. This could also be due to the absence of lipid-rafts when sphingomyelin is not present to interact with cholesterol. Finally, SLB **4** exhibited both features. The average fluorescence of the entire area was more intense, but the image also displayed distinct fluorescence aggregates, bigger than those observed previously (Figure 15 d). These aggregates are thought to be caused by the presence of GM1 within the SLB, as this lipid molecule is known to promote the seeding of Aβ aggregation and fibrillation.

Eventually, the models SLB **1**, **2** were selected for further experiments. The former was chosen for its simplicity and comparison purpose with previous research. The latter was selected because it combined both simple composition and the highest degree of adsorption of the peptide. SLB **3** and **4** were discarded despite of their physiological relevancy because the reproducibility of their formation was very poor and susceptible to more defects than the two other SLBs.

### 3.1.3 *Dependency of the adsorption of Amyloid-β on the peptide concentration*

Before studying the adverse effects of the peptides on the SLB models, the affinity of Aβ for SLB **1** (DOPC:DOPS) was measured. In order to characterize the early-stage adsorption of Aβ , SLBs were incubated with two types of fluorescently labelled peptides (Aβ (1-40) and Aβ (1-42)) at various concentration. For each sample, 1% of the peptides were fluorescently labelled. The SAF collection was used to detect the emission of lipids-bound peptides only and the fluorescence of supernatant peptides in bulk solution could be neglected. SAF signal was monitored over a fixed area of the SLB ($(9.8 \times 9.8)\mu m^2$ or $(37.5 \times 37.5)\mu m^2$), with peptide concentrations ranging from 1 µM to 40 µM, during at least 6 hours after the start of the incubation. The fluorescence intensity was averaged over the complete area of each scan.

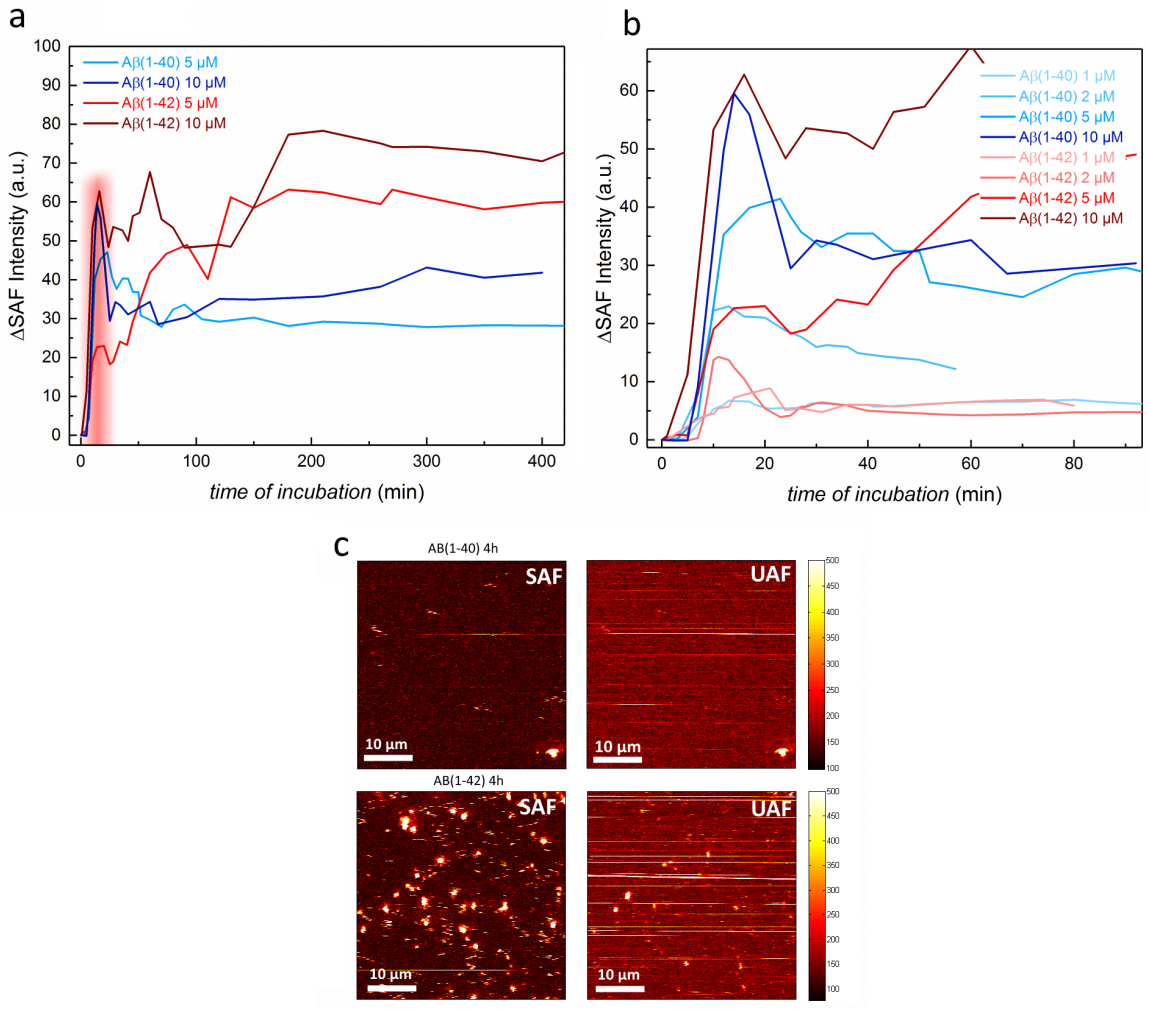


Figure 16: Evolution of the SAF signal over incubation of SLB with fluorescent peptides. (a) Long-time adsorption of Aβ(1-40) and Aβ(1-42). Short-time adsorption is highlighted in red. (b) Detailed short-time adsorption for low concentrations of Aβ. (c) Comparison between SAF/UAF imaging of 5 μM Aβ(1-40) and Aβ(1-42) after 4 hours of incubation.

The evolution of the fluorescence intensity was then plotted as a function of the incubation time (Figure 16 a). Results revealed a particular evolution of the signal divided in two time-ranges. For an incubation time up to 30 minutes, all solutions showed a fast increase in fluorescence intensity, followed by a systematic decrease of fluorescence intensity. These results were interpreted as a fast adsorption of the peptides followed by a partial desorption due to weak unspecific interactions. This behavior is well known as "overshooting" and known also from the adsorption of other proteins[214–216]. Different hypotheses have been formulated to explain the overshoot, but the most accurate for this experiment is based on the surface coverage and lateral protein-protein interactions. Briefly, many pep-

tides continuously adsorb on the surface in a metastable conformation. As the density of adsorption increases, electrostatic repulsions between peptides bearing net charges of equal sign promote the desorption of these metastable adsorbates, unless some of them undergo conformational changes which enhances their binding[214, 215]. This overshooting time range is hereafter referred to as short-time adsorption (depicted by the red shade on Figure 16 a). During the short-time adsorption, Aβ(1-40) displayed a higher fluorescence increase than its more toxic counterpart Aβ (1-42) for concentrations between 1 µM and 5 µM (Figure 16 b). However, this tendency was reversed beyond 10 µM, namely at concentrations equal or superior to the critical micellar concentration (cmc) of Aβ 's[217]. Around and beyond cmc range, Aβ(1-42) is known to exist as higher order aggregates than Aβ(1-40). This explains Aβ(1-42) subsequent higher fluorescence intensity during overshooting, since the first adsorbed species already are bigger aggregates.

Once the minima of SAF intensity have been reached after the overshooting described previously, extended time of adsorption yielded different behaviour for each type of peptide. Aβ(1-40) exhibited either a plateau or a slow increase when the time of incubation was prolonged beyond 24h. On the other hand, Aβ(1-42) showed a further increase in fluorescence intensity after only one hour: Aβ(1-42) accumulates several irregular jumps of intensity before reaching another plateau. SAF imaging of the area allowed to correlate these fluctuations with the appearance of fluorescent aggregates on the SLB (Figure 16 c). On the UAF imaging, bright stripes are visible and attributed to the motion of these fluorescent aggregates in the bulk solution during the scanning process. Some of them will eventually adsorb durably on the interface and increase the SAF intensity. These fluorescent aggregates are thought to be the result of peptides oligomerization. As shown by the comparison of imaging between the two peptides, Aβ(1-42) exhibited a stronger and faster tendency than Aβ(1-40) to form these aggregates and nucleation sites on top of the SLB after the short-time adsorption/desorption phase. This was especially obvious at concentrations above 5 µM. This outcome is also in accordance with previous reports showing the higher propensity of Aβ(1-42) to aggregate, due to the influence of the longer C-terminus[52, 218].

Therefore, the outstanding signal of Aβ(1-42) could have three explanations. It was either due to the adsorption on the SLB of peptide aggregates pre-formed in solution ; or caused by peptides stacking on aggregates already adsorbed ; and/or simply caused by an enhanced adsorption of monomers due to a higher affinity for the lipids. The quantification

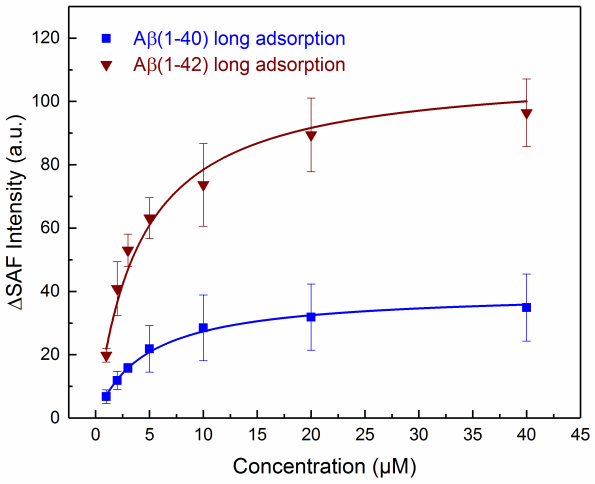


Figure 17: Maxima of fluorescence intensity after 6 hours of incubation as a function of Aβ concentration.

| | $K_d$ (μMol) | $I_{max}$ (a.u.) |
|---|---|---|
| Aβ (1-40) | 4.24 ± 0.28 | 39.96 ± 1.27 |
| Aβ (1-42) | 3.48 ± 0.37 | 110.17 ± 9.08 |

Table 2: Values obtained from the Langmuir isotherm fitting of the graph in Figure 17 with equations 8,9.

of Aβ(1-40) and Aβ(1-42) respective affinity was required to assess this hypothesis. To quantify the affinity of the peptides for the SLBs, the maxima of the average intensity of the area after 6h of adsorption were plotted as a function of the peptide concentration (Figure 17). This curve was then fitted with a Langmuir isotherm (equation 8)[219]. Fitting yielded values for the unspecific adsorption constant ($K_u$), which were then expressed as dissociation constant ($K_d$) to quantify this affinity (equation 9).

$$I = I_{max} \frac{K_u \times C}{K_u \times C + 1} \tag{8}$$

$$K_u = \frac{k_a}{k_d} = \frac{1}{K_d} \tag{9}$$

Where I is the measured fluorescence intensity, $I_{max}$ is the maximum fluorescence intensity reached at higher concentration, and $k_a$, $k_b$ being the kinetic constants for unspecific adsorption and desorption respectively (results depicted in Table 2). The values calculated

for $K_d$ were $(4.24 \pm 0.28) \times 10^{-6}$ M for Aβ (1-40) and $(3.48 \pm 0.37) \times 10^{-6}$ M for Aβ (1-42). Despite the high limitation of the Langmuir isotherm model to describe protein adsorption events, the range of these values is in accordance with other studies[212, 220]. From these data, it is supposed that the slightly higher $K_d$ value for Aβ (1-40) reflects a weaker interaction with lipid molecules than Aβ (1-42). This could be expected for the less toxic type of peptide, although the difference of affinity is too small to justify all the discrepancies encountered in SAF.

Despite having a similar values for $K_d$, the $I_{max}$ of each peptide is drastically different, as showed in Figure 17: Aβ (1-42) maximum SAF intensity is almost 3-folds higher than its counterpart. During these experiments, Aβ (1-42) yielded a higher SAF intensity than Aβ (1-40) when aggregates became visible on the interface. From that moment, the SAF intensity increased until a plateau is reached, demonstrating that the aggregates are adsorbed durably and not reversibly. Since the results yielded a similar affinity of both peptides for the lipids, this increase in surface fluorescence was likely the consequence of the deposition and subsequent growth of these aggregates. More Aβ (1-42) adsorbed on the surface than Aβ (1-40) because they were in oligomeric state. So, the "higher" affinity of Aβ (1-42) for the SLB is nothing but a secondary factor to explain its higher SAF signal. Additionally, the fact that Aβ (1-42) is the prior component of senile plaques in the brain[221, 222] supports the hypothesis that it aggregates more rapidly than Aβ (1-40) and interacts durably with the lipids at the early stage of the disease, while Aβ (1-40) is slower to oligomerize. In the absence of oligomers, the maximum adsorption of non-aggregated peptides is limited by the saturation of the surface with monomers. Furthermore, the adsorption of monomers was highly reversible, at least during the overshooting period (i.e. the desorption is observed up to 30 minutes of incubation). This limitation would explain why the non-aggregating Aβ (1-40) peptide yielded less signal than Aβ (1-42), prone to form oligomers.

To confirm this supposition, the evolution and average intensity of the non-aggregated Aβ (1-42) layer was selectively monitored and compared with the data obtained from its aggregates (Figure 18). From its constant SAF value, it is clear that the layer of adsorbed non-aggregated Aβ is in equilibrium and saturation with the incoming flow of peptides once the surface is saturated. Moreover, the SAF intensity of the non-aggregated layer of Aβ (1-42) (Figure 18 a, bottom line) was similar to the average SAF intensity of Aβ (1-40) in Figure 16 a. This confirms that the presence of Aβ (1-42) aggregates was the main

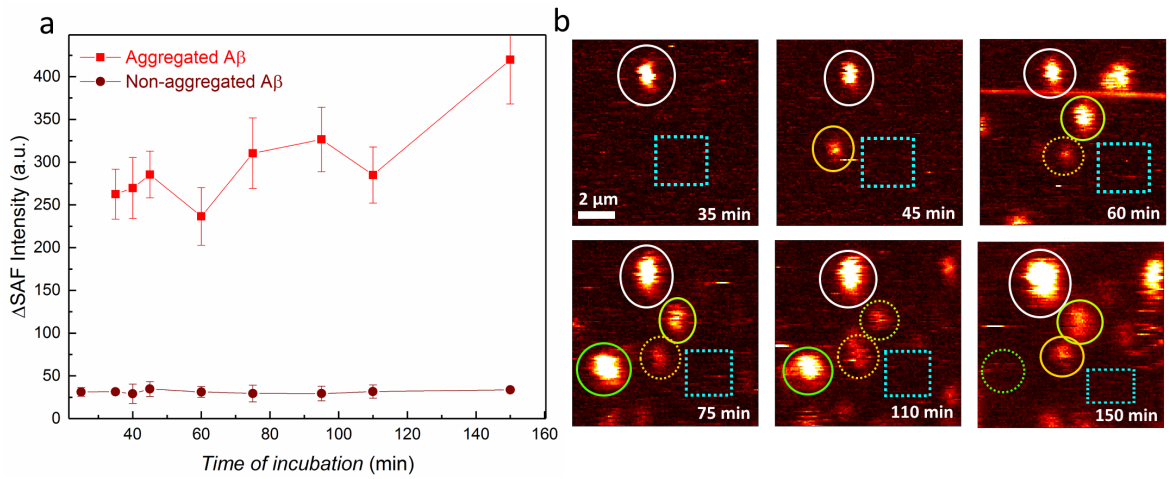


Figure 18: (a)Evolution of SAF intensity as a function of time for non-aggregated layer and aggregated sample of 10 µM fluorescent Aβ (1-42). (b) SAF imaging data with the tracking of the aggregates over time displayed by colored circles (each colored circle corresponds to one of the aggregates which remain at similar location). The SAF intensity of the first aggregate (white circle) and non-aggregated area (blue box) are displayed in (a).

source for the discrepancies in maximum SAF intensity: without these aggregates, the two peptides would exhibit comparable SAF signal. Unlike the non-aggregated peptide areas, the fluorescent aggregates displayed in Figure 18 b exhibited an increasing intensity. The aggregates were adsorbed tightly enough at the lipid bilayer so that most of them could be "tracked down" by SAF imaging. This is represented in Figure 18 b where each circle corresponds to the follow-up of one aggregate, a dashed circle indicating that the same aggregate partially desorbed. They seemed to spread or desorb punctually, but the lateral position of many of them remained similar over a time-span of more than 2 hours. These measurements confirmed the assumption that both non-aggregated monomeric Aβ s show a similar adsorption affinity. The discrepancies in the adsorption behaviour of Aβ (1-40) and Aβ (1-42) were obviously caused by the aggregates and did not come from the affinity of individual, non-aggregated, peptides.

### 3.1.4 *Reversibility of the adsorption of Amyloid-β*

Many proteins initially bind loosely on surfaces and only increase their affinity after structural changes have occurred over time. This behaviour was encountered in the last experiment. Both Aβ s exhibited a successive adsorption/desorption phase and weak interactions

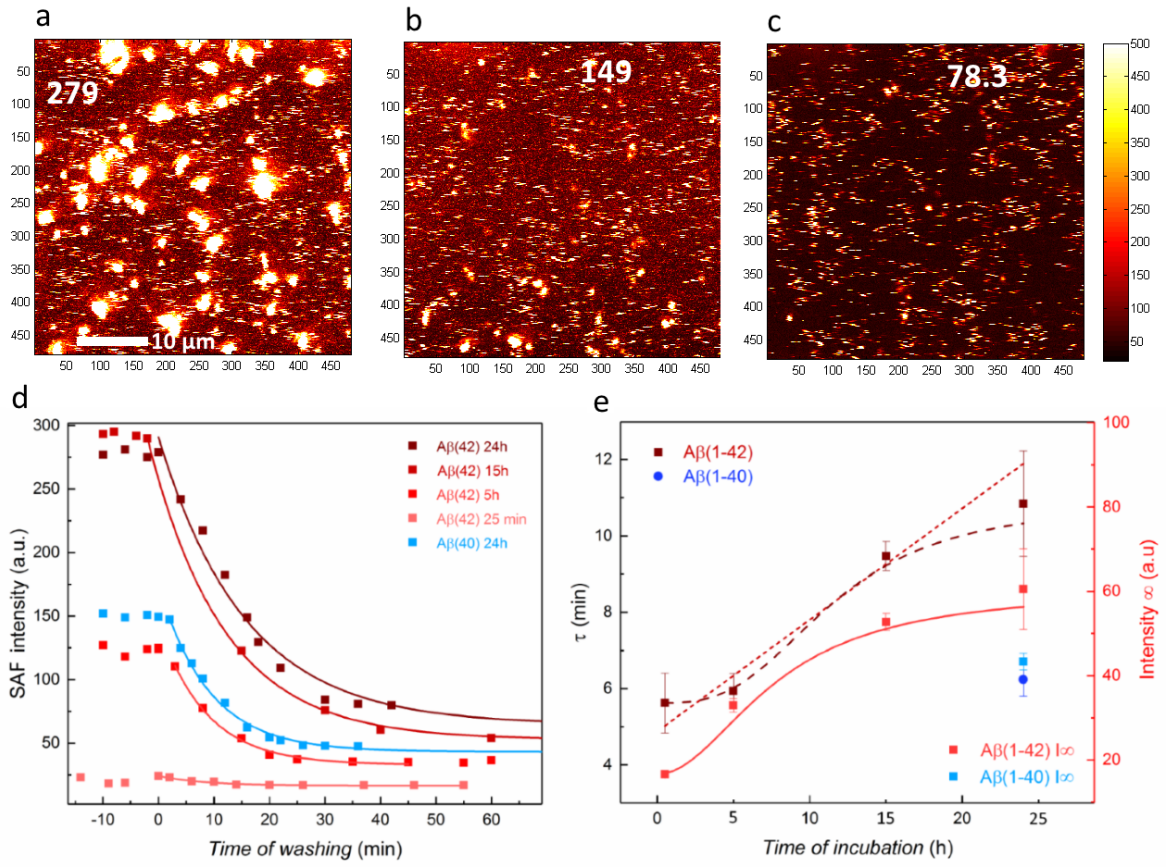


Figure 19: SAF imaging of 5 µM fluorescent Aβ(1-42) (a) after 24 hours of incubation on SLB, (b) after 15 min of washing with PBS, (c) after 1 hour of washing with PBS (average intensities are displayed in the top). (d)Evolution of the SAF intensity of 5 µM Aβ after washing with PBS. Each curve corresponds to a different time of incubation before the washing step. (e) Evolution of half-life time ($\tau$) and the minimum SAF intensity ($I_\infty$) in function of the incubation time before washing.

with the SLB, before some aggregated structures adsorbed durably on the SLB. As an example, quantification of the affinity of Aβ(1-42) using the SAF intensity of the short-time adsorption would yield a $K_d$ value of $(33.51 \pm 0.14) \times 10^{-6}$ M. This represents an affinity 10-folds lower than found using the SAF intensity after a longer incubation, and usually reported in literature. It also illustrates perfectly how the affinity of the peptide increased through the restructuration of the molecule over time. As a result, desorption kinetic of the peptides can strongly depend on the time that has been passed since the first adsorption events[223]. However, building this hypothesis from the adsorption curve only was insufficient to elaborate a proper model for the adsorption of Aβ . For that purpose, the reversibility of the adsorption after different times of incubation was investigated as well.

Therefore, 5 µM of fluorescent Aβ was incubated on SLB **1** (DOPC:DOPS) and the flow of peptides was exchanged with pure PBS buffer after various times of incubation has been passed (Figure 19 a,b,c). The decrease in SAF intensity was fitted with an exponential decay function (Figure 19 d), from which the half-life time $\tau$ (i.e. the time necessary for half of the peptides to desorb) and minimum intensity $I_\infty$ were extracted (equations 10, 11).

$$I = I_0 \times e^{-t/t_1} + I_\infty \tag{10}$$

$$\tau = \ln 2 \times t_1 \tag{11}$$

The first observation simply confirmed the results stated in previous section about the respective affinities of the peptides : after the same time of incubation and washing, the remaining fluorescence of Aβ(1-42) was higher than the fluorescence of Aβ(1-40). Although an attempt was made to find a linear dependence between the half-life time of Aβ(1-42) and the time of incubation, $\tau$ was better described by a sigmoid function (Figure 19 e). The same observation applied to $I_\infty$, indicating a good correlation between the two parameters. The resilience of Aβ to washing exhibited a strong enhancement when aggregates started to cover the surface (between 5 and 15 hours of incubation before washing). Next, both $I_0$, the half-life time, and $I_\infty$ reached a limit value. This showed that the affinity of the aggregates increased over time during their coverage of the SLB, as suggested previously.

However, the non-linear evolution of $\tau$ - and, by extrapolation, the affinity - is interesting for the discussion of the model of adsorption. While it is obvious that the affinity could not increase indefinitely, the plateau at the beginning of the x-axis in Figure 19 e suggested that the first adsorbed species, which are not aggregated, already exhibited their limit of affinity. Only through the process of oligomerization, occurring after 5 to 15 hours of incubation, would the peptides undergo a change of their affinity over time. Finally, the range of minima intensities $I_\infty(16.63 - 60.57)$ after washing was small compared with the range of initial intensities $I_0(24.08 - 290.10)$ before washing. This information, coupled with the SAF imaging, suggested that the remaining peptides species were similar, no matter how long Aβ was incubated before washing. These remaining peptides were monomeric or small oligomeric species and seemed already adsorbed on the surface before the coverage with the most massive aggregates. This is unexpected, as the aggregated species were thought to be a decisive factor in the resistance of Aβ to washing from the SLB. This last

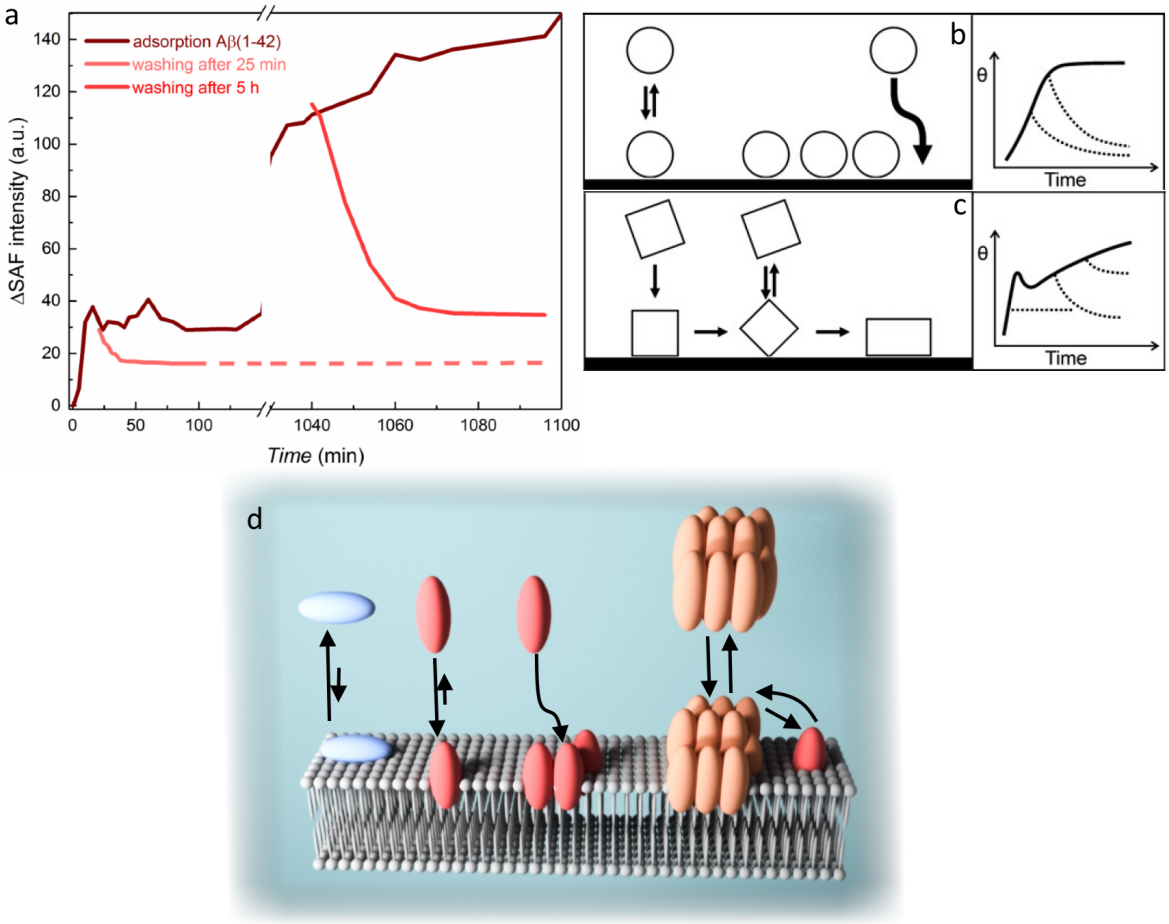


Figure 20: (a) Plot of the adsorption model for Aβ elaborated from the results obtained in previous experiments. (b) Cooperative adsorption model. (c) Three-states adsorption model. (d) Scheme of the adsorption model of Aβ.

observation was critical for the elaboration of the adsorption model : it meant that a fraction of monomeric or small oligomeric species have been subjected to a state-transition that increased their affinity for the SLB. Hence, they were the very last peptides adsorbed on the SLB after washing.

Combining the results of the adsorption process of Aβ and its reversibility, a model of adsorption phenomenon can be elaborated. The model resemble those developed by Rabe et al. with some adaptations (Figure 20 a, b, c). Briefly, the "cooperative adsorption model" states that pre-adsorbed proteins on the surface attract bulk proteins vertically to the surface due to the overlap of the electrostatic forces of the protein and the surface. When the lateral electrostatic repulsions between the proteins is too strong, approaching molecules are guided in the vicinity of pre-adsorbed proteins (Figure 20 b)[216]. On the other side, the "three-states model" describes how an overshooting effect is obtained, due to

the irreversible adsorption of first proteins which undergo fast orientation change toward reversibly adsorbed species. A third relaxed and more stable adsorption state is slowly reached and lead to a global increase of adsorbate after overshooting (Figure 20 c)[224]. The cooperative adsorption model corresponds remarkably to the images of aggregated Aβ recorded in SAF, where the aggregates were closely packed and spread along the surface. It also fits the washing experiments where $I_\infty$ converged toward a minimum range after the time of incubation has reached a threshold. The three-states model is also interesting because of its description of the overshooting effect followed by a second increase of adsorbed peptides. However, it must be nuanced to account for the discrepancies about the reversibility of adsorption. In the experiments with Aβ , no fully-irreversible adsorption could be confirmed since the washing during the overshooting period still yielded a small removal of peptides. It is assumed that (at least) two different states of Aβ with different affinities adsorbed simultaneously on the SLB. Once the surface coverage had reached a limit, peptides were too densely packed and the metastable states desorbed from the lipids due to the electrostatic repulsion. Only the most stable states could withstand this repulsion. This process yielded the overshooting effect observed during the short-time adsorption. The ratio between stable and metastable states explains very well the discrepancies between Aβ (1-40) and Aβ (1-42) concerning the desorption process. the latter is expected to favour the adsorption of the more stable state on lipids, perhaps because of its longer hydrophobic C-terminus[52]. Following the overshooting effect, the surface was mainly saturated with stable peptides which can cooperatively attract bulk solution peptides in their vicinity. This process leads to the formation of patchy aggregates on the surface. Alternatively, pre-aggregated species can adsorb on the surface. In the two cases, aggregates were obviously not the most stable species since some of them still desorbed entirely. However, their affinity and resilience to washing still showed a slight enhancement over time. This could be the consequence of a rooting of the aggregates as they attracted and stacked an increasing amount of incoming Aβ s (Figure 20 d).

### 3.1.5 *Influence of calcium ions on the adsorption of Amyloid-β*

The probable bidirectional relationship between Aβ and calcium ions in Alzheimer disease has long been hypothesized[225]. Aβ can disturb $Ca^{2+}$ homoeostasis, notably by formation of cation-selective channels[226–228]. On the other hand, dysregulation in the dynamics

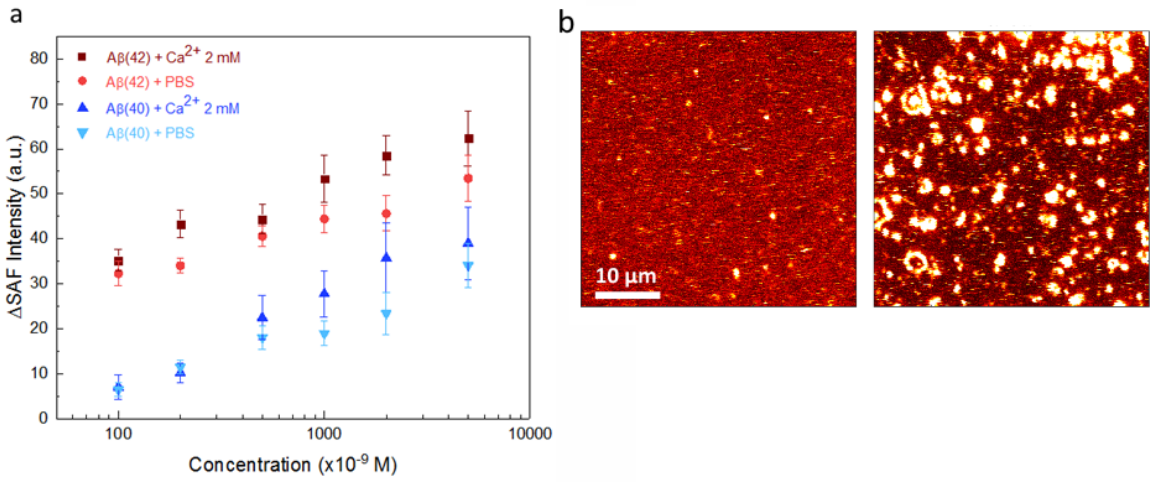


Figure 21: (a) Average SAF signal in function of different concentrations of adsorbed Aβ dissolved in pure PBS or PBS with 2 mM of $CaCl^2 \bullet 3H_2O$). (b) SAF imaging of 200 nM Aβ (1-42) adsorbed on SLB when dissolved in pure PBS (left) or 2 mM calcium buffer (right).

of $Ca^{2+}$ ions can modify the brain metabolism and trigger the release of Aβ peptides[229]. Interactions between Aβ and $Ca^{2+}$ also promotes the formation of oligomeric species[198] and would facilitate the binding of the peptide on the membrane via formation of ionic bridges[210]. For all these reasons, some experiments described in this thesis have been reproduced and compared, using PBS with 2 mM of $CaCl^2 \bullet 3H_2O$ instead of simple PBS. Following the methods of other groups, the content in calcium of the buffer is largely higher than the normal calcium concentration in cultured neurons (100-140 nM) [226, 230]. Therefore, the influence of $Ca^{2+}$ on Aβ is expected to be exacerbated.

First, the monitoring of the adsorption of Aβ on SLB **1** (DOPC:DOPS) was reproduced at low concentrations with the peptide dissolved in calcium buffer. The average fluorescence intensity of the area was measured after 5 hours of incubation with the peptides. As a matter of fact, dissolution in membrane buffer increased the amount of adsorbed peptides on SLB, compared with the adsorption of peptides dissolved in PBS (Figure 21 a).

This effect is thought to be the consequence of new interactions between Aβ and calcium ions. Computational studies explain this effect by the formation of the previously mentioned ionic bridges : $Ca^{2+}$ is supposed to act as a link between the polar head group of the lipids and the peptides, negatively charged at neutral pH[231]. It also strengthens the electrostatic interactions between charged residues of Aβ and the SLB[232]. Analysis of the SAF imaging reveals that $Ca^{2+}$-containing buffer promoted a different way of adsorption

than PBS (Figure 21 b) : $Ca^{2+}$ clearly increased the amount of aggregated species on the surface, even at concentrations as low as 200 nM. An increase of peptides aggregation could be expected since the ion-bridges can also occur between two negatively charged peptides. However, the non-aggregated adsorbed peptides exhibited a lower fluorescence intensity of $29.53 \pm 3.44$ a.u. when Aβ was dissolved with $Ca^{2+}$ ions, while the non-aggregated peptides had a fluorescence intensity of $40.26 \pm 5.81$ a.u. when dissolved in PBS. It is then assumed that although $Ca^{2+}$ increased the amount of peptides near the surface, this effect was mainly obtained through formation of peptide-peptide bonds promoting aggregation. The surface of the SLB was not more saturated by Aβ in $Ca^{2+}$ than in PBS buffer. The reason why PBS still exhibited a higher saturation of the surface than the calcium buffer can be due to their respective ionic strengths. The ionic strength of the calcium buffer was slightly higher than pure PBS. Hence, the calcium buffer yielded a stronger screening of the electrostatic charge of the lipid polar heads. This feature could have hindered the interactions between peptides and the SLB (see previous section).

In addition, the increase of fluorescence intensity due to calcium was not observed at concentrations beyond 1-2 µM Aβ . Beyond 2 µM of peptides, aggregation had been observed in PBS solution as well, and this factor is not specific of $Ca^{2+}$-buffer anymore. From these experiments, it is concluded that the presence of $Ca^{2+}$ could mainly trigger the aggregation of Aβ and occasionally act as a bridge between the peptides and the lipid bilayer. However, the influence of this bridging effect on the adsorption is significant only at concentrations lower than 1-2 µM. Beyond this limit, the flux of peptides coming from the bulk solution toward the membrane is supposed to overcome the influence of the calcium and the bulk concentration is high enough to yield aggregation without the influence of ionic bridges.

### 3.1.6 *Characterization of the aggregation state of Amyloid-β samples*

The exact role of Aβ in Alzheimer disease and its symptoms is still under debate, but nowadays the idea that the oligomeric species are responsible of the neurotoxicity is widely spread[42, 65, 233]. However, the biological synthesis of Aβ from the amyloid-precursor-protein releases the monomeric form of the peptide. Although some groups include pre-aggregated peptides in their sample, this work aimed to mimic the interaction with Aβ from scratch, hence starting with the monomeric peptides. Beyond this requirement, SAF

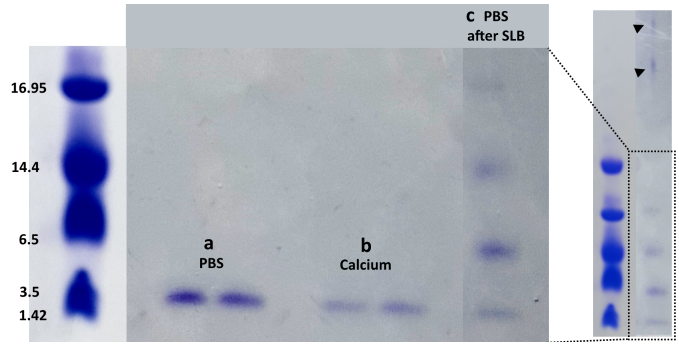


Figure 22: Native-PAGE with subsequent Coomassie blue staining of Aβ(1-42) (a) dissolved 24h in PBS, (b) dissolved 24h in membrane buffer (5 mM of $Ca^{2+}$), (c) dissolved in PBS and collected after 24h of incubation with SLB.

imaging showed the appearance of fluorescent peptide clusters, obviously in an aggregated state. Therefore, the characterization of these aggregates is relevant for this thesis.
To check the oligomerization state of the peptide, Aliquots of Aβ(1-42) were dissolved during 24 hours in the buffers used for the experiments, then separated by Native-PAGE electrophoresis according to their mass (Figure 22). Dissolution in PBS only yielded the monomeric form of the peptide after separation. The same result was obtained when dissolved in membrane buffer, despite its content in calcium ions, supposed to accelerate the oligomerization of Aβ [198]. This conservation of the monomer can be the result of the storage at room temperature instead of biological temperature. Yet, some aggregates - or oligomers - of Aβ were formed and observed as fluorescent aggregates in previous experiments. In order to determine the size of the oligomeric species in this type of sample, a fraction of 5 µM peptide solution was collected after 24 hours of incubation on SLB **1** (DOPC:DOPS) and peptides were separated using the same technique (Figure 22 c). On this gel, bands were visible at a higher mass than the monomer. Mainly dimeric and trimeric forms of Aβ were collected, with traces of tetrameric oligomers. Based on the color intensity of the bands, the dimeric form was dominant. However, from the intensity of fluorescence in previous experiments, it was supposed that bigger oligomers were formed and adsorbed on the SLB. But because of their relatively low concentration, their bands were barely visible and smeared at the top of the gel. From these experiments, it is showed that the starting peptide material is preserved as monomers even in $Ca^{2+}$-containing buffer. Interestingly, the oligomerization process is triggered by incubation in the presence of the lipid bilayer when the concentration of Aβ is too low to produce the nucleation of aggregates in solution (i.e. below critical micellar concentration).

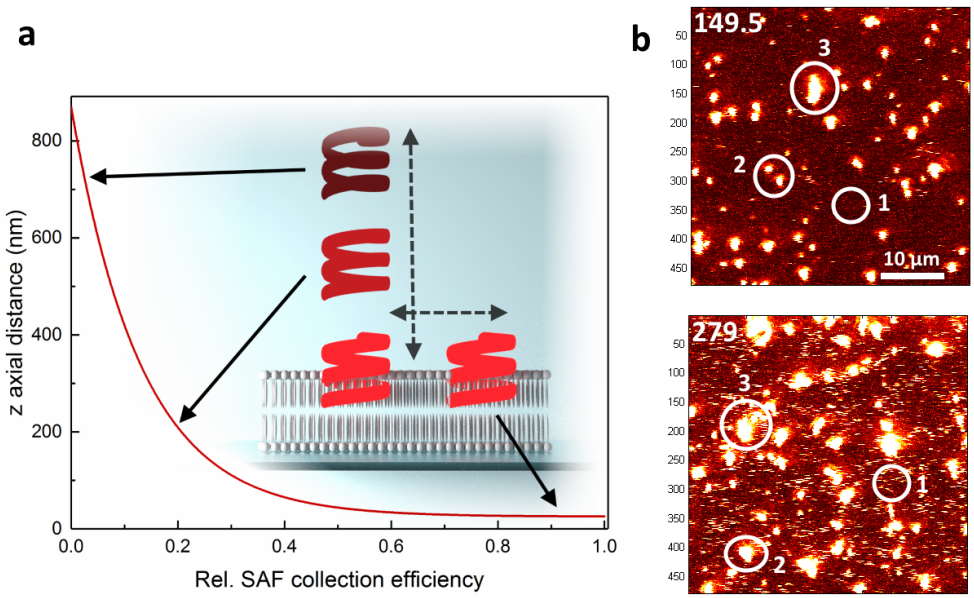


Figure 23: (a) Axial detection profile of SAF objective with angle of acceptance of 62°-75°. The possibilities of diffusion of Aβ within the SAF detection volume are correlated to a fictional detection efficiency. (b) SAF imaging of 5 µM Aβ (1-40)(top) and Aβ (1-42)(bottom) after 24h of incubation on SLB. Numbered circles design the aggregates targeted with FCS.

### 3.1.7 *Characterization of the diffusion coefficient of Amyloid-β*

Besides the quantification of the affinity of Aβ peptides for the lipid bilayer, their diffusion around the surface was also determined. Fluorescence correlation spectroscopy (FCS) is a method to measure the diffusion of emitting species by monitoring the variation of their signal within a defined detection volume. The monitored signal can be the SAF collection, hence analyzing the motion within the interfacial region. Fitting of the correlation curve with the proper model allows to extract the diffusion coefficient ($D_L$) of the fluorophore. Aβ can theoretically diffuse in three dimensions: Aβ can diffuse in two dimensions along the SLB surface (x and y axis) and/or adsorb on or desorb from the surface (z axis). However, the detection of the signal depends of the collection efficiency function, which is subject to an exponential decay along the optical axis (z) in the case of SAF objective[202]. This feature forced to adapt the fitting of the SAF-FCS curve, so that the decaying signal of Aβ moving along the optical axis is properly integrated in the fitting (Figure 23 a). Using the SAF 3D-FCS fitting, values of $D_L$ were calculated for 5 µM Aβ (1-40) and Aβ (1-42) after 24h of incubation on SLB (Table 3). From the SAF imaging, monitored areas

displayed inhomogeneous fluorescence and aggregates. This result recalled the previous section, where different sizes of oligomers were identified with Native-PAGE. Fluorescent aggregates were selectively targeted for FCS and sorted according to their size on the SAF imaging : target 1 represented the first layer of adsorbed peptides without any visible aggregation, target 2 was attributed to the smallest aggregates with a diameter between 1-3 µm, and target 3 referred to the aggregates whose diameter was equal to or greater than 4 µm (Figure 23 b). There was an inverse proportionality between the size of the aggregates and the $D_L$. As expected, bigger fluorophores diffused slower. However, there was also a net difference in the diffusion of the two types of peptide. All targets considered, Aβ (1-42) diffused approximately from 6 to 15-folds slower than Aβ (1-40). Considering the whole set-up of the experiment being the same for both Aβ s, there are only two parameters that can influence their diffusion near the interface: their mass and their affinity for the SLB. The influence of the mass can be discussed using the equation of diffusion developed by Albert Einstein during his thesis at the University of Zürich (1905) (equation 12).

$$D = \frac{k_B T}{6\pi\eta r_0} \tag{12}$$

Where $k_B$ is the Boltzmann constant and $\eta$ is the viscosity of the solvent. Considering Aβ as a small globular protein and the mass $m$ of a molecule to be proportional to the volume $4\pi r_0^3/3$ , it is found that $D_L \propto 1/m^{\frac{1}{3}}$ . Considering the target 1 as the signal emitted by monomeric and dimeric Aβ (the two dominant species characterized by Native-PAGE), the theoretical mass of the other targets was estimated by proportionality with $D_L$ (reported in Table 3). From the mass calculation, the approximate number of peptides constituting the aggregates was derived. Targets 2 in Aβ (1-42) contains around 2 times more peptides than in Aβ (1-40). As for targets 3, Aβ (1-42) contains 4 - 5 times more peptides than in Aβ (1-40). These results offer a potential explanation for the discrepancies in $D_L$ between the two Aβ s. If Aβ (1-42) aggregates were more voluminous than Aβ (1-40) it is expected that they would diffuse slower. However, even the diffusion of target 1 - supposedly of similar size for both peptides - displayed a huge difference in $D_L$ despite the small difference in molecular weight.

| | $D_L(\times 10^{-12} m^2 s^{-1})$ | $mass_{from\ D_L}(\#peptides)$ |
|---|---|---|
| **Aβ (1-40)** | | |
| target 1 | $29.6 \pm 5.8$ | $4329.9 - 8659.8 \quad (1-2)$ |
| target 2 | $24.8 \pm 5.6$ | $13566.2 - 16293.6 \quad (\approx 3-4)$ |
| target 3 | $20.15 \pm 5.3$ | $23276.2 - 35598.3 \quad (\approx 5-8)$ |
| **Aβ (1-42)** | | |
| target 1 | $4.7 \pm 0.8$ | $4514.1 - 9028.2 \quad (1-2)$ |
| target 2 | $2.3 \pm 0.7$ | $21911.3 - 36315.1 \quad (\approx 5-8)$ |
| target 3 | $1.4 \pm 0.5$ | $108971.8 - 170206.2 \quad (\approx 20-38)$ |

Table 3: Values obtained for the diffusion coefficient of both types of Aβ peptide after 24h of incubation on SLB. $D_L$ is extracted from SAF-FCS fitting of different targets (see Figure 23 b). The theoretical mass and amount of peptides in each target is calculated from the $D_L$ and equation 12.

Therefore, it seems evident that the mass of the peptides did not influence the diffusion on its own, but the respective affinities of each peptide for the SLB also played a role. The higher affinity of Aβ(1-42) for the lipids may have hindered its diffusion at the surface and its desorption from the bilayer. From comparison between the molecular weight of the two Aβs and their respective $D_L$, the interactions with the bilayer seems to exert a greater influence on the diffusion near the surface than the mass of the peptides. The mass could have a bigger impact on the diffusion once Aβ is completely desorbed from the SLB and too far apart from the lipid molecules to interact with them. Moreover, the mass calculation from FCS confirmed the assumption made in previous section, that aggregates bigger than tetramers (i.e. up to 40 peptides) could be formed on the SLB. It seems that the formation of these oligomers occurred rarely and their low amount prevented their detection with the Native-PAGE electrophoresis. However, other studies about the aggregation of Aβ also showed that oligomers of higher order (average amount up 50 peptides) were formed after only few hours[234].

## 3.2 FLUORESCENT SUPPORTED LIPID BILAYER

### 3.2.1 *Formation of supported lipid bilayer of different compositions*

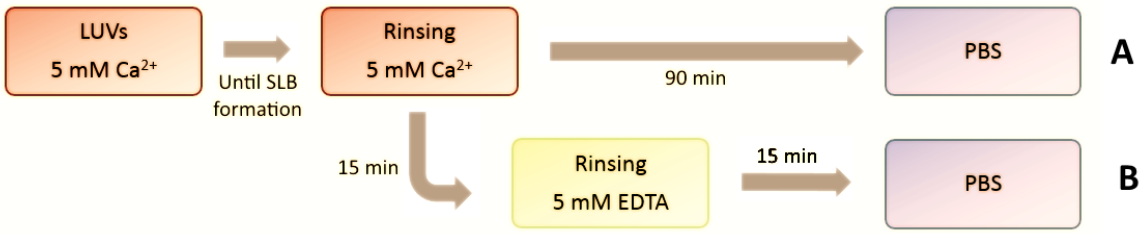


Figure 24: Overview of the two general protocols for the establishment and washing of the supported lipid bilayers described in this thesis.

As written in Section 3.1.2 different compositions of SLB were attempted to be formed. The basic protocol for the formation of SLB (explained in Chapter 2) required some adaptation depending on the lipids present in solution. First, a study of the stability of the bilayer was conducted with a protocol elaborated recently to study the interaction of SLB with α Synuclein[160, 235]. The major concept of the protocol is to spread the solution of lipid unilamellar vesicles (LUVs) on the substrate, then to rinse it with a determined buffer to remove the undisrupted LUVs. Finally, the freshly formed SLB is let to equilibrate with the buffer used in further experiments. During the first step, LUVs are dissolved in membrane buffer (containing $Ca^{2+}$). $Ca^{2+}$ ions are known to destabilize the lipid structure[236]. While this effect is desirable to disrupt the vesicles adsorbed on the substrate and force the desorption of non-disrupted vesicles, prolonged incubation with $Ca^{2+}$ has been showed to remove lipid molecules from the bilayer itself or to perturb its diffusion[237]. On the other hand, EDTA-containing buffer has been showed to yield a restructuration and stabilization of the SLB while complexing the $Ca^{2+}$ ions[238]. Therefore, two methods were used to form the SLB on the glass substrate. The first one consisted in a single rinsing step with the membrane buffer before equilibration with PBS. The second one involved two shorter rinsing steps : a preliminary washing with membrane buffer followed by a rinsing with EDTA to remove the free calcium ions (Figure 24).

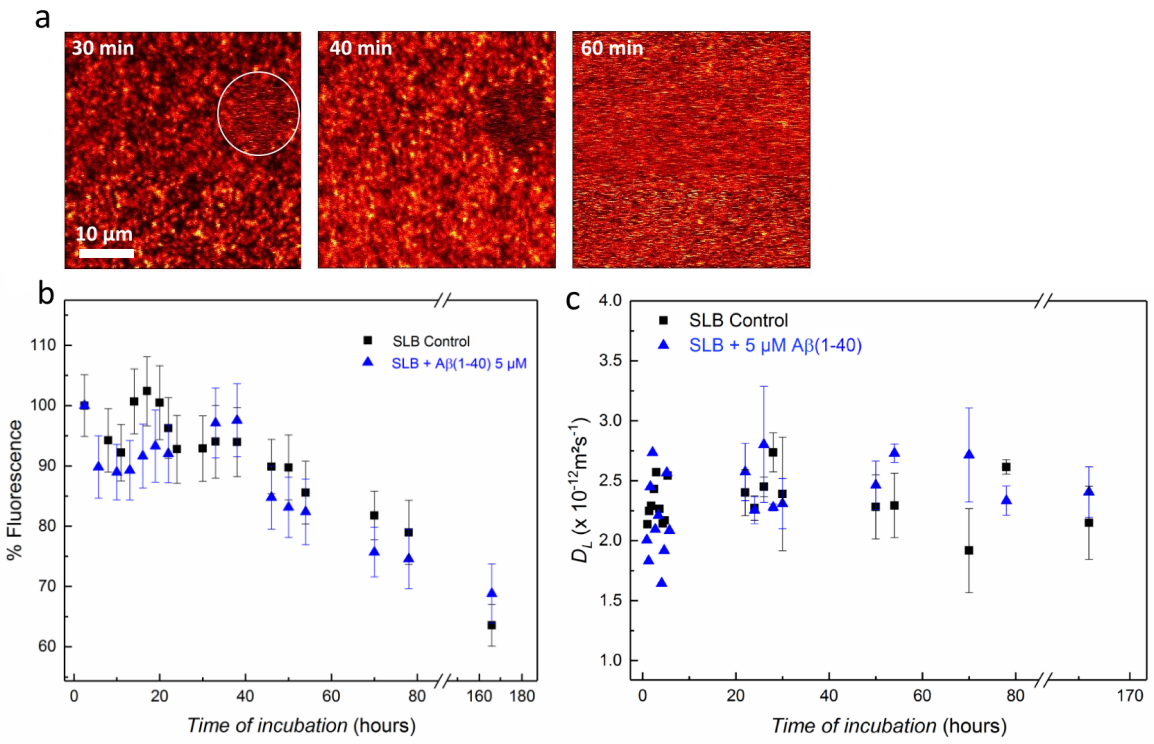


Figure 25: (a) SAF imaging of the formation of a DOPC:DOPS SLB using protocol B (EDTA rinsing step, see Figure 24). The white circle points the first zone of restructuration of the SLB. (b) Evolution of the SAF signal and diffusion coefficient $D_L$(c) of the SLB over one week, with and without incubation with 5 µM Aβ (1-40).

In order to evaluate the stability of the SLB, fluorescent DOPE-Atto647 was incorporated in the lipid mixture to visualize the bilayer with SAF upon its formation on the substrate. The protocol B used by Hähl et al.[160] was the first to be tested and included the rinsing step with EDTA. The progressive adsorption and disruption of the LUVs could be monitored by SAF imaging. Lateral scanning lines became visible only few minutes after the exchange of buffer and are characteristic of disrupted vesicles forming a lipid bilayer patch (Figure 25 a). The stability of the SLB **1** (DOPC:DOPS) under constant flow of PBS was assessed during a time span of 7 days by checking the bilayer integrity and fluorescence intensity with SAF imaging, and the lipid diffusion $D_L$ by SAF-FCS (Figure 25 b,c). After one week, the fluorescence intensity decreased of approximately 35% while the value for $D_L$ remained constant. Also from the FCS curve, the values of $G_0$, inversely proportional to the amount of fluorescent molecules, raised from $0.137 \pm 0.025$ to $0.251 \pm 0.009$. This means that some fluorescent molecules are lost from the bilayer over time, and the decrease in fluorescence is not due to photobleaching. Still, these data showed that the SLB was per-

fectly stable during at least 42 hours. At the same time, this type of SLB was incubated with 5 µM Aβ (1-40) as a first observation of the impact of the interaction with the peptides. The results are displayed in this section though, because they emphasize the resistance of the SLB formed with Hähl's protocol. Even after 7 days of incubation with Aβ, the SLB exhibited no significant difference with the control. From the previous section, it is known that at this concentration and after such a time of incubation, the peptides likely adsorbed and aggregated on the bilayer. Therefore, it was surprising to observe no impact on the SLB. Similar preservation of the fluorescence have already been observed for this type of SLB with another peptide (α Syn)[237] while the same experiment with another protocol for the formation of the SLB yielded different results[235]. One hypothesis to explain that contradictory outcome is that the SLB formed after restructuration with EDTA was actually too stable and resilient to the influence of all peptides. The second hypothesis is that the complete chelation and removal of all remaining calcium ions hinders the adsorption of Aβ. Therefore, the protocol A without any rinsing with EDTA was conserved for the formation of SLB in further experiments.
Using adaptation of the protocol A, SLBs of different lipid compositions were formed (mentioned in Section 3.1.2):

1. (DOPC:DOPS) with a lipid ratio of (65:35)
2. (DOPC:DOPS:Chol) with a lipid ratio of (50:15:35)
3. (DOPC:DOPS:Chol:SM) with a lipid ratio of (40:10:25:25)
4. (DOPC:DOPS:Chol:SM:GM1) with a lipid ratio of (40:10:20:20:10)

Their stability during a time span of 48 hours and under a constant flow of PBS was monitored and compared (Figure 26). The resistance of SLB**1** is lower when formed with protocol A than with protocol B, and its fluorescence dropped of 30-35% after only two days instead of one week. This effect is thought to come from the absence of calcium removal with ETDA. However, the stability is still considered sufficient for observing the impact of Aβ in further experiments.

Compared with SLB **1**, the stability of other SLBs remained similar, although slightly higher after 40 hours of lifetime. It is assumed that incorporating other lipids in the bilayer induces the formation of so-called "lipid rafts" which are produced by the interaction and packing of sphingomyelin with cholesterol. Those lipid rafts confer an enhanced stability and resistance to some detergents on the SLB[239]. Another proof of the formation of

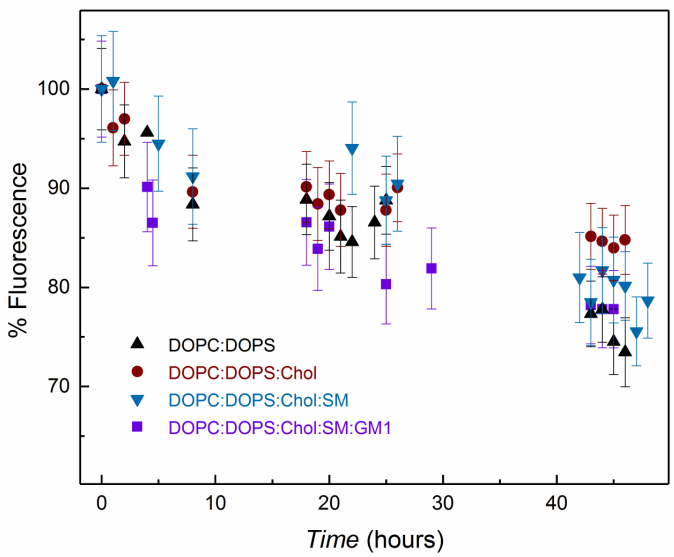


Figure 26: Evolution of the SAF intensity in function of time of SLBs prepared with protocol A (without EDTA, see Figure 24) for different lipid compositions.

such micro-ordered domains in the lipid bilayers is provided by measuring their lateral diffusion coefficient. The $D_L$ decreased with the sophistication of the SLB, as expected when rafts or liquid-ordered phases appear within the membrane[240, 241] :

1. (DOPC:DOPS) $D_L = 2.51 \pm 0.37 \times 10^{-12} m^2 s^{-1}$
2. (DOPC:DOPS:Chol) $D_L = 1.47 \pm 0.62 \times 10^{-12} m^2 s^{-1}$
3. (DOPC:DOPS:Chol:SM) $D_L = 0.40 \pm 0.28 \times 10^{-12} m^2 s^{-1}$
4. (DOPC:DOPS:Chol:SM:GM1) $D_L = 0.47 \pm 0.16 \times 10^{-12} m^2 s^{-1}$

Despite the successful formation of all these SLBs, only the SLB **1** and **2** were selected for further investigation of the interaction with Aβ. Their formation is more straightforward than the other SLBs and was more reproducible. Besides, their lateral diffusion coefficient were in the range of previous studies involving Aβ or amyloidogenic peptides, which might prove helpful for a comparison purpose.

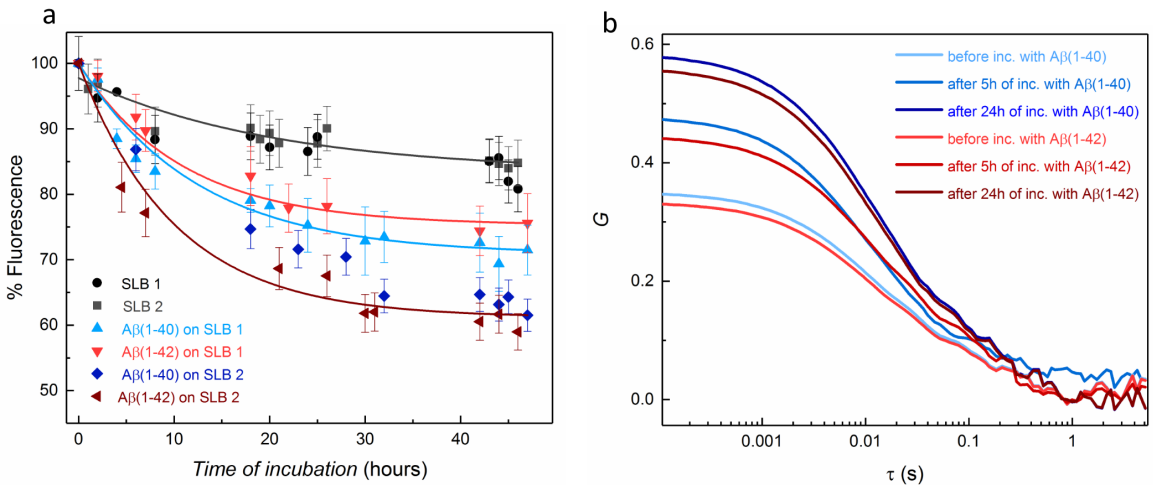


Figure 27: (a) Evolution of the SAF intensity of SLBs in function of time of incubation with 0.5 µM Aβ (1-40) and Aβ (1-42). (b) Correlation curves obtained from the SAF-FCS of fluorescent SLB (DOPC:DOPS) incubated with the same conditions.

### 3.2.2 *Influence of the interaction with Amyloid-β on the structure of supported lipid bilayers*

In the previous sections, the model of adsorption of Aβ on SLB have been hypothesized by characterizing its affinity of adsorption and the evolution of its structure over time, and after washing with PBS. Yet, no information was gained concerning the impact of these interactions on the substrate itself. Therefore, fluorescent SLB **1** (DOPC:DOPS) and SLB **2** (DOPC:DOPS:Chol) were incubated with non-labelled Aβ (1-40) and Aβ (1-42) at different concentrations. The concentrations of the peptide were 0.5 µM, 5 µM, 25 µM and 50 µM. Compared with quantifications made in the brain of rats, these concentrations are beyond the average concentration of "free diffusible" Aβ in the brain (≈ 6 nM)[242, 243]. However, they cover the range of concentrations used to mimic Alzheimer disease process in most studies. Besides, estimation of the free diffusible concentration of Aβ does not or poorly takes account of the local membrane concentration where peptides are gathered during the progression of the disease.

Three different effects could be observed, depending on the concentration of peptides: a decrease of the average SLB fluorescence intensity; the formation of fluorescent lipid aggregates; and eventually the disruption of the bilayer. Incubated with these samples of Aβ , images of the SLBs were recorded periodically in both SAF and UAF channels at

different concentrations and at incubation times up to 48 hours. Within these 48 hours of incubation, three different effects could be observed, depending on the concentration of peptides: a decrease of the average SLB fluorescence intensity; the formation of fluorescent lipid aggregates; and eventually the disruption of the bilayer.
Even at the lowest concentration of peptide (0.5 µM) the fluorescence exhibited a decrease of approximately 25 % for SLB **1** and 35 % for SLB **2** (Figure 27 a). A lipid control confirmed that this effect was not only due to photobleaching or natural damaging but indeed reflected an influence of the peptides. The discrepancies between the two SLBs can be explained by the results obtained in Section 3.1.2, where the preferential adsorption of Aβ on cholesterol-containing membrane is reported. It seems logical that an enhanced adsorption of peptides increased the impact of such adsorption on the substrate, hence the bigger decrease in fluorescence when Aβ was incubated on SLB **2**. When increasing the concentration of peptides, this decrease of the SAF signal of SLB was also enhanced, as expected if a larger amount of peptides (and likely aggregated oligomers) adsorbed on the bilayer. However, this decrease of fluorescence reached a limit around 50% loss. The curves obtained from the SAF-FCS measurement proved once more that this effect was actually due to a lower amount of fluorophores rather than photobleaching. This finding comes from the analysis of the $G_0$, which increased with when the incubation with Aβ was prolonged, implying a lower number of molecules in the detection volume (Figure 27 b). Therefore, it is assumed that the fluorescence decrease is caused by a loss of fluorescent lipids, namely that Aβ reduced the average amount of lipid molecules in the area of its adsorption. Furthermore, when comparing the loss of fluorescence caused by Aβ (1-40) and Aβ (1-42), the two peptides yielded similar results with no clear stronger impact for any of them. The reduction of the amount of lipids is then assumed to come from unspecific and similar interactions coming from both peptides.

Besides the conclusions coming from monitoring of the average fluorescence, information about the structure and morphology of the SLBs could be collected from the analysis of the SAF images. Modification of the SLB integrity could be observed by fluorescence imaging, whose extent depended on the concentration of Aβ and the lipids composition. At a concentration of 0.5 µM, the only observable effect was the decrease of fluorescence, hence related to the loss of lipid molecules described above. The scale of the darkening increased at 5 µM to reach 45-50% loss of fluorescence.
Another effect was visible on the SLB incubated with 5 µM Aβ : the formation of fluores-

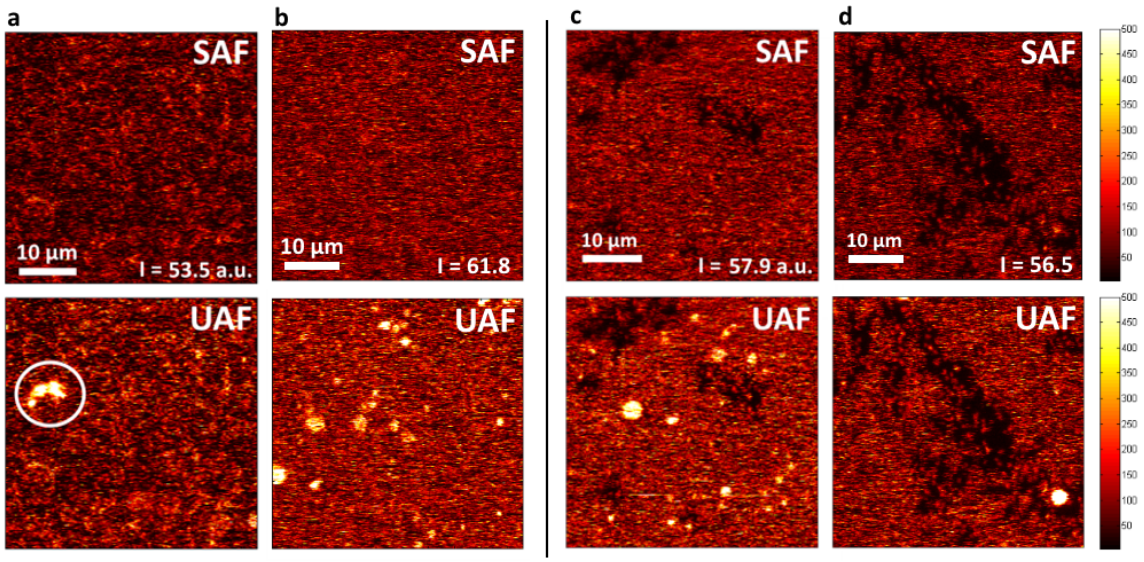


Figure 28: SAF and UAF imaging of SLBs recorded after 24 hours of incubation with Aβ (1-42) peptide. (a) SLB **1** with 5 µM Aβ . (b) SLB **2** with 5 µM Aβ . (c) SLB **1** with 50 µM Aβ . (d) SLB **2** with 50 µM Aβ .

cent clusters mainly observable in the UAF channel (Figure 28 a). The signal of these lipid clusters was more intense in the UAF than in the SAF channel. This interesting feature can be explained by a protrusion of the lipids growing beyond the interface and the maximum detection efficiency of SAF. Since the SLB formation implies a preliminary washing of most of the unbound lipid vesicles, lipids clusters should not have been caused by residual vesicles and were more likely formed from the interfacial lipids themselves which protruded above the bilayer. It is interesting to point out that the minimum Aβ concentration for the formation of these lipid clusters coincides with the concentration at which peptide aggregates were observed in PBS (cfr. Section 3.1.3). Therefore, it might be an indication that peptide aggregation and lipid clustering are two concerted events. The clustering of lipids also depended on the lipid composition: again, cholesterol-containing membrane (SLB **2**) accelerated the formation of the fluorescent lipid aggregates.

When Aβ concentration reached 50 µM, the formation of dark areas in the SLB could be observed after approximately 15-24 hours of incubation with the peptide (Figure 28 b). Such dark areas are likely attributed to a local desorption of the two lipid leaflets from the interface. These "holes" within the SLB had an initial diameter around 2-3 µm. The formation of smaller pores with a diameter size of 16 nm have been reported after 20 min for Aβ directly mixed with liposomes[244]. But such small pores were beyond the lateral resolution of our microscope (550 $\pm$ 50 nm). A longer monitoring showed the holes spreading

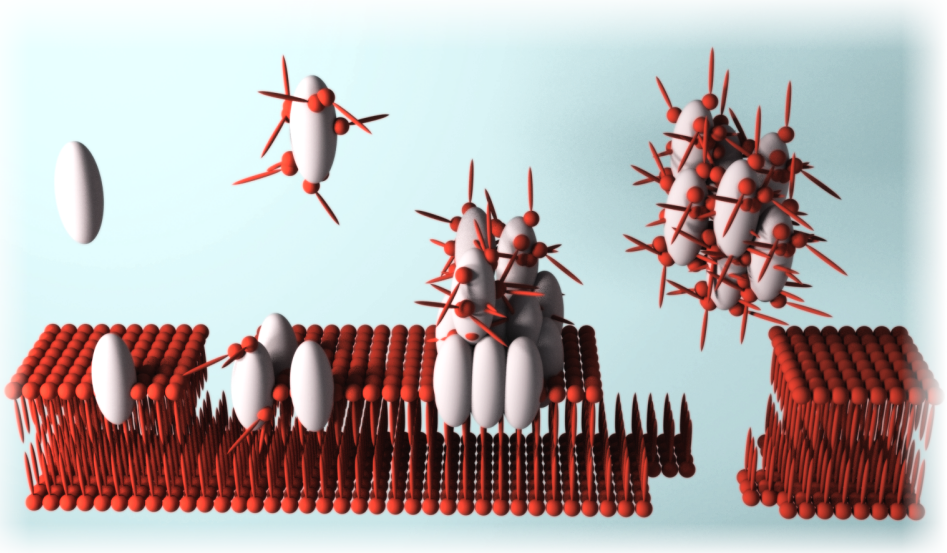

Figure 29: Scheme of the hypothesized mechanism of toxicity of Aβ upon interaction with a lipid bilayer. A progressive and concentration/aggregation-dependent lipid removal process leads to a thinning and potential disruption of the SLB.

among the SLB and consequently resulted in a bilayer disruption. A comparison between Aβ (1-40) and Aβ (1-42) was attempted but no reproducible trend could be observed. Both peptides yielded similar impacts on the SLBs, with the most critical effects exhibiting variations between the two peptides from one experiment to another (i.e. the time of incubation before the clustering of lipids or the disruption of the SLB).

From these results it appears that a part of the toxicity of the two amyloidogenic peptides could arise from a progressive and concentration-dependent lipid removal process (Figure 29). The interactions with the peptides can induce an extraction of some lipid molecules from the bilayer, resulting in a decrease of fluorescence and thinning of the membrane when the lipid-peptide complex desorbs from the surface. These extracted lipid molecules could have clustered as a side-effect of the aggregation between peptides encountered at higher concentration, assuming that each peptide maintained its interaction with the extracted lipids while aggregating. At some point, the aggregated lipid-peptide structures may become too massive and unstable to withstand the flow of solution inside the measuring cell, hence being washed away and forming holes within the bilayer. These holes can eventually yield the disruption of the SLB. This hypothesis is in agreement with other theories despite the discrepancies in SLB compositions, affinities or steady-state ex-

periments within these studies[211, 235].
Although a concentration of 50 µM Aβ is physiologically irrelevant[243], lower concentration of the peptide also yielded a loss of fluorescence, which is still attributed to an extraction of lipid molecules. This effect could be sufficient to destabilize the structure of the membrane bilayer by reducing its thickness. Such event can hinder biological functions localized around the membrane and eventually promote cellular death.

### 3.2.3 *Influence of the interaction with Amyloid-β on the diffusion coefficient of supported lipid bilayers*

Another important feature of lipid bilayers is the intrinsic mobility of lipid molecules and their lateral diffusion within the lipid leaflets[75, 245]. Fluorescently labelled SLBs were studied by SAF-FCS upon incubation with Aβ at different concentrations, using the signal collected by the SAF channel. Fluorescence correlation plots were then fitted with a 2-dimensional diffusion model. Fitting allowed calculation of the diffusion coefficient ($D_L$) which quantifies the lateral diffusion of lipid molecules inside the SLB (equations 4 and 5, Table 4). When monitoring random areas of the bilayer, SLB **1** incubated with Aβ(1-40) did not exhibit any significant change in the diffusion of its lipids, no matter how high was the concentration of Aβ(1-40).
On the other side, Aβ(1-42) eventually decreased the diffusion of the lipids at a concentration of 25 µM. This effect appeared after at least 3 hours of incubation. Such a delay before displaying any impact on the $D_L$ of lipids likely correlates this influence with the formation and adsorption of the aggregated peptide species. The formation of oligomers has been observed with 5 µM Aβ(1-42) within an hour of incubation with SLB (cfr. Section 3.1.3) but if they were still present during these FCS experiments, they seemed unable to influence the diffusion coefficient of the SLB. Previous SAF imaging of the peptides showed that after the time of incubation required to decrease the $D_L$ of lipids, massive fluorescent aggregates were already formed on the surface (see Figure 16 c). The difference of influence between Aβ(1-40) and Aβ(1-42) could come from their difference of affinity for the lipids and/or the size and amount of their aggregates (cfr. Section 3.1.7).
The affinity of each peptide for the SLB has already been characterized and seemed too similar to exert a real influence of the hindrance of the lipids (Section 3.1.3).
The fact that the only peptide to promote an impact on the diffusion of the lipids was Aβ(1-

| $D_L$ of SLBs ($\times 10^{-12} m^2 s^{-1}$) | before incubation | after 20 h of incubation |
|---|---|---|
| SLB **1** | | |
| 0.5 µM Aβ (1-40) | 2.88 ± 0.22 | 3.01 ± 0.10 |
| 5 µM Aβ (1-40) | 2.78 ± 0.27 | 3.06 ± 0.07 |
| 50 µM Aβ (1-40) | 2.91 ± 0.11 | 3.14 ± 0.05 |
| 0.5 µM Aβ (1-42) | 2.94 ± 0.42 | 2.91 ± 0.40 |
| 5 µM Aβ (1-42) | 2.96 ± 0.15 | 2.43 ± 0.06 |
| 25 µM Aβ (1-42) | 2.95 ± 0.38 | 1.90 ± 0.18 |
| SLB **2** | | |
| 0.5 µM Aβ (1-40) | 1.43 ± 0.42 | 1.53 ± 0.39 |
| 5 µM Aβ (1-40) | 1.23 ± 0.54 | 1.17 ± 0.13 |
| 50 µM Aβ (1-40) | 1.89 ± 0.32 | 1.51 ± 0.40 |
| 0.5 µM Aβ (1-42) | 1.36 ± 0.28 | 1.21 ± 0.46 |
| 5 µM Aβ (1-42) | 1.61 ± 0.12 | 1.43 ± 0.35 |
| 25 µM Aβ (1-42) | 1.31 ± 0.23 | 1.35 ± 0.17 |

Table 4: Values obtained for the diffusion coefficient of SLB **1** and **2** before and after 20h of incubation with both types of Aβ peptide.

42), and its higher propensity to aggregate, support the oligomeric hypothesis. In addition, the hindrance of the lipids diffusion required a time of incubation with the peptides long enough to assume that oligomers have been formed. This could be regarded as another proof of the oligomeric nature of toxic Aβ , if the condition for the hindrance of the lipids diffusion coincides with the adsorption of aggregated peptides.

SLB **2** was incubated with the same conditions, but no modification of $D_L$ was detected after one day of incubation, even with Aβ (1-42). The absence of influence on the diffusion of lipids is thought to come from the liquid-ordered phase within the SLB. Liquid-ordered phase naturally slows down the diffusion of lipids, as showed by the value of $D_L$ before

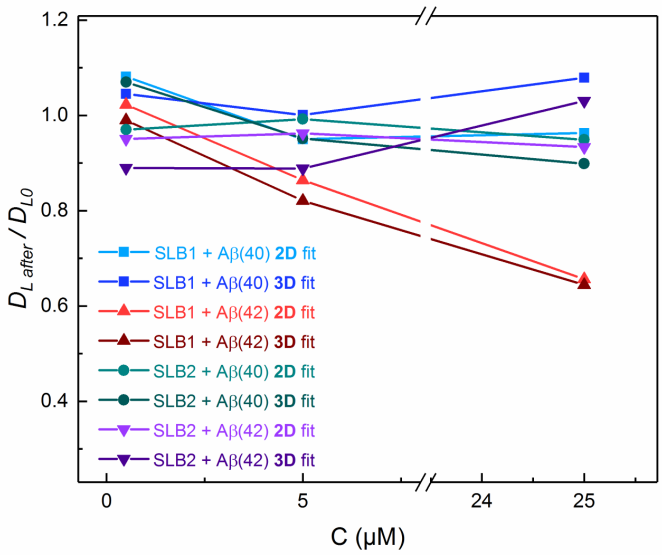


Figure 30: Plot of the change in diffusion coefficient of SLBs before and 20 hours after incubation with Aβ ($D_{L\,after}/D_{L\,0}$) in function of the concentration of peptide. $D_L$ has been calculated from SAF-FCS with both 2 and 3-dimensional fitting.

incubation and in Section 3.2.1. Therefore, Aβ aggregates probably diffused faster than the lipids in SLB **2** and lost the property to hinder the motion of the lipids to which they bound. This result indicates that the intrinsic mobility of the adsorbed peptide species could also be an important factor to determine their ability to slow down the lipids diffusion.

From the previous conclusion came the idea that lipids only lost their freedom of motion if they were bound and "anchored" on slower peptide aggregates which hindered their diffusion. In that case, affected lipids should be dragged by the motion of Aβ 's and follow their displacements. But the motion of peptides is not limited to 2-dimensional translation, as they might desorb and diffuse in the bulk solution. To uncover similarities between the diffusion of lipids and peptides, the results of SAF-FCS for the SLB were also fitted with the SAF-3D model. The values for $D_L$ obtained with the SAF-3D model were 10-folds lower than with the 2D model, probably because the diffusion of the lipids was to slow for a fitting assuming axial motion. But interestingly, the ratio of change in $D_L$ before and after incubation with peptides ($D_{L\,after}/D_{L\,0}$) was conserved (Figure 30). This result suggests that the same movements are responsible for the fluctuations of fluorescence of the SLB, before and after incubation.

Indeed, the diffusion of lipids before incubation is obviously limited to lateral diffusion at the top of the interface, while the direction of diffusion of lipids after incubation was yet unknown. If new directions of diffusion after incubation with Aβ had been observed

(i.e. if the lipids have diffused axially) the ratios $D_{L\,after}/D_{L\,0}$, both calculated by 2D or SAF-3D fitting, would have given different results. On the contrary, identical ratios meant that only the speed of diffusion was modified, but the direction of diffusion remained identical. Since the initial diffusion of lipids is only lateral, similar motion before and after incubation with Aβ implies that the targeted lipids are still diffusing by lateral translation only. This is in contradiction with the previous assumption that peptides dragged the lipid molecules interacting with them. However, the latter results were obtained by targeting homogeneous areas of the lipid bilayer (according to SAF imaging). When targeting the lipid clusters mainly visible in UAF (cfr. Section 3.2.2) and fitting the FCS curves with the SAF-3D model, their $D_L$ reached a value of $(1.99 \pm 0.17) \times 10^{-12} m^2 s^{-1}$ which was close to the coefficient of diffusion of Aβ (1-42) aggregates. Similar $D_L$ for the peptides and the lipids with SAF-3D fitting tends to confirm the hypothesis of lipids dragged by Aβ oligomers. It is concluded that Aβ was only able to influence the diffusion of lipid molecules within the SLB when the bigger oligomers were formed and massively adsorbed on the bilayer. The diffusion of lipids hindered by the peptides was still limited to lateral diffusion for the lipids forming the bilayer. On the other side, lipids already extracted from the bilayer and clustered above the surface were dragged and followed the motion of the peptide, which behaved like a lipid-carrier.

The last hypothesis still raised some contradiction with the previous experiments about the bilayer integrity. Since Aβ (1-40) successfully promoted lipid removal from the surface at the highest concentrations, it should also exhibit some of the oligomeric structures able to hinder the lipid diffusion(see Section 3.2.2). Hence, the FCS experiment was adapted: instead of averaging the diffusion of random spots of the SLB, lipids were specifically targeted around the disruption of the bilayer (Figure 31 a, b). After fitting with a 2D model, correlation curves showed that lipids next to a damage in the bilayer indeed had a slower diffusion coefficient, hence a reduced mobility (Figure 31 b). Not only that, but the reduction of mobility was inversely correlated with the distance from these damages (Figure 31 c). Beyond a distance of 14-15 µm from the disruption of the SLB, lipids incubated with Aβ (1-40) showed no reduction of $D_L$ anymore, like described in the beginning of this section. On the contrary, incubation with Aβ (1-42) generally induced a reduction of lipids $D_L$ even further from the holes in the SLB. It is concluded that the previous model is still valid : a hindrance of lipid motion is obtained when massive oligomeric species are adsorbed on

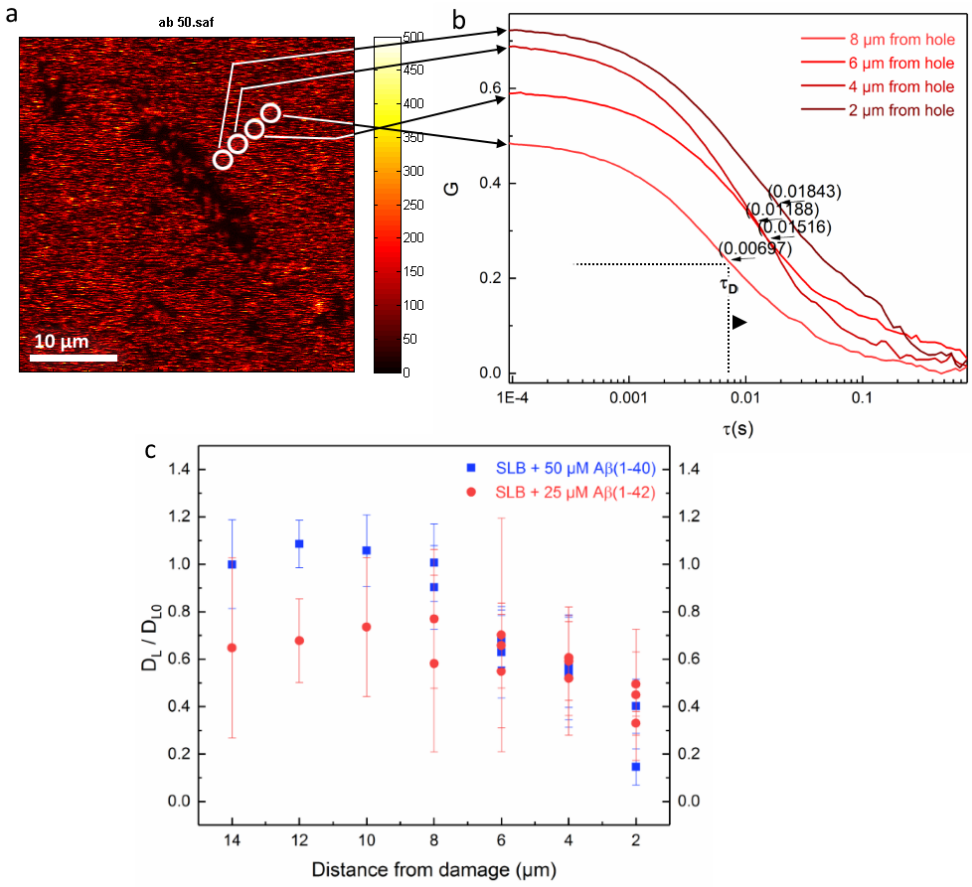


Figure 31: (a) SAF imaging of SLB **1** after 6h of incubation with 50 µM of Aβ (1-40) and localization of FCS monitoring spots. (b) Corresponding autocorrelation curves of SLB **1** with annotation of the diffusion time ($\tau_D$). (c) Comparison of the change in diffusion coefficient of SLBs before and 20 hours after incubation with Aβ ($D_{L\ after}/D_{L\ 0}$) in function of the distance from the disruption of the bilayer.

the SLB. This condition is easily fulfilled when the bilayer is incubated with Aβ (1-42), but is only met around the most critical damages of the SLB when incubated with Aβ (1-40).

### 3.2.4 *Reversibility of the impacts of Amyloid-β on supported lipid bilayers*

Different effects were elaborated in the previous sections, due to the interaction between SLB and peptides. Additionally, the reversibility of the adsorption of Aβ on SLB was investigated in Section 3.1.4. Therefore, the subsequent reversibility of its effects was also enquired. fluorescent SLB **1** was incubated with 25 µM Aβ (1-42) during 20 hours, then the flow of sample was exchanged with pure PBS in order to rinse the surface from adsorbed

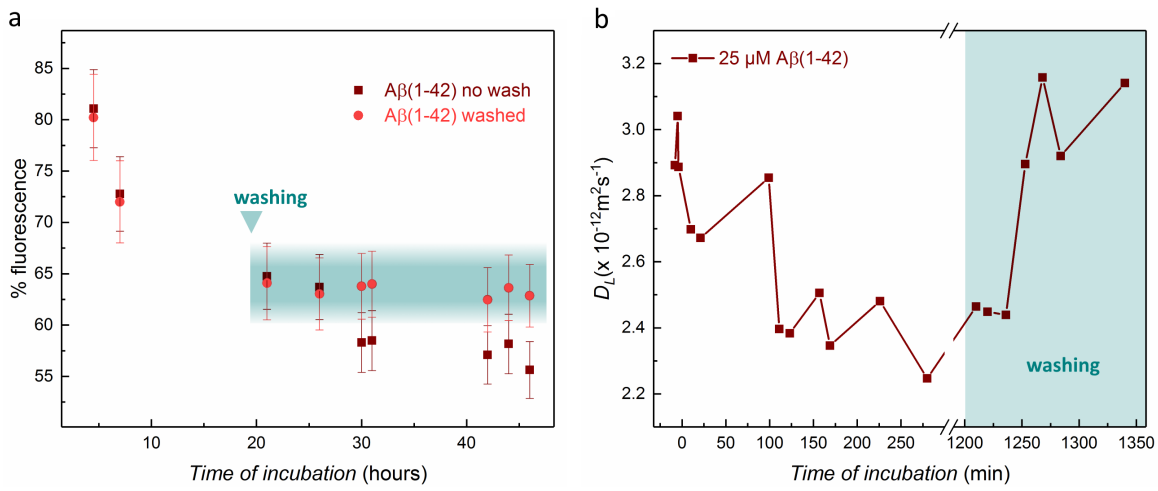


Figure 32: SLB was incubated during 20h with 25 μM Aβ(1-42), subsequently washed with PBS and not washed, respectively. (a) Evolution of the SAF intensity of SLB incubated with Aβ with and without rinsing step. (b) Evolution of the diffusion coefficient $D_L$ of SLB calculated from SAF-FCS with 2D fitting. $D_L$ dropped during incubation with the peptide, then returned normal value after washing Aβ.

peptides. Obviously, the rinsing of adsorbed peptides did not reverse the fluorescence loss encountered by the SLB. However, the decrease of fluorescence was stopped around the actual value reached before washing, while prolonged incubation maintains the loss of fluorescence until lower values (Figure 32 a). This result implies that the process responsible for lipid loss was quenched when Aβ was removed from the surface. From Section 3.1.4 it is known that few peptide species remain on the surface after rinsing but their impact on SLB is then too small to induce more desorption of lipid molecules from the surface. On the other side, the diffusion coefficient of lipids was also measured after washing Aβ (Figure 32 b). $D_L$ decreased of about 30 % after few hours of incubation with 25 μM Aβ (1-42), like in previous section. Interestingly, the rinsing procedure induced a reversion of the mobility hindrance, back to normal diffusion after ca. one hour. This result confirmed the assumptions made concerning the influence of Aβ on the diffusion of lipids. It is known from Figure 19 a,b and c that only the smallest peptide species remained adsorbed on the SLB after washing. In the present experiment, the desorption of bigger oligomeric species through washing is associated with a recovery of the normal diffusion of the lipid molecules. Also, the delay for recovery of original $D_L$ (approximately one hour) matches the delay to reach the minimum of SAF intensity during the rinsing of fluorescent peptides

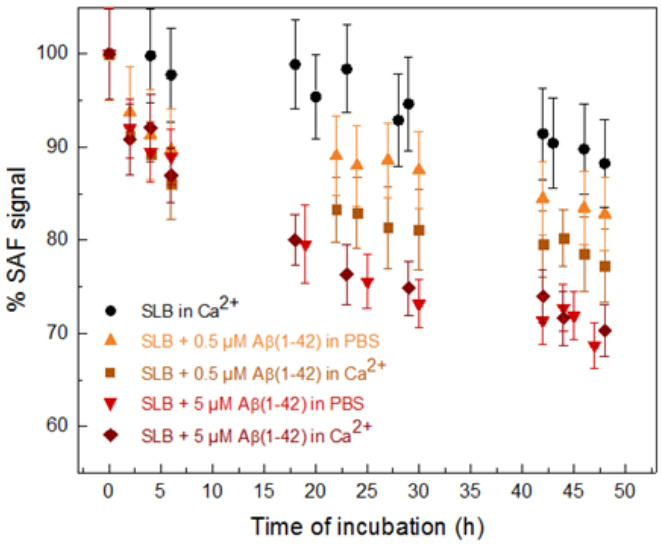


Figure 33: Comparison of the SAF signal of SLB **1** incubated during 48 hours with Aβ (1-42) dissolved either in pure PBS or buffer containing 2 mM $Ca^{2+}$.

(cfr Figure 19 d). This is considered as another proof of the oligomeric nature of the most harmful Aβ species.

### 3.2.5 *Influence of calcium ions on the effects of Amyloid-β on supported lipid bilayers*

The influence of calcium ions on the adsorption process of Aβ has already been investigated in Section 3.1.5. It was found out that $Ca^{2+}$ enhanced the adsorption and the oligomerization of Aβ on SLB at low concentration (below 5 µM) when compared to pure PBS solvent. Therefore, it was expected that calcium could also influence the effects of the interaction of the peptides on the SLB. fluorescent SLB **1** was incubated with Aβ (1-42) dissolved at different concentrations in PBS buffer containing 2 mM $Ca^{2+}$. The results were compared with the effects observed in previous sections when Aβ was dissolved in pure PBS. Calcium ions enhanced the decrease in fluorescence of SLB when interacting with the peptides at 0.5 µM (Figure 33). This outcome has several possible explanations. As $Ca^{2+}$ triggers the oligomerization of Aβ peptide at low concentration, it may promote more damaging within the SLB since oligomers are thought to be the most toxic species. Additionally, dynamic simulations showed that calcium ions stimulate a deeper insertion of Aβ inside the bilayer[232], which is correlated with a stronger disordering or thinning

| $D_L$ of SLB **1** ($\times 10^{-12} m^2 s^{-1}$) | before incubation | after 20 h of incubation |
|---|---|---|
| 5 µM Aβ (1-42) in PBS | 2.96 ± 0.15 | 2.43 ± 0.06 |
| 25 µM Aβ (1-42) in PBS | 2.95 ± 0.38 | 1.90 ± 0.18 |
| 5 µM Aβ (1-42) in $Ca^{2+}$ | 2.78 ± 0.20 | 2.39 ± 0.17 |
| 25 µM Aβ (1-42) in $Ca^{2+}$ | 2.81 ± 0.32 | 2.04 ± 0.22 |

Table 5: Comparison of $D_L$ values of SLB **1** incubated with Aβ (1-42) in PBS and with 2 mM $Ca^{2+}$.

effect[246, 247]. Stronger disordering or thinning of the SLB means that the interactions between lipid molecules are weaker, hence more easily extracted out of the bilayer by Aβ. Another straightforward explanation is based on the previous conclusion that lipid removal is a concentration-dependent process. Since calcium ions increase the amount of adsorbed peptide – aggregated or not - the amount of extracted lipid molecules would be enhanced as well. Nevertheless, a conclusion similar to the adsorption experiment (Section 3.1.5) was made when the concentration of peptide was increased to 5 µM. At this concentration, the adsorption and aggregation features of Aβ were identical when dissolved in PBS or $Ca^{2+}$ buffer. Similarly, the loss of fluorescence induced by 5 µM Aβ was identical for both buffer. This tends to favor the idea that calcium acted through an enhanced adsorption and oligomerization rather than a disordering effect.

Finally, the influence of the peptide over the mobility of the lipid was measured by FCS. The values of $D_L$ of the lipids after incubation with the peptide in $Ca^{2+}$ are close to those obtained when Aβ is dissolved in PBS (Table 5). It was concluded in the previous sections that the aggregation state of the peptides interacting with the SLB was the critical parameter to influence the diffusion of the lipids. Since there was no further reduction of the diffusion coefficient of SLB, the aggregation of high concentrated peptides interacting with the SLB seemed unaffected by the change of solvent. This conclusion excludes an enhanced oligomerization of Aβ at high concentration in $Ca^{2+}$ buffer, compared with PBS. Such outcome was predictable since the minimum concentration to observe an effect on the diffusion coefficient of lipids was beyond 5 µM. At this concentration, it was already observed that the aggregation process between Aβ peptides exhibited no change regarding the buffer used for dilution.

# 4

# RAMAN MEASUREMENTS

## 4.1 RAMAN SPECTROSCOPY OF SUPPORTED LIPID BILAYER

### 4.1.1 *Detection of supported lipid bilayer in standard conditions*

Raman spectroscopy is a label-free characterization technique whose sensitivity is lower than fluorescence but gives an insight in the structure of the sample. The effects of the interaction between Aβ and SLB were investigated in the previous chapter, but the results lacked details about the molecular structure of the molecules. Raman spectroscopy is an ideal complementary method. Despite the fact that collected photons are inelastically scattered instead of emitted, the principles behind the supercritical angle spectroscopy technique can also be applied to Raman signal. Therefore, it was attempted to characterize specifically the molecules involved in the interactions between Aβ and the SLB, namely the molecules situated near the interface, by collecting the photons scattered above the critical angle.

Such technique of characterization was referred to as supercritical angle Raman (SAR). Classical Raman spectroscopy - or undercritical angle Raman (UAR) - was simultaneously performed. First, the structure of the SLB **1** was investigated with SAR/UAR. A fluorescent imaging control was performed to assess the proper formation of the bilayer on the surface, while another fluorescence-free sample was used for Raman measurements. Although the formation of the bilayer could be confirmed by fluorescence, it was found out that the current system could not collect the Raman scattering from a unilamellar bilayer with SAR, nor with UAR (Figure 34). The thickness of the SLB was measured to be only 4.93 nm[160], fact that leads to a clear dominance of supernatant water molecules background in the UAR spectrum, despite their intrinsic low Raman scattering cross-section. The interfacial selectivity of the supercritical angle system prevented dominance of the water band at 3300 $cm^{-1}$ in SAR. However, the characteristic peaks of the lipid molecules were still not visible. As mentioned previously, the thickness of the SLB probably limited the amount of photons

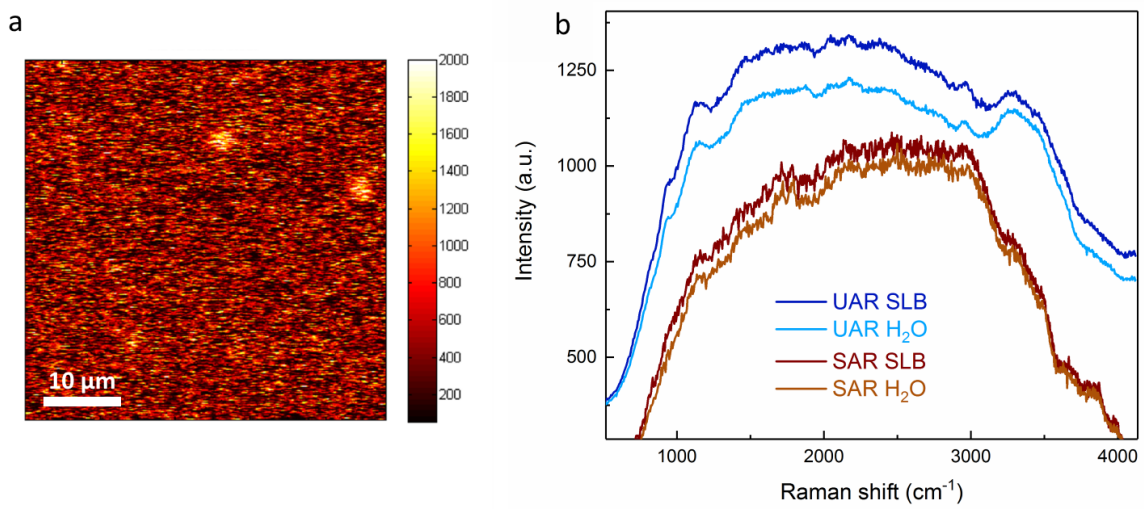


Figure 34: (a) SAF imaging of SLB **1**. (b) corresponding SAR spectra of SLB **1** compared with pure water.

scattered by the lipids, a drawback combined with the intrinsic low sensitivity of Raman spectroscopy. These features explained the difficulty to detect the SLB. This disadvantage was confirmed in other reports, therefore the study of such membrane model via Raman spectroscopy is usually achieved by the use of enhancement techniques[248–250].
From the last results, it was concluded that a unilamellar SLB would not influence the Raman spectrum of an experiment with both lipids and peptides. In other words, the Raman signal of Aβ will not be disturbed by the scattering of the SLB, and will only display the structure of Aβ.

### 4.1.2 *Detection of supported lipid bilayer vesicles or multilayer*

"Signal to noise" ratio of the SLB seemed to be the critical parameter to achieve its detection with Raman. To confirm that the reduced amount of lipid molecules in the SLB was the cause for its absence of Raman signal, measurements were performed while targeting specific areas of the sample exhibiting multilamellar bilayers or undisrupted vesicles. These lipid structures were expected to gather enough molecules to overcome the dominance of water background and to emit enough signal for its detection in UAR or SAR. Omission of the extrusion process described in Chapter 2 yielded this stacking of phospholipids since discrepancies in the size of the vesicles by preventing a proper disruption and fusion into a single bilayer. The use of a minute amount of fluorescent lipids permitted to specifically target these stacking areas by fluorescent mapping of the sample. The collected spectra

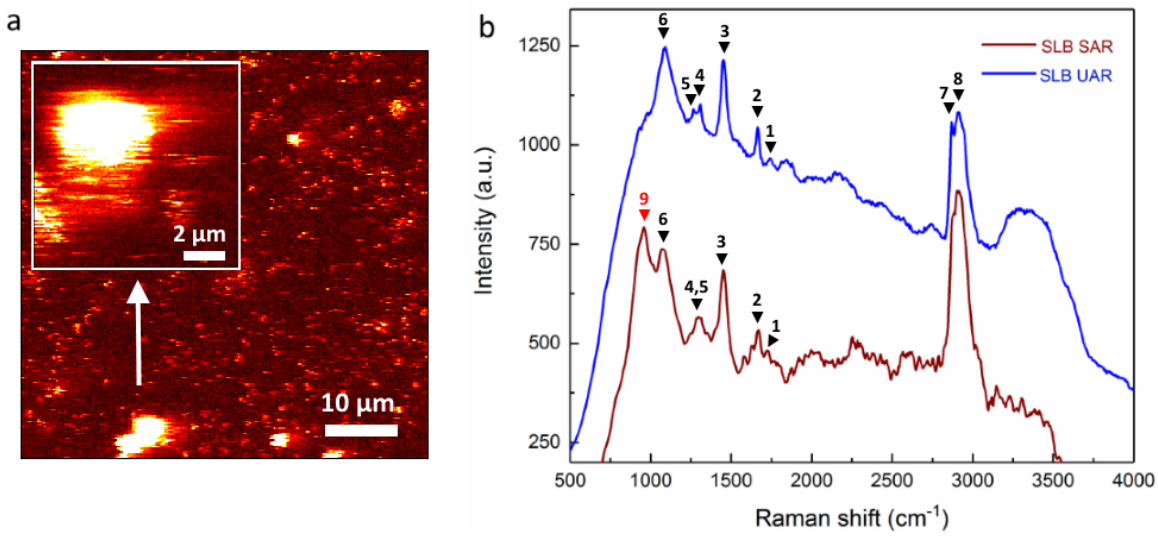


Figure 35: (a) SAF imaging of lipid multilayers/vesicles typical of SLB **1** without the extrusion step. (b) corresponding SAR/UAR spectra of multilamellar lipids structure/vesicles with minute amount of DOPE-Atto647. See Section 4.1.2 for the interpretation of the peaks

displayed a great fluorescence band component, yet the peaks protruding from the fluorescence baseline allow the characterization of the lipids and proved this method to overcome the low amount of signal of a single SLB which prevented its detection.

The main component of the SLB being DOPC, its Raman spectrum served as reference for the interpretation of the following results. The C=O ester stretching vibration was detected at 1742 $cm^{-1}$ (1) and the peak around 1665 $cm^{-1}$ (2) corresponded to C=C stretching vibration from unsaturated fatty acid chains. A sharp $CH_2$ scissoring mode at 1451 $cm^{-1}$ (3), a small $CH_2$ twisting mode at 1309 $cm^{-1}$ (4) and =C-H *in plane* deformation at 1265 $cm^{-1}$ (5) were also observed, although these last two peaks are broadened in the SAR spectrum. Another broad band situated at 1084 $cm^{-1}$ (6) was attributed to C-C stretching mode. The interpretation of the peaks at 2872 $cm^{-1}$ (7) and 2902 $cm^{-1}$ (8) in the CH region was more suspicious since their shape fitted exactly the $CH_2$ symmetric stretching and fermi resonance peaks, appearing normally at 2847 $cm^{-1}$ and 2882 $cm^{-1}$ in references[251]. One sharp peak at 958 $cm^{-1}$ (9) corresponded to O-P-O symmetric stretching and was specific of the SAR spectrum, hence the interfacial region[252]. The intensity of this peak might be caused by the packing of lipid polar head near the interface.

In conclusion, the Raman spectra of lipid molecules could be obtained without enhancement techniques by targeting multilamellar structures and increasing the amount of lipids inside the detection volume. However, these multilamellar structures are not observed

with the protocol of the experiments with Aβ. Therefore, other methods should be tested in order to observe both the lipids and the peptides simultaneously with Raman.

### 4.1.3 *Surface-enhanced-Raman spectroscopy of supported lipid bilayer*

Apart from the stacking of lipid molecules, many other techniques are available to increase the Raman signal of the sample. Among them, the use of plasmonic resonance produced by silver or gold nanoparticles on vibrational light scattering is widely used and known as surface-enhanced Raman spectroscopy (SERS). Various methods are used to bring those metal plasmon in the vicinity of the sample. In this experiment, the knowledge of our group to synthesize silicon nanofilaments (SNFs) functionalized for chemical catalysis was exploited. SLB **1** was formed on the surface of a SNFs layer synthesized from trichloromethylsilane (TCMS) and functionalized with gold nanoparticles (average diameter size of 7.5 nm) (Figure 36 a). The nanofilaments were synthesized and characterized by Zhang Xiaotian. Plasma treatment of the nanofilaments ensured that the substrate was still hydrophilic to allow the proper adsorption of lipid vesicles.
The formation of the SLB on both unfunctionalized and gold-embedded SNFs was assessed by fluorescence control before Raman experiments. SAF imaging of the surface was possible although the focus could not be as precise as in other measurement, due to the absence of water molecule directly above the glass coverslip. The successful formation of the SLB was confirmed, but the bilayer exhibited some defects as the surface was less homogeneous than for SLBs directly adsorbed on a glass slide (Figure36 b). The mobility of the SLB was also affected by the substrate, as showed by SAF-FCS measurements (Figure 36 c). Fitting of the correlation curve with a 2-dimensional model yielded a $D_L$ of $(1.54 \pm 0.67) \times 10^{-12} m^2/s$ which is slower than the diffusion of normal SLB **1**. However, those defects were considered not problematic for the Raman experiments, since this technique will be used to extract information about the chemical structure and bonding, not about the general morphology of the bilayer. Following fluorescence controls, Raman measurements were conducted with a non-fluorescent SLB.

Two additional control experiments were performed before performing the SERS measurements, to check the influence of the SNFs on the spectrum. Raman scattering of lipid vesicles/multilayers were recorded for lipid adsorbed on the surface of unfunctionalized SNFs (without gold nanoparticles, hence without surface-enhancement), and for SLB de-

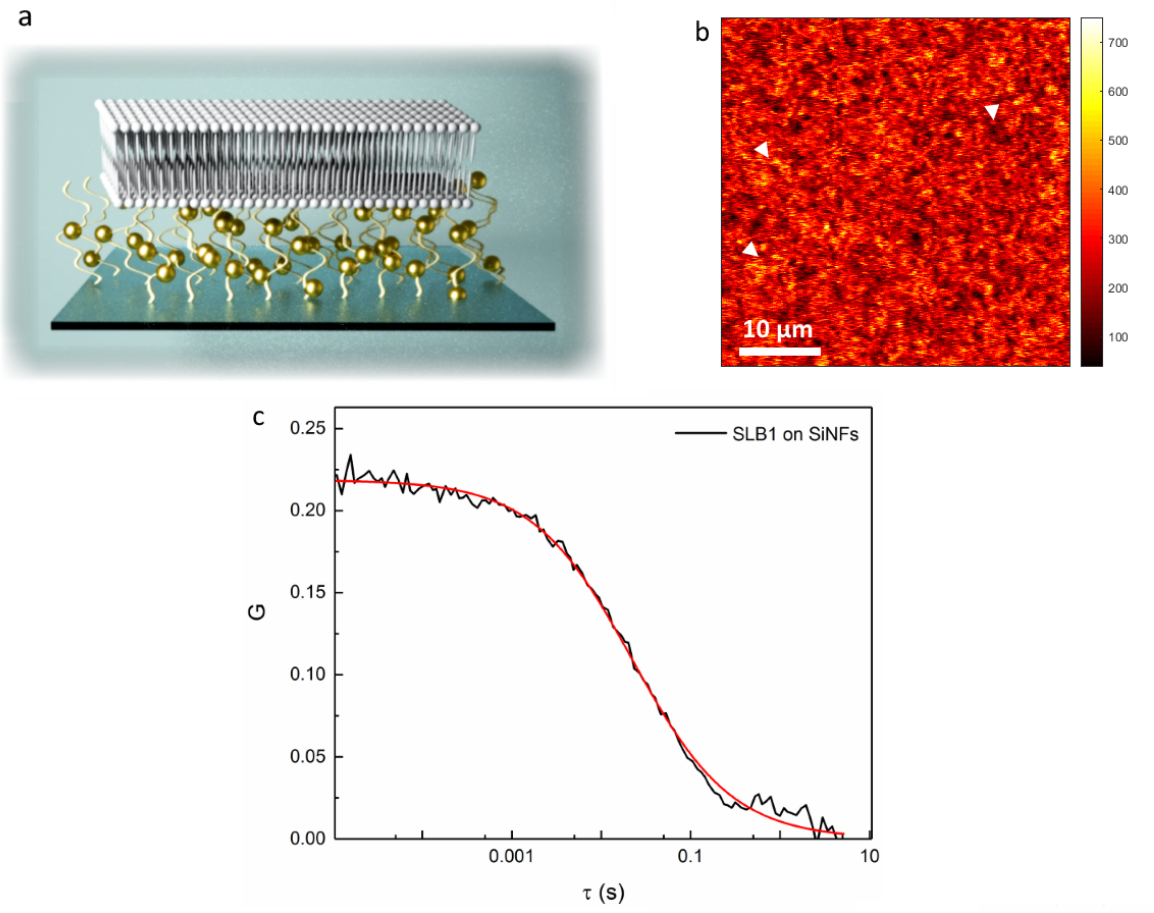


Figure 36: (a) Scheme of the SERS technique: gold nanoparticles embedded in silicon nanofilaments serve as a support for the formation of the SLB. (b) SAF imaging of the SLB **1** formed on nanofilaments substrate. Examples of defects are depicted by the white arrowheads. (c) correspondent SAF-FCS curve of SLB.

posited on coverslip simply covered by a 20 nm layer of gold (i.e. similar to the standard method for SERS). The latter was used to provide the surface-enhancement effect without the physical influence of the SNFs bed.

The UAR spectra of lipids formed on SNFs without gold nanoparticles and on bare glass were identical (Figure 37 a), adding another proof that the deposition of the lipids on the SiNFs carpet did not cause severe alteration of the lipid structure. Peaks of the lipids were observed at 1659 $cm^{-1}$, 1448 $cm^{-1}$, 1303 $cm^{-1}$, 1270 $cm^{-1}$ and 1082 $cm^{-1}$; corresponding to C=C stretching vibration, $CH_2$ scissoring mode, $CH_2$ twisting mode, =C-H *in plane* deformation and C-C stretching mode respectively.

On the other side, the presence of the gold layer or gold nanoparticles profoundly affected the Raman scattering of the lipids (Figure 37 a). A $CH_2$ scissoring mode peak at 1430

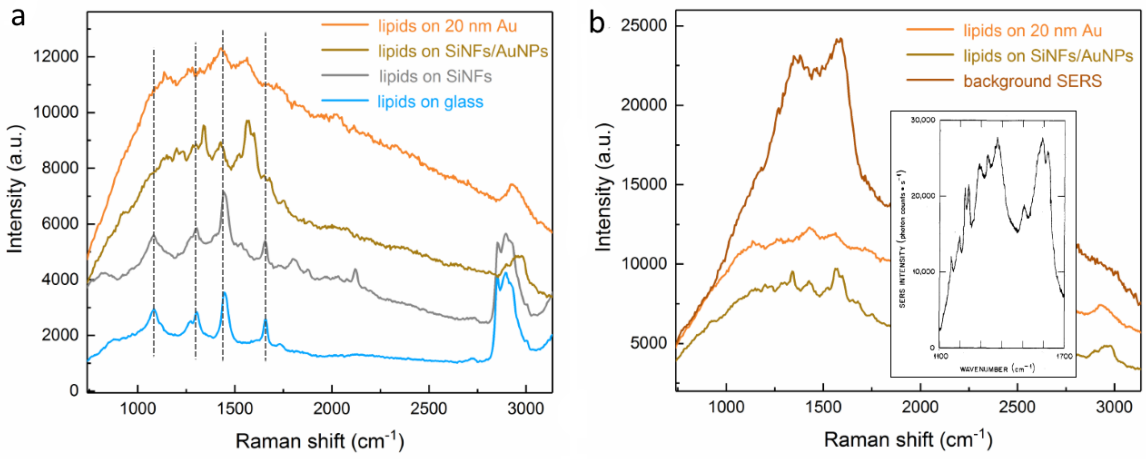


Figure 37: (a) Comparison of the UAR spectra of lipids deposited on a hydrophilic glass slide, on SNFs, on SNFS functionalized with gold nanoparticles and on glass covered with a 20 nm thick layer of gold. (b) Comparison of the different UAR spectra obtained with SERS effect. The inserted spectrum is the SERS of 1-nitropyrene on a layer of silver (from [253]).

$cm^{-1}$ was the only lipid vibration remaining in the 500-2000 $cm^{-1}$ range when the SLB was formed on the layer of gold. Another peak observed at 1563 $cm^{-1}$ was unexpected and will be discussed below.

By comparison, the UAR spectra of SLB formed on gold-functionalized SNFs exhibited sharp peaks characteristic of lipids (Figure 37 a). Those peaks coming specifically from the vibration of the lipids will be extensively detailed with the analyze of Figure 38. However, an intense peak at 1566 $cm^{-1}$ was observed and recalled the previous peaks obtained with a simple layer of gold. Another peak at 1339 $cm^{-1}$ was also visible. The interpretation of these two peaks was troublesome, since they correspond to the vibration of aromatic/hetero-ring and nitro-compound containing nitrogen atoms. In Figure 37 b, the inserted spectrum obtained from SERS of 1-nitropyrene on a 80 nm layer of silver also showed a high similarity, which seemed to confirm the origin of those vibrations. However, those chemical vibration unlikely originated from the lipid sample and did not correspond to the Raman spectrum of the objective oil either (whose peaks could have affected the spectra due to an improper focus). The maximum intensity of these peaks was correlated with an exact focus on the surface of the coverslip covered with gold, and any displacement of the focus of few nanometers was enough to discard these vibrations. More importantly, these peaks could be observed even in the absence of any sample or background buffer (Figure 37 b). It seemed that these two peaks specific from gold substrate or nanoparticles

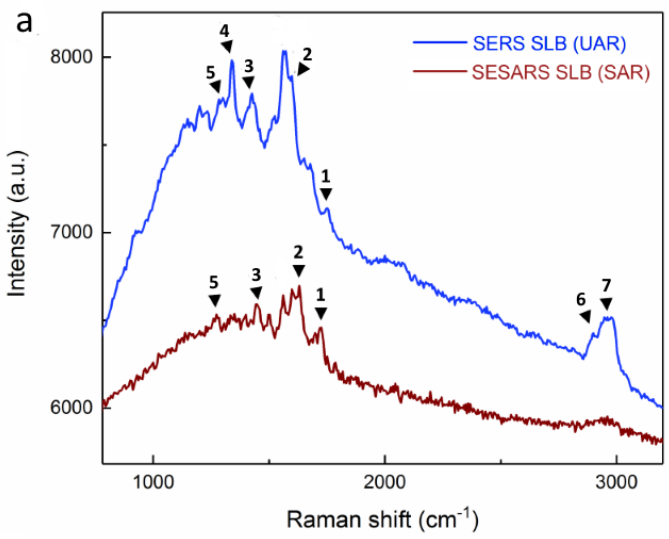


Figure 38: Surface-enhanced SAR and UAR spectra of SLB **1** formed on the layer of SiNFs functionalized with gold nanoparticles to perform surface-enhanced Raman spectroscopy.

were due to the photoluminescence effect of the metal[254]. The origin of the photoluminescence is the same than the enhancement effect of SERS and consists in an amplification of the electric field around the metal (approximately until 10 nm away from the surface plasmon). Therefore, the background signal of the layer of gold likely has hidden the scattering of the SLB deposited on it. On the other side, gold nanoparticles disseminated within the SNFs layer did not overload the Raman spectra with the metal photoluminescence, while still allowing the SERS effect to amplify the signal of the SLB.

Apart from the gold photoluminescence, the SNFs functionalized with gold nanoparticles used for SERS (UAR) and the supercritical angle equivalent (SESAR) allowed the detection of photons scattered by a single supported bilayer (Figure 38). The peak at 1750 (UAR) / 1725 (SAR) $cm^{-1}$ (1) is identified as C=O ester stretching vibration. SAR spectrum displayed a peak at 1630 $cm^{-1}$ (2) attributed to C=C stretching vibration from fatty acid chains. The correspondent peak in UAR is broadened by the photoluminescence effect and shifted at 1615 $cm^{-1}$. Both the C=O and C=C stretching peaks exhibited a red-shift toward smaller wavenumbers with both detection angles when compared with reference experiments. This is associated with a lower frequency of vibration. Since the deposition of lipids on SNFs did not yield any change in the Raman spectra, their reduced frequency of vibration is possibly the consequence of the gold nanoparticles which can hinder the vibrations of the chemical bonds if they desorbed from the SNFs. Such desorption of the

nanoparticles was indeed observed when using the functionalized SNFs for chemical catalysis. The interaction of gold nanoparticles with lipid bilayer has been reported to increase the ordering of the lipid phase[255], which in turn is expected to yield a decrease of the frequency of vibration[256].

The peak at 1448 $cm^{-1}$ (3) was easily attributed to $CH_2$ scissoring mode, while the peaks at 1339 $cm^{-1}$ (4) and 1274 $cm^{-1}$ (5) in UAR might correspond to blue-shifted $CH_2$ twisting mode and =C-H *in plane* deformation respectively. The last peaks at 2895 $cm^{-1}$ (6) and 2947 $cm^{-1}$ (7) were typically in the CH region and attributed to $CH_2$ and $CH_3$ asymmetric stretching.

This experiment showed that the detection of an unilamellar supported lipid bilayer on SNFs was made possible by the SERS technique, and can be applied to the supercritical angle collection of scattered photons. However, some shifts were observed for the peaks of the lipids, mainly attributed to an influence of the gold-functionalized environment. Eventually, the SERS/SESARS technique might be used to simultaneously gather information about the structure of the SLB and Aβ peptides when they interact together.

## 4.2 RAMAN SPECTROSCOPY OF PEPTIDES

### 4.2.1 *Detection and characterization of Bovine Serum Albumin*

Raman spectroscopy can be used to characterize polypeptide chains by analyzing specific regions of the spectrum which reflects the secondary structures present within the protein. As it was the first time that the supercritical angle technique was used to detect Raman signal of proteins, the first experiments consisted to ensure the efficient detection and characterization bovine serum albumin protein (BSA). Indeed, the detection of the Raman signal of proteins can be challenging due to the low probability of a photon to be inelastically scattered and because of the small Raman cross-section of polypeptides[257]. BSA was a good starting target because of its size and inexpensive acquisition. Furthermore, its native structure is well known and consists mainly of α-helix. Therefore, different concentrations of BSA were dissolved in distilled water and Raman spectra were acquired for both UAR and SAR detection.

Figure 39 (a) displays the SAR spectra acquired for concentration ranging from 10 to 60% (w/v). At the lowest concentration, almost no signal could be distinguished with certitude

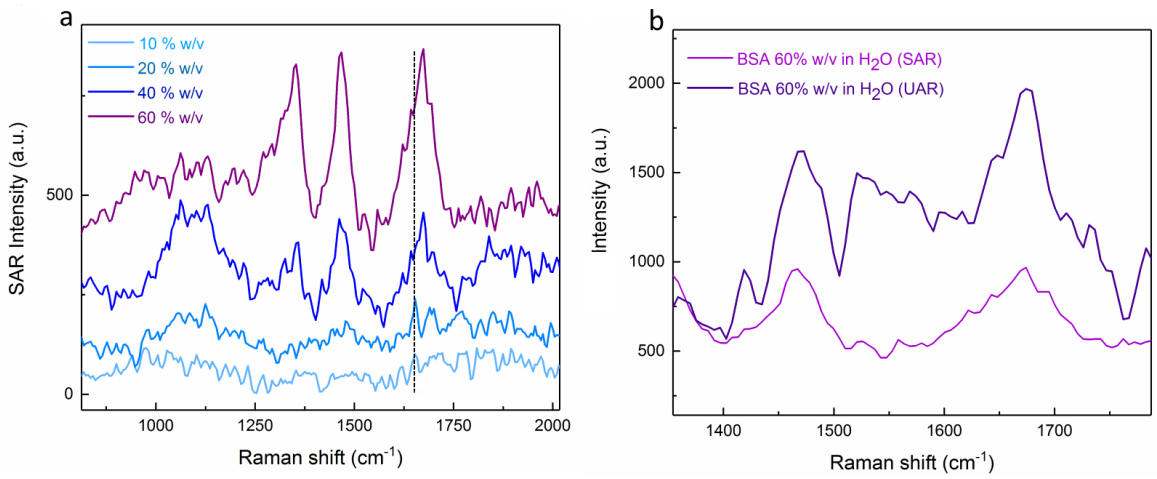


Figure 39: (a) SAR spectra of BSA protein at different concentrations (w/v) in distilled water. (b) SAR and UAR spectra of BSA protein at 60% (w/v) in distilled water.

from the background. This was not surprising considering both the low sensitivity of Raman spectroscopy for peptides and the small volume of detection with the SAR technique, limiting the amount of sample (cfr. Section 4.1.1). Starting from 20% (w/v) the peaks from the $CH_2$ scissoring mode (1467 $cm^{-1}$) and the amide I region (1640-1690 $cm^{-1}$) protruded slightly from the background. A small but sharp peak was observed at 1651 $cm^{-1}$ and characteristic of the expected $\alpha$-helix. However, at 40% (w/v) this $\alpha$-helix peak became broadened in a larger, dominant peak at 1674 $cm^{-1}$. This peak was also dominant at 60% (m/v) BSA. In the literature, such Raman shift in attributed to $\beta$-sheet secondary structure. $\beta$-sheet is not typical of BSA protein, but is often related to toxic aggregation processes of polypeptides. The conversion of BSA $\alpha$-helix structure into $\beta$-sheet after some aggregation process was surprising but not inconceivable since it was met at the highest concentrations. At 60% (m/v) - which was equivalent to 10 mM of BSA - the sample even turned into a "gel-like" solution due to the high density of proteins. In these conditions, the proteins were likely to interact and aggregate. This is a disadvantage of the low sensitivity of SAR, since it requires concentrations so high that the aggregation process dominates native structures. Additionally, such "gel-like" solution might be inconvenient to handle.

Besides the peak from amide I, the peak of $CH_2$, the peak of tryptophan residues (1342 $cm^{-1}$) and amide III (1271 $cm^{-1}$) were also visible at higher concentrations. The same results were obtained when analyzing the UAR spectra (Figure 39 b) although the signal was more intense and had a better resolution. This effect is thought to be caused by the bigger volume of collection of the UAR technique, which exhibits no exponential decay in the

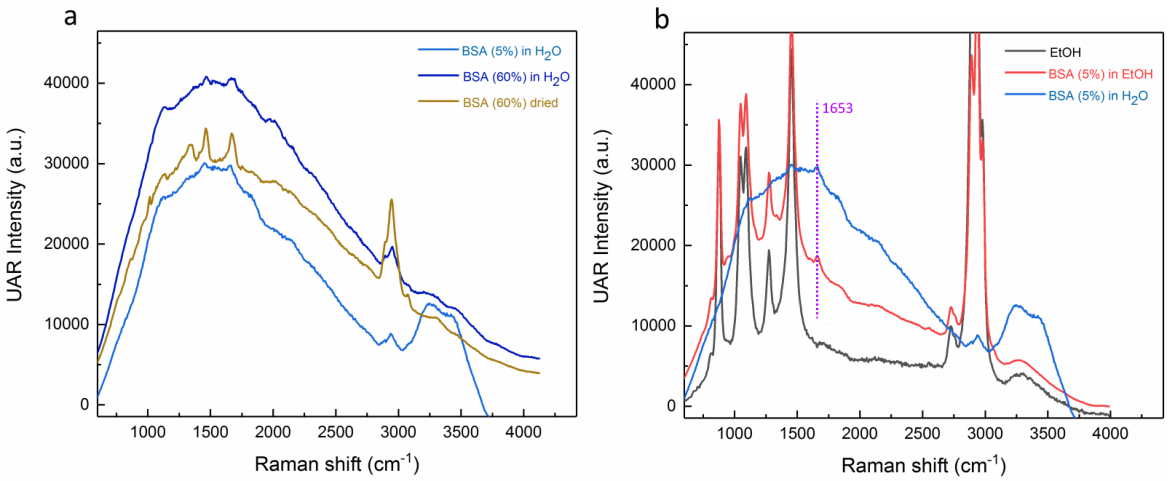


Figure 40: (a) UAR spectra of BSA protein at different concentrations (w/v) in distilled water and after 24h of solvent evaporation. (b) Comparison of UAR spectra of BSA protein at 5% (w/v) in distilled water and ethanol.

efficiency of collection and more scattered signal. The presence of bands around 1531 and 1568 $cm^{-1}$ is characteristic of indole rings - from which tryptophan is a derivative - and was the only significant difference between the peaks of UAR and SAR. The UAR spectrum itself, however, was found to exhibit a specific broadband envelope underlying the peaks in the whole range of Raman shift (Figure 40 a). This broadband was first thought to be caused by fluorescence of the sample (like showed in Section 4.1.2) but prolonged exposition in order to photobleach the sample did not alter its intensity. Furthermore, a decrease of the volume of water in the sample also promote the disappearance of this broadband. On the other hand, an increasing concentration of protein resulted in an increase of both the intensity of this broadband and the peaks of protein. Finally, a change of solvent for ethanol decreased the intensity of the broadband for an equivalent concentration of BSA (Figure 40 b). All these features excluded the fluorescence explanation as the source of this broadband. It was previously observed and referred to as "pseudo-Raman" band because of the incompatibility with fluorescence process [258]. This pseudo Raman band was supposedly caused by the interactions between the polypeptide chains. Water exhibited the greatest broadband because the solvent composed of the smallest molecules maximized the interaction between the proteins. The size of ethanol molecules allowed fewer interactions between the polypeptide chains, hence yielded a smaller broadband when used as a solvent.

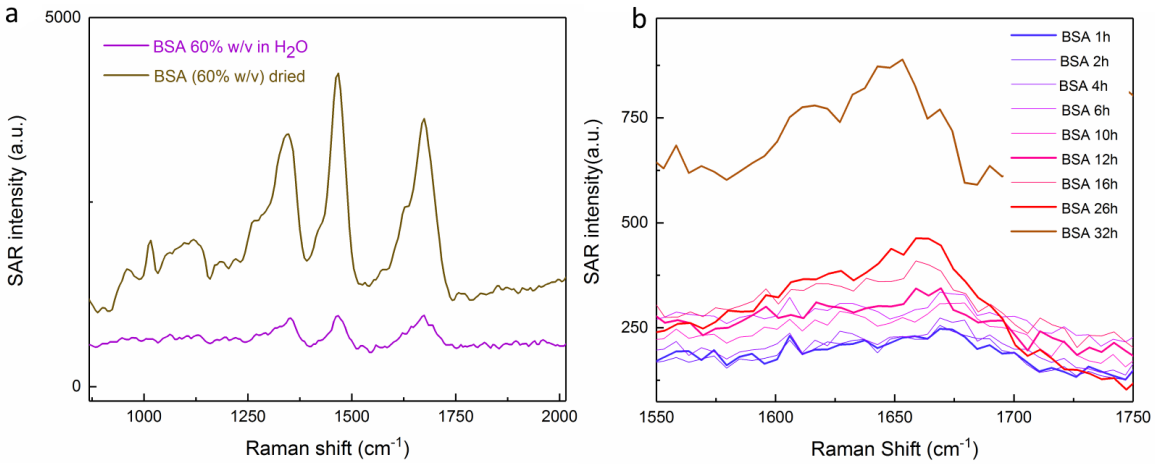


Figure 41: (a) Comparison between the SAR spectra of the 60% (w/v) BSA sample before and after solvent evaporation. (b) Evolution of the Amide I region of the SAR spectra from 20% (w/v) BSA with progressive solvent evaporation.

However, dissolution in water was the prerequisite to mimic the natural interaction between peptides and SLB, despite the concentration being the limiting factor of SAR. A solution to partially overcome the need for high concentrations without relying on surface-enhancement techniques was inspired by Angelis et al[259]. They used superhydrophobic surfaces to let a droplet of highly diluted sample evaporate, hence concentrating the solute inside an almost perfect sphere maintained by water repulsion. Although the SLB was not a superhydrophobic substrate, progressive evaporation of the solvent would concentrate the targeted proteins on the top of the surface, accessible to both SAR and UAR detection. Constant recording of the Raman signal allowed to detect the characteristic peaks of the proteins before complete evaporation of the solvent. In this way, the secondary structure of the protein could be elucidated as soon as the collection of photon is sufficient. Therefore, the technique was attempted with a BSA sample. First, a comparison between diluted and dried BSA at 60% (m/v) was made. The dryness of the sample and the consequent concentration reached at the surface drastically enhanced the detection and resolution of the Raman peaks (Figure 41 a). In a second attempt, a solution of 20% (w/v) BSA was monitored during several hours with SAR spectroscopy. The progressive evaporation of the solvent rendered possible the detection of amide I peaks (Figure 41 b). The most interesting observation was that the amide I peak of native $\alpha$-helix could be detected at 1653-1660 $cm^{-1}$ before the concentration is high enough to induce aggregation into another structure. From these results, it was expected that even A$\beta$ might be detected and

characterized with SAR despite the smaller size of this peptide, if the solvent is let to evaporate. However, it must be noted that the concentration estimated for SAR detection - roughly between 20 and 40% (w/v) - would represent a larger molar concentration for Aβ than for BSA (typically between 50 and 100 mM Aβ).

### 4.2.2 *Differentiation of two proteins according to axial distance*

The strength of supercritical angle spectroscopy is its selectivity for surface-bound emitters. While the detection and characterization of BSA has been achieved with both SAR and UAR in the previous section, the results showed an unique structure for both angles of detection, hence did not exploit the axial distinction of the two techniques when they are combined. In the following experiment, the success of this feature was tested through the detection of two proteins of known and distinguishable structures, whose axial separation and confinement was predictable.

This was accomplished by functionalization of a glass coverslip with biotin molecules. Biotin was covalently linked through amide bonds after an amino-silylation of the glass surface. The coverslip was then incubated with a first solution of streptavidin, which is known to form one of the strongest non-covalent interactions with biotin and topped with a solution of BSA. Therefore, a sample expected to yield surface-bound streptavidin and bulk supernatant BSA would be differentiated by SAR/UAR combination (Figure 42 a).

First, the success of the substrate biotinylation was checked with attenuated total reflectance infrared (ATR-FTIR) spectroscopy (Figure 42 b). The starting step was the amino-silylation of the glass surface with 3-aminopropyl triethoxysilane (APTES) dissolved in toluene. All the IR spectra displayed an intense and broad peak in the 1000 $cm^{-1}$ region attributed to Si-O-Si network bonds. The peak also probably includes the Si-OH vibration around 950 $cm^{-1}$[260]. One of the asymmetric stretching modes of the Si-O-Si protruded slightly more at 1155 $cm^{-1}$ (1) after treatment with the APTES. Some other peaks were more specific of the new chemical moieties. The new stretching modes of $CH_2$ at 2932 $cm^{-1}$ and 2886 $cm^{-1}$ were initially absent from the glass slide. The absorption band between 3000 and 3300 $cm^{-1}$ exhibited a particular shape which was associated with the presence of symmetric and asymmetric stretching modes of $NH_2$ (2), normally present at 3290 and 3300 $cm^{-1}$[261]. Peaks at 1490 $cm^{-1}$ (3) and 1567 $cm^{-1}$ (4) were attributed to $NH_2$ deformation modes of the amine groups which, according to literature, are linked

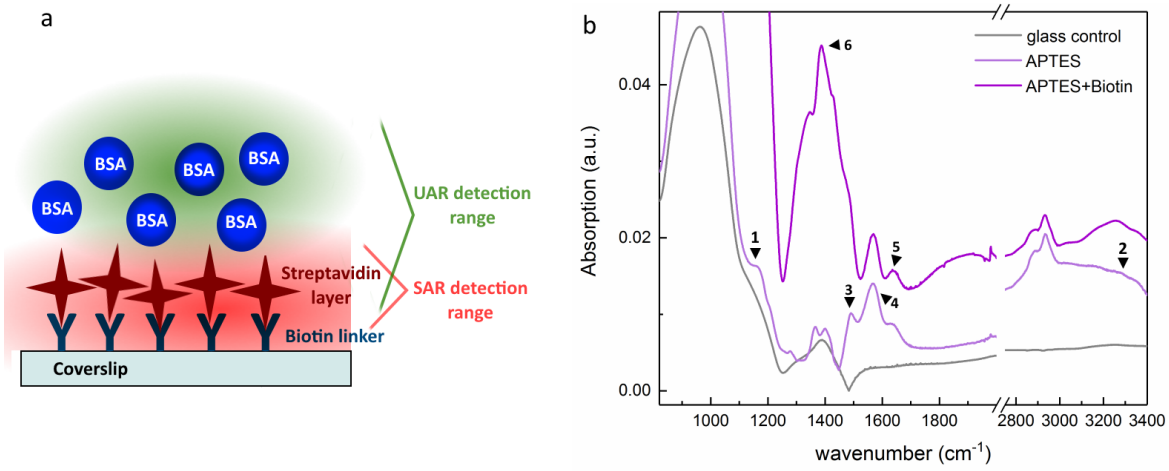


Figure 42: (a) Scheme of the experiment. A coverslip functionalized with biotin is used to ensure the vicinity of streptavidin proteins near the surface, while BSA are floating in the bulk solution. The former is expected to be detected by SAR while the latter would only be detected in UAR. (b) ATR-FTIR spectra of the coverslip after each step of the functionalization with biotin.

through hydrogen-bonds with Si-OH group to form cyclic-like structures. Comparison between the spectra of bare glass and glass after treatment with APTES confirms the successful linkage of the amine group on the coverslip. The attachment of biotin molecule was assessed with ATR-FTIR as well. The peak at 1567 $cm^{-1}$ is still present but an amide function at 1645 $cm^{-1}$ (5) is slightly more protruding, indicating a partial attachment of biotin to the glass via amide bonds. The intense peak at 1392 $cm^{-1}$ (6) can be due to the O-H bending of carboxylic acids, confirming that noncovalently bound biotin molecules are still adsorbed on the sample. A final test of affinity was made by immersing the biotinylated glass slide in a solution of fluorescent streptavidin for 1h, then by washing in a PBS buffer and regular monitoring of the remaining fluorescence. By comparison with a control coverslip without biotin, it was obvious that the functionalization of the glass-slide permitted to retain more streptavidin than the control. Especially during the first two hours when the gap is the most important, although the fluorescence intensity is still twice higher after 20h of immersion in PBS. Therefore, a glass slide was subjected to the same protocol and incubated with a solution of label-free streptavidin, on which was dropped another solution of BSA. The final solution was composed of 40% (w/v) in streptavidin and 20% (w/v) BSA, and was characterized with Raman spectroscopy (Figure 43).

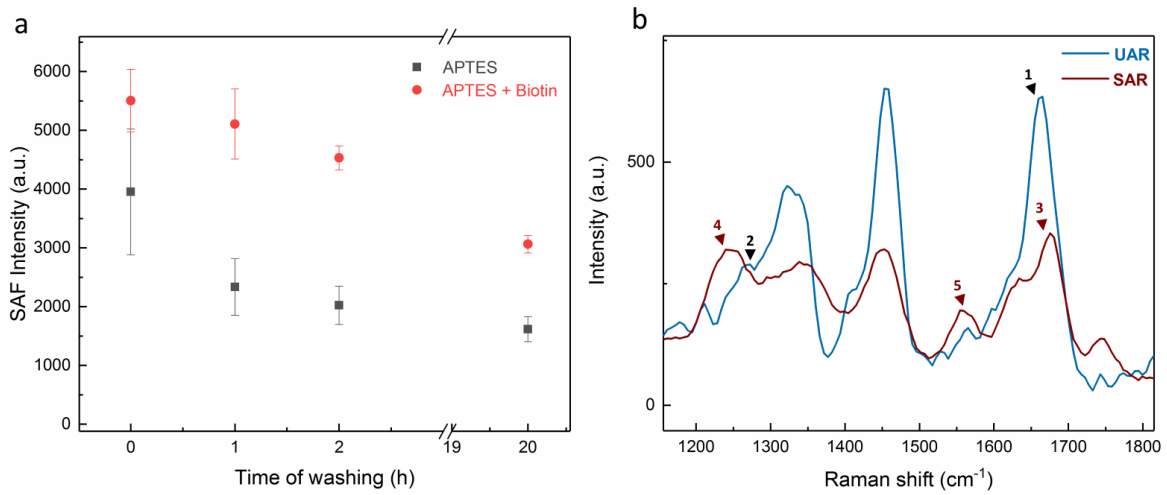


Figure 43: (a) Comparison of the remaining fluorescence between a control glass slide and a biotinylated coverslip after incubation with fluorescent streptavidin (10 µg/mL) and continuous washing in PBS buffer. (b) SAR and UAR spectra of the biotinylated coverslip incubated with an first solution of streptavidin, then a solution of BSA (40% (w/v) and 20% (w/v) respectively).

The UAR spectrum displayed three determinant peaks in the 1000-2000 $cm^{-1}$ shift region. The amide I peak at 1659 $cm^{-1}$ (1) and amide III peak at 1267 $cm^{-1}$ (2) are attributed to an $\alpha$-helix secondary structure. Peaks from the $CH_2$ scissoring and aliphatic side-chain stretching vibrations are visible at 1458 $cm^{-1}$ and 1322 $cm^{-1}$ respectively. When compared with literature, the shift and even the shape of these peaks seemed to faithfully match the spectra of bovine serum albumin[262]. The SAR spectrum on the other hand brought a different characterization. The amide I peak was shifted at 1675 $cm^{-1}$ (3), corresponding to $\beta$-sheet structure which is typical of streptavidin protein. The discrepancy was even more obvious for the amide III peak protruding at 1243 $cm^{-1}$ (4), also attributed to $\beta$-sheet. The tryptophan peak at 1554 $cm^{-1}$ (5) is also slightly more resolved than in the UAR spectrum, as suggested by reference paper[263]. Although some influence from BSA could be observed in the shape and width of the amide I and III peaks, the SAR/UAR comparison could be used to successfully characterize two proteins in function of the axial distance between their specific structure and the interface of the coverslip.

### 4.2.3 *Characterization of Amyloid-β*

#### 4.2.3.1 *Amyloid-β (1-42)*

In order to study the interaction between a lipid bilayer and Aβ, Raman spectroscopy was used to elucidate the secondary structures exhibited by the peptide when adsorbed on the surface of the lipids. Because of the relatively small size of the peptides (40 and 42 amino acids), the secondary structure was considered to represent the general conformation of the molecule despite the lack of resolvable tertiary structure. As stated in Section 4.1.1 and Section 4.1.2, a standard unilamellar SLB could not be detected by classical Raman spectroscopy. Therefore, The Raman scattering of Aβ incubated on SLB **1** could be collected without any contribution of the lipids in the resolved spectrum.
First, aliquots of Aβ(1-42) (0.22 mM - 0.1% (w/v)) were incubated on SLB **1**. Because the sensitivity of the classical Raman technique for the small peptide Aβ was really low, the technique used to detect the signal of BSA was employed on Aβ samples (see Section 4.2.1). Briefly, UAR and SAR signals were collected continuously et saved after averaging of 20 scans while the buffer was slowly evaporated. Special attention was given to the amide I and amide III regions which contained the main information to elucidate the secondary structure of proteins. Especially, the amide I peak was deconvoluted with Gaussian fitting to characterize quantitatively the different secondary structures present within the sample.

Aβ(1-42) exhibited discrepancies between the UAR and SAR spectra (Figure 44 a). Firstly, the UAR intensity was higher than SAR, and was explained by the bigger collection volume of the undercritical angle technique. In addition, the areas of the deconvoluted peaks and their ratios were different between the UAR and SAR spectra. These variations of the ratio between the deconvoluted peaks were independent of each spectrum intensity. Finally, analogous peaks of UAR and SAR exhibited different Raman shifts. These observations showed that the Raman scattering - and by definition the structure - of the peptides were influenced by their proximity with the interface and with the SLB.
Concretely, the SAR amide I of Aβ(1-42) could be deconvoluted into two peaks whose maxima were at 1660 and 1689 $cm^{-1}$ respectively (purple and red in Figure 44 a). The former had a shift value corresponding to a structure between an α-helix and a disordered structure, while the latter could be attributed to a β-sheet structure blue-shifted towards higher frequencies of vibration. Both secondary structures seemed to appear in the supercritical

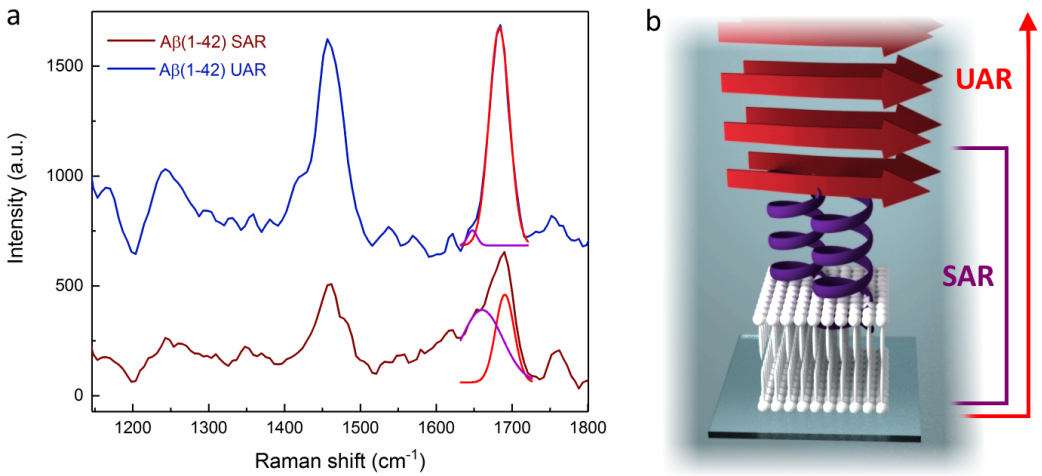


Figure 44: (a) Amide I and III regions of SAR and UAR spectra of Aβ(1-42) incubated on SLB **1** after partial evaporation of the buffer (27h). (b) Hypothetical structure of Aβ(1-42) adsorbed on SLB. α-helix (purple) is closer to the interface (detected in SAR) while β-sheet structure (red) is dominant in bulk solution (detected in UAR).

angle scattering region, near the SLB. However, the β-sheet peak area only represented 46.9% of the α-helix peak, which was slightly dominant in SAR.

The UAR amide I was also deconvoluted into two peaks, situated at 1648 and 1683 $cm^{-1}$ and attributed to α-helix and β-sheet. In the UAR spectrum, the area of the α-helix peak only represented 3% of the β-sheet peak, and was hardly distinguishable from the baseline. Another proof of the predominance of β-sheet in the UAR spectrum was found in the amide III region where the peak at 1242 $cm^{-1}$ was protruding from the baseline, and attributed to the same β-sheet structure. This Amide III β-sheet peak was harder to observe in the SAR spectrum, hence the structure was probably located further away from the SLB.

This reversed tendency of the secondary structure observed for Aβ(1-42) in UAR and SAR was interpreted as a preferential folding towards the α-helix structure when the peptide was close to the SLB. This explanation was in agreement with previous works where an α-helix structure displayed an enhanced stability in organic solvent or other media of low polarity[164, 264, 265]. According to these results, the electrostatic charge of Aβ is more uniformly distributed in the α-helix structure, making its insertion into a non-polar hydrophobic structure - such as a lipid bilayer - more favourable. On the opposite, Aβ seemed prone to adopt a random coil structure in aqueous media, or to fold as β-sheet when a critical concentration was reached. This was confirmed by the large predominance of the β-sheet peak in the UAR spectrum, where most of the scattered light came from

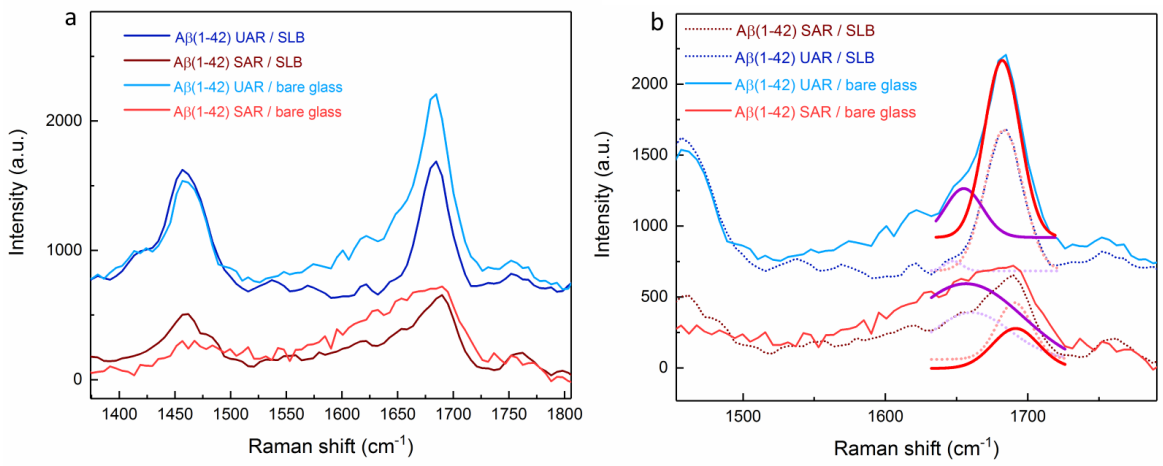


Figure 45: (a) Comparison between the amide I region of Raman spectra of Aβ(1-42) incubated either on SLB **1** or on a bare glass slide. (b) Deconvolution and comparison of the Raman amide I peak of Aβ(1-42) adsorbed on the two previous substrates.

the volume above the interfacial SLB. The most interesting conclusion about these UAR and SAR spectra is that both secondary structures were observed simultaneously on the same area of the sample and were only sorted by their axial distance from the SLB. This differs from a common hypothesis about the fibrillation process in which there is a conversion from the adsorbed peptide structure toward the fibril macro-structure (i.e. β-sheet stacking)[212, 264, 266, 267]. In the results described in this thesis, the α-helix secondary structure adopted by Aβ(1-42) at the beginning of its adsorption on the SLB still remained as an "anchor-like" structure even after the aggregation of additional peptides into β-sheet structure (Fig. 44 b).

To validate the assumptions about the selective folding of Aβ(1-42), an attempt was made to elucidate its structure with Raman when the peptide was dissolved without the presence of any lipid bilayer structure. No specific interactions were expected between the peptide and the bare glass coverslip. As a consequence, the SAR signal of Aβ was more difficult to observe because of the lower interfacial concentration, but the partial evaporation of the buffer ultimately led some peptides in the supercritical angle detection range. Comparison between the amide I peaks of the peptide with and without SLB is displayed in Figure 45 (a) and the deconvolution is showed in Figure 45 (b). The first observation was that the amide I peak was broadened in absence of any lipid bilayer structure. When comparing the spectra with and without SLB, discrepancies were found for the Raman

shifts and the areas under the peaks.

In the SAR spectrum, the β-sheet component only represented 18.8% of the α-helix (by opposition, 46.9% when adsorbed on SLB), showing a decreased contribution of the β-sheet structure. In addition, the peak at 1667 $cm^{-1}$ displayed a higher intensity, which is correlated to the scattering of unfolded peptides.

In UAR, the α-helix component of the amide I peak also became more prominent and its proportion increase from 3% to 29% $cm^{-1}$. It was also blue-shifted from 1648 to 1658 $cm^{-1}$. The analysis yielded the same conclusion that the peptides exhibited fewer β-sheet structures when there was no SLB to adsorb on. Theoretical models for the structure of Aβ indicate that it folds in a predominantly α-helix structure with β-sheet conversion in membrane-like, apolar media[268]. On the contrary, water turns the conformation of the peptide into a compact series of loops and strand without defined α-helix or β-sheet[269]. Therefore it has been suggested that α-helix represents an intermediate step in the aggregation process of Aβ. However, a first transition from random coil toward α-helix is indicated as the result of the addition of lipid vesicles in the peptides buffer. In the spectra of this thesis, the increasing proportion of α-helix signal without SLB was contradictory. However, it must be emphasized that the α-helix peak was either subjected to a blue-shift toward the unstructured region, or adjacent to another band characteristic of this random coil (at 1667 $cm^{-1}$). Therefore the α-helix structure, although present without lipid influence, seemed to exhibit more variations than the helix adsorbed on the SLB and some peptides clearly displayed a preferential unfolded conformation.

#### 4.2.3.2 *Amyloid-β (1-40)*

Raman spectra of Aβ(1-40) were also recorded upon adsorption on SLB/bare glass and analyzed similarly to Aβ(1-42) (Figure 46 a). The resolved secondary structures of the two peptides after adsorption on SLB were different.

Aβ(1-40) adsorbed on SLB displayed a β-sheet peak at 1687 $cm^{-1}$, which was dominant in both SAR and UAR. In addition, the amide III peak at 1243 $cm^{-1}$ in UAR also assessed the presence of β-sheet in bulk solution. In the UAR spectrum, the left part of the amide I peak was deconvoluted into a peak at 1639 $cm^{-1}$ which could be attributed to the scattering of the α-helix structure and represented 96.6% of the β-sheet peak area. However, despite having almost identical ratios, the peak of α-helix is extremely broadened compared to the β-sheet peak. It is supposed that although some α-helices were detected, their structure is highly unstable and yielded structural variations exhibiting different vibrational scattering.

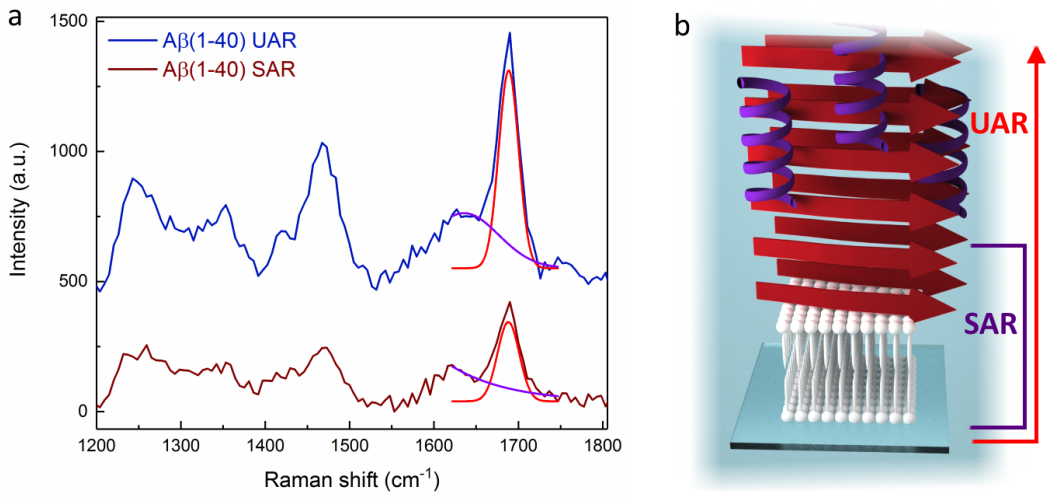


Figure 46: (a) Amide I and III regions of SAR and UAR spectra of Aβ(1-40) incubated on SLB **1** after partial evaporation of the solvent (30h). (b) Scheme of the hypothetical structure of Aβ(1-40) adsorbed on SLB according to the Raman results. α-helix (purple) is only detected in UAR while β-sheet is present in both SAR and UAR spectra.

In the SAR spectrum, besides the β-sheet peak at 1687 $cm^{-1}$, the deconvoluted amide I yielded a peak at 1624 $cm^{-1}$. However, α-helix could hardly be attributed to such a red-shifted peak. In this experiment with Aβ(1-40), clear α-helix structures were only observed far from the SLB since they appeared selectively in the UAR channel. This is opposed to the results obtained for Aβ(1-42) and with the usual hypothesis of Aβ aggregation, although the α-helix peak in UAR was so broadened that it maintained some uncertainty about the characterization.

A possible interpretation of these results is that the peptides which were folded into an α-helix structure upon aggregation on the SLB have desorbed and were not concentrated near the lipid bilayer anymore, unlike Aβ(1-42). α-helices (or similar structures) were rather mixed with the dominant β-sheet above the SLB (Figure 46 b). This desorption of α-helix peptides could be due to the weaker adsorption and insertion of Aβ(1-40) within the SLB, already reported in Section 3.1.3 and Section 3.1.4. The longer hydrophobic C-terminus of Aβ(1-42) favoured the insertion inside the bilayer and the conservation of the α-helix structure in folded peptides.[52]. On the other side, the shorter Aβ(1-40) folded into α-helix structure were not inserted as deeply as Aβ(1-42). They could have desorbed more easily and interacted with aggregates already formed, ending up beyond the axial detection of the SAR technique. Alternatively, the lack of defined α-helix structures for Aβ(1-40) could

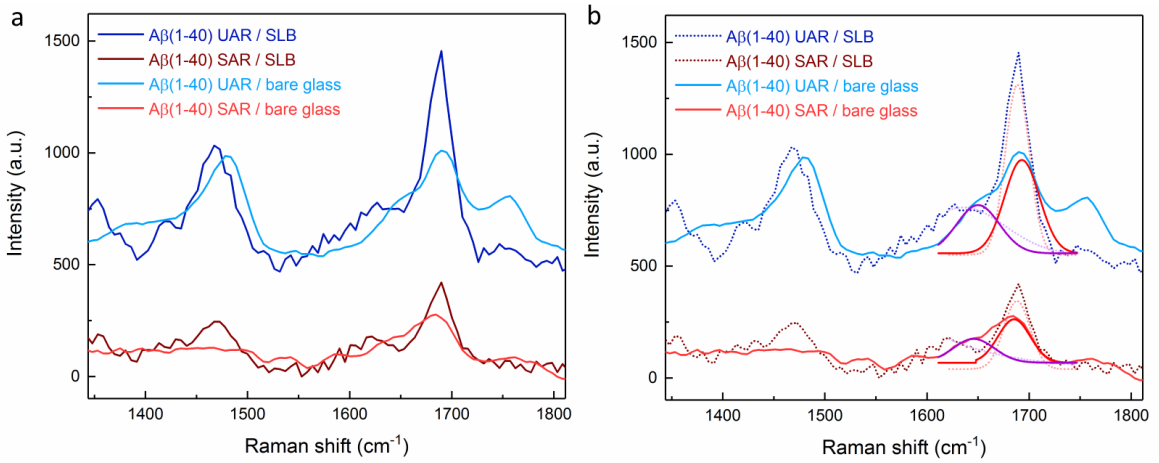


Figure 47: (a) Comparison between the Raman spectra of Aβ(1-40) incubated either on SLB **1** or on a bare glass slide. (b) Deconvolution and comparison of the Raman amide I peak of Aβ(1-40) adsorbed on SLB or glass coverslip.

be the proof of a real conversion of α-helix toward β-sheet, induced by the interaction with the SLB[268].

When incubated without SLB, Aβ(1-40) yielded other Raman diffraction spectra (Figure 47 a,b). In UAR, the general intensity of the amide I decreased, and the deconvoluted peak assigned to α-helix shifted from 1639 $cm^{-1}$ to 1650 $cm^{-1}$ which was now exactly in the range corresponding to the helix structure. In addition, its ratio with respect to β-sheet slightly decreased down to 83.2%.

The changes were more pronounced in the SAR spectrum, where a peak appeared at 1645 $cm^{-1}$, where there was initially no peak scattered from peptides adsorbed on the SLB. This new peak had a ratio of 70.5% with the corresponding β-sheet scattering. These results seemed to indicate that the conversion of α-helix into β-sheet hypothesized previously did not occur without the presence of the lipid environment. However, the presence of α-helix structure itself was previously related to membrane-like media.

It is possible that the structure observed was not a fully formed α-helix but another similar structure : $3_{10}$-helix. Vivekanandan et al. have reported that Aβ(1-40) in aqueous solution could exhibit $3_{10}$-helix as a tighter version of the α-helix, playing the role of an intermediate toward the fully structure helix. Structural similarities between the two helix could explain the apparent results of Raman spectroscopy, meaning that only partially folded intermediates were observed[270]. The ratio of the peaks of $3_{10}$-helix and β-sheet were

similar in both SAR and UAR, meaning that no preferential folding relative to the axial distance from the interface was observed.

### 4.2.4 *Surface-enhanced-Raman spectroscopy of Amyloid-β adsorbed on a supported lipid bilayer*

#### 4.2.4.1 *SERS of Amyloid-β (1-42)*

In Section 4.1.3 the Raman spectrum of an unilamellar SLB was obtained by SERS using a layer of silicon nanofilaments and gold nanoparticles as a substrate for the formation of the bilayer. Afterwards, this SLB was incubated with an aliquot of Aβ(1-42) (0.22 mM = 0.1% (w/v)) and the Raman signal was collected. The plasmonic surface-enhancement allowed the direct detection of the signal of the peptides, without the need of evaporation of the solvent.

The SAR spectrum before and after incubation with Aβ is displayed in Figure 48 (a). An intense peak at 1651 $cm^{-1}$ (purple arrow) correlated to the α-helix secondary structure appeared after incubation with the peptide. The same structure was confirmed by the peak protruding at 1266 $cm^{-1}$ (purple arrow). A peak at 1561 $cm^{-1}$ (1) was already observed before incubation, but broadened with C=C signal and explained by the gold photoluminescence (see Section 4.1.3). However its intensity increased drastically after incubation with the peptide. Heterocyclic rings were now a plausible source for the increased intensity of this peak, since each Aβ possesses three histidine residues ($His_6$, $His_{13}$ and $His_{14}$). The peak at 1561 $cm^{-1}$ (1) and at 1327 $cm^{-1}$ (2) were attributed to neutral imidazole side chain by Ashikawa et al.[271] Indeed, the peak at 1327 $cm^{-1}$ (2) was not visible before incubation with the peptides. In addition to the analysis of the peak of the peptide with SAR, the disappearance of the peaks of the SLB at 1448 $cm^{-1}$, 1630 $cm^{-1}$ and 1725 $cm^{-1}$ was observed. This effect was thought to be caused either by an overlapping with the signal of the peptides or by the removal of the lipid molecules from the surface, as it was already observed by fluorescence in the previous chapter (see Section 3.2.2).

The UAR spectrum is displayed in Figure 48 (b). An immediate identification could be done on the amide I and amide III peaks appearing only after incubation with the peptide. Peaks at 1651 and 1274 $cm^{-1}$ (purple) were identified as α-helix but the peak at 1677 $cm^{-1}$ and the small peak at 1244 $cm^{-1}$ were specific of β-sheet structure. This result is an example of how the selectivity between UAR and SAR could provide important results when

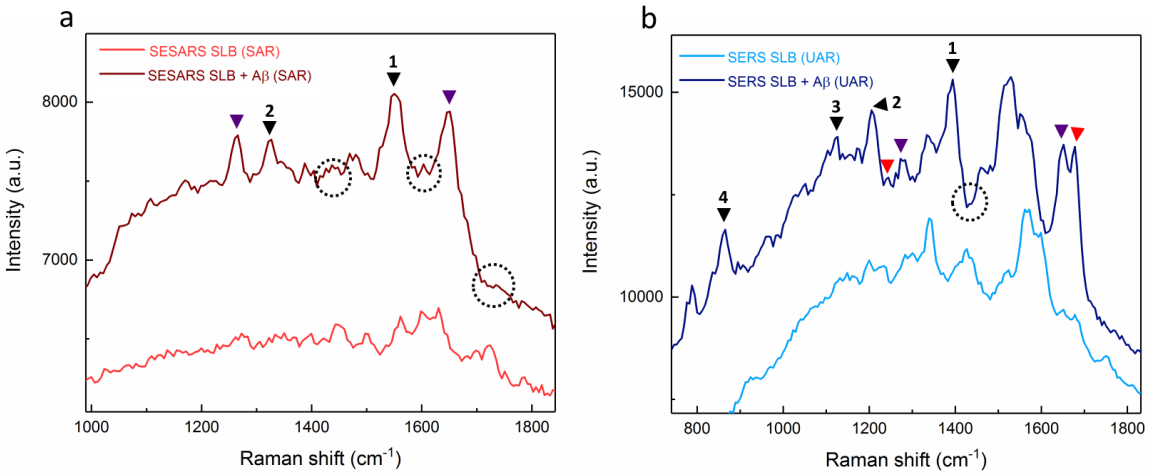


Figure 48: Surface-enhanced SAR (a) and UAR (b) spectra of SLB **1** formed on a layer of silicon nano-filaments functionalized with gold Nanoparticles, before and after incubation with Aβ (1-42).

the two were combined, even with a surface-enhancement technique : the UAR spectrum alone would only have permitted the detection of both α-helix and β-sheet structures without any information about their localization. But the presence of only one specific structure in SAR/SESAR (i.e. the α-helix) brought the conclusion that although it was also detected with UAR, it was actually located near the surface of the SLB. On the other hand, SAR spectrum alone would not have allowed the detection of all the structures exhibited by Aβ. These results confirmed the previous hypothesis of Section 4.2.3.1 about the structure adopted by Aβ (1-42) upon adsorption on the bilayer (Figure 44 b), but did not require the solvent evaporation. This is an important feature that improves the validity of the model elaborated so far.

Some other features were observable when comparing the UAR spectra before and after incubation with the peptides. The broad peaks situated between 1561 $cm^{-1}$ and 1630 $cm^{-1}$ seemed red-shifted to 1540-1600 $cm^{-1}$ as if the correspondent chemical moieties were subjected to a lower frequency of vibration. In addition, the characteristic peaks of lipids at 1750 and 1448 $cm^{-1}$ were not visible anymore after incubation with Aβ, as it was already observed in SESAR. The very intense peak at 1394 $cm^{-1}$ (1) could be characteristic of the histidine residues of the peptides. The gold photoluminescence peak at 1330 $cm^{-1}$ was broadened by the contribution of histidine vibration. The peak at 1205 $cm^{-1}$ (2) was hardly attributed since Raman charts correlate this shift with ethers or tryptophan. Finally, the peak at 1126 $cm^{-1}$ (3) corresponded to C-N bond and the one at 865 $cm^{-1}$ (4) was

attributed to Tyrosine residues. Not attributed peaks might be the enhanced signal of impurities.

In conclusion, surface-enhancement technique still permitted to detect the peaks of Aβ peptides without the need to evaporate the solvent. Moreover, comparison of the data from SERS and SESAR confirmed the assumptions made in previous sections about the structure adopted by the peptides upon adsorption of the SLB. Unfortunately, no more information about the structure of the lipid molecules could be extracted from this experiments, since their signal disappeared after incubation with the peptides. The overlapping of the signal of a unilamellar bilayer with the signal of high concentrated Aβ is likely the cause of this loss of data.

#### 4.2.4.2 *SERS of Amyloid-β (1-40)*

Incubation of SLB with peptides and characterization by surface-enhanced Raman was repeated with Aβ(1–40). The comparison of the SESARS spectra before and after incubation with Aβ are displayed in Figure 49. The two main differences were the apparition of an intense α-helix peak at 1640 $cm^{-1}$ (purple) and a group of peaks around 1300 $cm^{-1}$. This region decomposed into three resonances: an amide III peak that was detectable at 1278 $cm^{-1}$ and the confirmed presence of α-helix structures. The peaks at 1300 (1) and 1327 (2) $cm^{-1}$ were attributed to the C-terminal methylene twisting vibration[272] and imidazole, respectively. The SERS (UAR) spectra are shown in Figure 49 (b). One feature that is typical of the lipid bilayer was the disappearance of the carbonyl peak at 1730 $cm^{-1}$ (1) after incubation with Aβ. In addition, a peak that initially protruded at 1280 $cm^{-1}$ was correlated with =C-H in-plane deformation. After incubation with Aβ, this peak was broadened into another peak at 1320 $cm^{-1}$ (2), which was probably related to the peptide and corresponded to a shifted imidazole signal. The amide III region was too broadened for accurate characterization, and the amide I region was used instead to determine the structure of the peptides. Two peaks were detected, corresponding to both α-helix (purple) and β-sheet (red) secondary structures. This result was identical to the structures observed for Aβ(1–42), indicating a preferential folding into helices near the membrane, with a concentration of β-sheets above the surface of the SLB. However, this seemed to be in contrast to the structure that was extracted previously from Aβ (1–40) using the spontaneous Raman signal (see Section 4.2.3.2), where no α-helices were observed near the SLB and only a small fraction of their Raman scattering was above the bilayer. A possible explanation

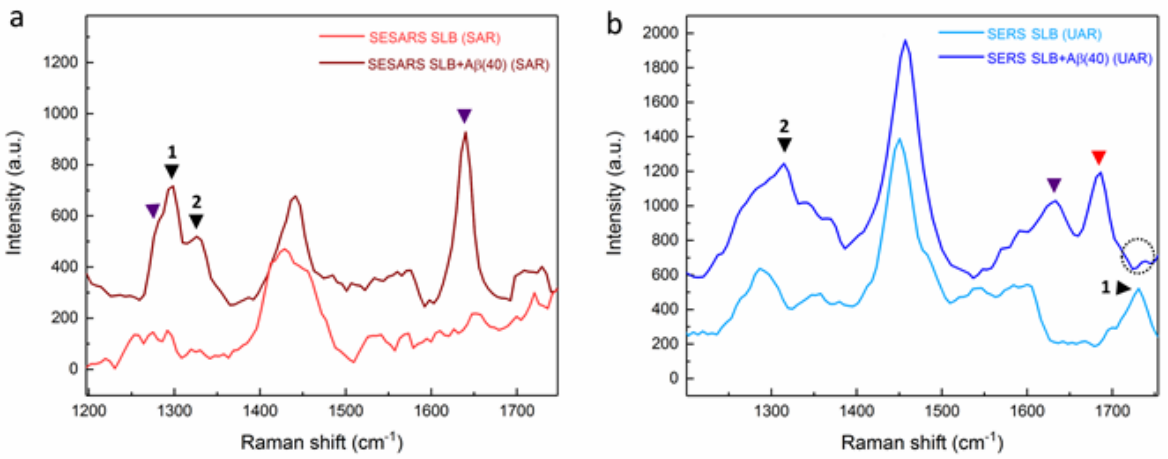


Figure 49: Surface-enhanced SAR (a) and UAR (b) spectra of SLB **1** formed on a layer of silicon nano-filaments functionalized with gold Nanoparticles, before and after incubation with Aβ (1-40).

for this apparent inconsistency is that results shown in Section 4.2.3.2 required a high local concentration of peptides, which is a trigger for the folding of Aβ into β-sheet and their stacking. The increased sensitivity of SERS allows the data to be recorded before the conformation change. SERS data recorded after the evaporation of the buffer confirmed this hypothesis: the β-sheet peak then became dominant in both spectra after, as in Section 4.2.3.2 (see Figure 50).

It should be mentioned that the α-helix structure was already observed for Aβ (1–42) with classical Raman spectroscopy, and preserved despite the high peptide concentration used in Section 4.2.3.1. Conservation of the α-helix at higher concentration might be the consequence of its stronger interaction with the SLB, as it limited its desorption from the membrane, then remaining in the helical structure.

### 4.2.5 *Elaboration of a model for the interaction and toxicity of Amyloid-β upon adsorption on a supported lipid bilayer*

The principal objective of this thesis was to investigate the interaction of Aβ with a model of cell membrane and to determine the process and the consequences of such interaction. Gathering all the results obtained with both fluorescence and Raman experiments, a proposition of interaction pathway is elaborated in this section.

It is assumed that Aβ interacts with the SLB with unspecific adsorption since no specific

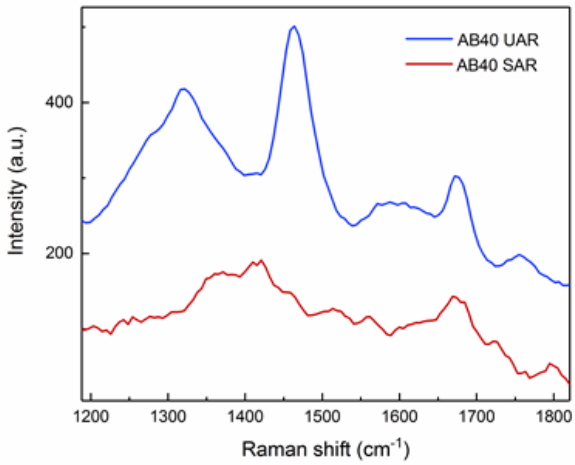


Figure 50: SERS (UAR) and SESARS spectra of Aβ (1–40) incubated on SLB after buffer evaporation over 24 h. Compared with the spectra in Figure 49 a) and b), the dominant secondary structure turned into β-sheets (1673 $cm^{-1}$). These changes from the spectra in Figure 49 to the spectra in Figure 50 seemed to demonstrate a conversion from the initial α-helix/β-sheet superposition into a dominant β-sheet stacking structure.

binder of the peptide was present within the bilayer. It is also known that the latest stages of interaction are featured by the presence of peptide aggregates which exhibit a β-sheet structure. Such structure can eventually lead to the formation of characteristic fibrillar aggregates around the neurons of Alzheimer patients, but was not observed in these experiments. This was not a problem since the mechanism of toxicity of Aβ is supposed to take place before this fibrillation process, when the peptides start to form smaller and soluble oligomers. At physiological concentration, the early stage of adsorption of Aβ is assumed to involve freshly produced monomers.

These conditions correspond to the lowest concentration described in this thesis. Aβ monomers first adsorb reversibly on the lipid bilayer, exhibiting a so-called overshooting effect. From the first adsorbed peptides, some will desorb while others remain at the surface of the SLB (Section 3.1.3). It is thought that the selectivity between remaining and desorbing peptides is due to different structures. Native structure of dissolved Aβ is considered to be unfolded, only in SAR/UAR experiments when no lipids were present in the peptide samples. However, the α-helix structure was observed with SAR at the top of the lipid bilayer for the most strongly adsorbed peptide (Aβ (1-42) - Section 4.2.3.1). The presence of this structure was confirmed in other studies and described as a more stable conformation toward hydrophobic environment. From these data, it is hypothesized that Aβ monomers can adsorb on

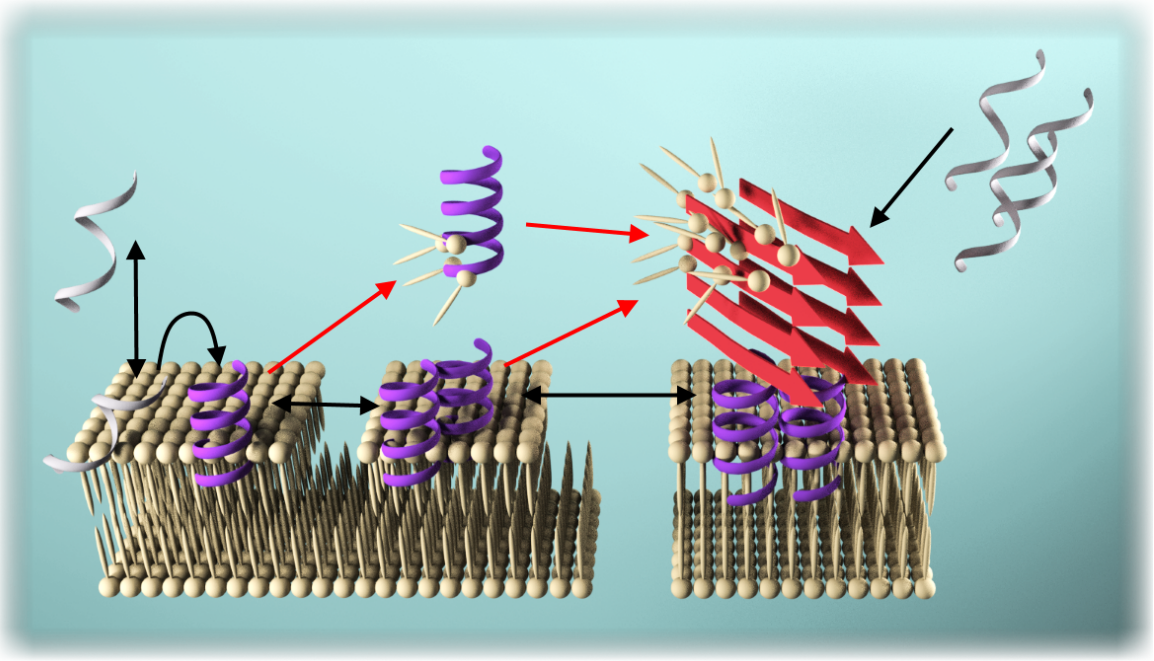

Figure 51: Hypothetical representation of the damaging process induced by Amyloid-β upon adsorption on a supported lipid bilayer. Peptides are represented exhibiting the secondary structures resolved with SAR/UAR experiments. "Toxic" damaging steps of the interaction pathway are indicated with red arrows.

SLB with an unfolded structure, then potentially undergo conformational change toward α-helix secondary structure which favours their interaction with lipid molecules. Aβ (1-42) exhibited a slightly stronger adsorption than Aβ (1-40), and displayed more α-helix Raman signal at the surface of the SLB therefore suggesting a correlation between the two observations. Not only does the α-helix structure enhance the stability of adsorbed Aβ inserted inside the SLB but it is also reported to strengthen the interaction between the peptides and lipid molecules.

Nevertheless, even the more stable peptides might be reversibly adsorbed, as showed by washing experiments (Section 3.1.4). Subsequently, desorbing Aβ is thought to promote the extraction of some lipid molecules from the SLB, when their mutual interactions overcome the hydrophobic interactions between aliphatic chains of fatty acids (Section 3.2.2). This extraction of lipid molecules can lead to a thinning of the lipid bilayer. Such modification of the thickness would likely be involved in a weakening of the resistance of the membrane. It is also logical to extrapolate such modification of the membrane to a hindrance of biochemical functions (i.e. permeation to ions or hindrance of catalysis involving membrane proteins).

Higher peptide concentrations were correlated with a higher tendency to aggregate but also with a more pronounced damaging of the SLB, such as a clustering of lipids or even a disruption of the bilayer. It is possible that the aggregation of Aβ on the surface of the SLB worsens the instability of the lipid-peptide structure. Too unstable aggregates are also susceptible to desorb from the bilayer and the extraction of the numerous lipids bound to the aggregates naturally results in a more severe alteration of the membrane.

### 4.2.6 *Raman characterization of α Synuclein adsorbed on supported lipid bilayer*

Previous experiments were conducted in our group with another amyloidogenic peptide correlated to Parkison's disease : α-Synuclein (α-Syn). The α-Syn peptide is more conserved than Aβ and is composed of 140 amino acids[273]. However, similarities are observed regarding their conformation: α-Syn is also reported to be natively unfolded in aqueous solution and to adopt various α-helical structures when interacting with lipids micelles or bilayers[274, 275]. Another likeness between Aβ and α-Syn lies in more recent theories concerning the role of their aggregation in their respective diseases. According to these hypotheses, the oligomers formed in the early stage of α-Syn aggregation would be the toxic species rather than the amyloid fibrils formed after aggregation[276]. The interaction between SLB and this peptide was previously investigated in our group, but no supercritical angle Raman spectroscopy was used yet. Therefore, the characterization of the structure of α-Syn was now attempted with SAR/UAR. As for Aβ, α-Syn Raman signal was monitored with and without interaction with a SLB substrate.

When incubated on a bare glass slide (Figure 52 a), α-Syn exhibited an amide I peak centered at 1652 and 1654 $cm^{-1}$ in SAR and UAR respectively. In SAR, another small peak at 1660 $cm^{-1}$ could also be found from the deconvolution. All these three peaks indicated the presence of an α-helix structure.
In UAR, a peak could be fitted at 1690 $cm^{-1}$, possibly caused by β-sheet photon scattering. This peak still represented 31% of the main amide I component. The dominant structure was an α-helix, although it was believed that α-Syn peptide gained a helical structure upon interaction with phospholipids. This apparent contradiction was already encountered with native Aβ in aqueous media (Section 4.2.3.1 and Section 4.2.3.2). However, characterization of native α-Syn in lipid-free media remains a contentious issue. In fact, in was suggested

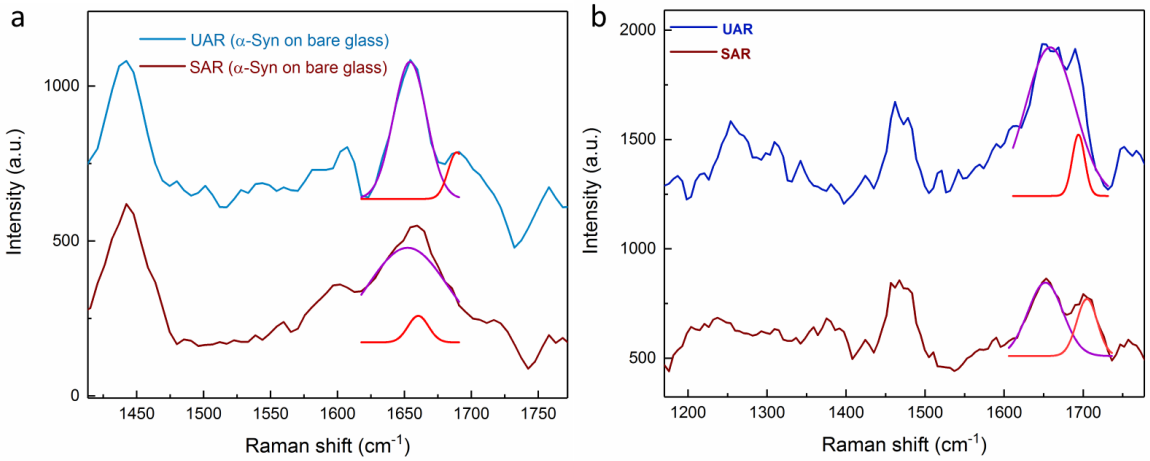


Figure 52: (a) SAR and UAR spectra of α-Synuclein incubated on a bare glass coverslip. (b) SAR and UAR spectra of α-Synuclein incubated on SLB **1**. Both spectra were recorded after solvent evaporation (31h-32h).

that α-Syn could exist in solution as a folded helical tetramer[277]. Although the amount of units forming the oligomers of α-Syn could not be determine in this experiment, it seems to confirm the possibility of a helical structure even in the absence of membrane-like media to induced structure transition.

The other sample was composed of a SLB incubated with α-Syn before submission to Raman spectroscopy (Figure 52 b). The amide I region was easily deconvoluted into two peaks. In the UAR spectrum, one peak with a broad summit at 1660 $cm^{-1}$ (purple) was attributed to the expected α-helix. The other peak at 1689 $cm^{-1}$ (red) was correlated to β-sheet structure but only represent 10% of the area of the α-helix peak. This reduced ratio compared with peptides incubated without SLB is surprising. There was no surface-enhancement in this experiment with α-Syn peptide, implying that the peak of α-helix structure was not artificially intensified and that α-helix is really dominant in the bulk solution. The amide III peak showed a broad band which was unsuccessfully deconvoluted but whose center was situated at 1255 $cm^{-1}$. Considering that the amide III peak of α-helix would be around 1270 $cm^{-1}$ and β-sheet peak would be around 1240 $cm^{-1}$, the detected broad peak at 1255 $cm^{-1}$ was interpreted as the presence of both secondary structures in the detection volume. A possible explanation for the smaller propensity of α-Syn to form β-sheet when incubated in presence of lipids is that the SLB favourized the helical structure and could even induce a transition from β-sheet to α-helix[278].

In the SAR spectrum, the amide I region was also deconvoluted into two peaks. The peak at 1653 $cm^{-1}$ (purple) was also featuring the $\alpha$-helix structure but the peak at 1705 $cm^{-1}$ (red) seemed excessively blue-shifted to correspond to the $\beta$-sheet structure. However, since no other vibration or chemical structure was more appropriate, the latter peak would cautiously be attributed to $\beta$-sheet. A compression of the global peptide structure might cause such increase in the frequency of vibration.

## 4.3 SUMMARY AND OUTLOOK

Aβ peptide is closely related to the infamous Alzheimer disease which spread among elderly people and causes many symptoms, the most remarkable being a progressive loss of memory. The main subject of this thesis was to carry out a close monitoring of the interaction between Aβ and a model of lipid membrane, then to observe, characterize and quantify the consequences of this interaction.
While being naturally produced in healthy individuals, Aβ still has no known function attributed to its presence in the brain. It has been hypothesized that in low concentration, it might have a protective effect for neuron membrane against metal ions. However, Aβ is mostly known for being the main constituent of aggregated substance surrounding the dead neurons of Alzheimer patients. Aβ belongs to a family of proteins and peptides which are prone to aggregate into β-sheet rich fibrils and induce severe diseases. The triggers for the aggregation process and the increase of Aβ concentration are still unknown (except for natural accumulation over aging) and conditions that favour the aggregation are not easily met *in vivo*, hence the profusion of *in vitro* experiments to elucidate the mechanisms of aggregation. In addition to the aggregation pathway, the exact cause for the death of neuron cells under the influence of Aβ is also in debate. The current scientific consensus is that the fibrils generated later during aggregation are not the most toxic species, but small oligomers would be more prone to induce toxicity towards the neurons, notably at the level of their lipid membrane. These toxic processes include lipid oxidation, formation of pores within the membrane and dysregulation of ionic homeostasis.

Although many information and hypotheses about Aβ are accepted by a great part of the scientific community, there are almost as many different models of study as there are different groups of research. Computed dynamic simulation[279], cell culture[280], peptides aggregated without lipid substrate[164], lipid membrane cross-linked with Aβ[244] or polymer-encased lipid-nanodiscs[281] are but few examples. Considering the diversity of models to study the interaction between Aβ and the lipid membrane, it seemed interesting to use a simple model which mimics the very beginning of this interaction, i.e. when the peptide starts to adsorb at the interface with the lipids. As the membrane curvature of the bigger cells could locally be considered as a flat surface, a supported lipid bilayer (SLB) model was selected. This model is straightforward to set-up and was formed on a trans-

parent glass coverslip which match perfectly the conditions for visible light spectroscopic measurements. The composition of the SLB was identical to previous studies with amyloidogenic peptides (α-Syn) for which the protocol of SLB formation has been optimized, and contained one third of negatively charged lipids.

Various techniques are commonly used to elucidate the effects of Aβ, such as fluorescence[211], NMR[282], AFM[164], circular dichroism (CD)[213] and Raman[283]. We choose to use supercritical angle spectroscopic techniques developed in our group, namely supercritical angle fluorescence (SAF) and supercritical angle Raman (SAR). The principle of the supercritical angle technique consists to collect the photons above the angle of total internal reflection of a glass-water interface. Photons coming from this direction are specifically emitted from surface-bound molecules or molecules located within few dozens of nanometers from the interface. Hence, the supercritical angle technique allows to selectively observe emitters located near the interface on which the SLB is formed. Therefore, the signal from the SLB, or Aβ interacting with the SLB, can be isolated from the bulk floating peptides which is still recorded on a separate channel. In addition to this selectivity, fluorescence was chosen for its sensitivity and imaging feature which would help to elucidate the effect of Aβ interacting with the SLB. Raman spectroscopy, on the other side, allows the characterization of molecular bounds and peptide secondary structures without the need to label the target.

Two types of peptides were used, Aβ (1-40) and Aβ (1-42) which were 40 and 42 amino acids long, respectively. Both are detected in the brain of Alzheimer patients and produced naturally, but Aβ (1-42) is known to have a higher aggregation tendency and to promote the aggregation of its counterpart as well.

At first, different compositions of lipids were used to yield a SLB similar to the natural composition of the membrane. This was done by including lipids such as cholesterol, sphingomyelin and ganglioside into the SLB. The amount of adsorbed peptide on these different SLBs were measurement by fluorescence and the more physiologically relevant SLBs generally yielded a higher adsorption of peptides. However, only the most basic (DOPC:DOPS) and cholesterol containing SLB (DOPC:DOPS:Chol) were used in further experiments since their formation were more reproducible than the other SLBs.

The affinity of adsorption of Aβ (1-40) and Aβ (1-42) on DOPC:DOPS SLB was quantified by monitoring the increase of fluorescence on the surface of the lipids in function of the time and concentration. The dissociation constant $K_d$ was extrapolated and Aβ (1-42) showed

a slightly higher affinity than Aβ (1-40). However, huge discrepancies in the total fluorescence intensity were measured between the two peptides. The main reason is that Aβ (1-42) formed fluorescent aggregates faster than its counterpart. The aggregates were also more tightly attached on the surface of the SLB, as showed by measuring the speed of diffusion of these aggregates. Our $K_d$ values were compared with other groups but the differences in lipid models highly influenced the results. A rather good agreement was found with the $K_d$ measured by Ariga et al.[220] but Thomaeir et al. measured a $K_d$ a hundred-fold higher with a specific composition of lipids[284].

Through these experiments, a model for the adsorption of the peptide on the SLB was proposed: the first adsorbed peptides were weakly interacting with the lipids and the adsorption was highly reversible. However, some peptides could undergo a transition toward a stronger interaction, probably a change in the structure of the peptide. Aβ (1-42) was more prone to perform this transition than Aβ (1-40). In addition, a cooperative component seemed to drive the adsorption of more peptides near the already adsorbed ones, hence forming the nuclei of aggregation that has been reported for Aβ . Again, Aβ (1-42) was faster to yield this aggregated state since the first adsorbed species were more tightly bound within the SLB and offer stable nuclei of aggregation. The cooperative and nucleation-dependent aspect of the aggregation was confirmed with Native-PAGE experiment which showed that interaction between the peptides and the lipids was an important trigger for the formation of multimeric peptide species. Besides the difference in the kinetic of aggregation, the type of aggregated species was also different between Aβ (1-40) and Aβ (1-42), as found by fluorescence correlation spectroscopy. From FCS data the speed of the different aggregates could be quantified and the mass and size of the oligomers were extrapolated. In general, Aβ (1-42) aggregated species diffused 6 to 15 folds slower and the mass of the oligomers was 2 to 10 folds higher than Aβ (1-40). The latter result showed that Aβ (1-42) aggregates are not only formed faster and more tightly bound to the SLB, but they are also more massive than those obtained from the aggregation of Aβ (1-40).

After having characterized the adsorption process of Aβ on SLB, the impact of such adsorption on the lipid membrane was investigated. Fluorescent SLB constituted of DOPC:DOPS and DOPC:DOPS:Chol were incubated with Aβ at different concentration, ranging from 0.5 to 50 µM. Abnormal effects were observed and their intensity dependent on the concentration of peptides. Even at the lowest concentration (0.5 µM), some effects could be observed on the SLB. After 24 to 48 h of incubation, the average fluorescence intensity of

the SLB had decreased. Autocorrelation curves showed that this decrease of intensity was due to a reduced number of fluorescent molecules in the detection area.

Increasing the Aβ concentration up to 5 µM yielded an additional effect as some areas of the SLB surface exhibited fluorescent clusters of lipids detected further away from the surface of the SLB. The protrusion of these lipid clusters is observed when incubated with peptides whose concentration also yielded the presence of peptide aggregates in previous experiment. Therefore, it is tempting to associate these two events, as aggregated peptides could extract lipids from the SLB. It would be interesting to use Förster resonance energy transfer (FRET) to prove this assumption.

Finally, increasing the peptide concentration up to 50 µM brought another effect as the surface of the SLB sporadically showed a total disruption of the lipid membrane.

All these abnormal effects related to the integrity of the SLB were observed with similar intensities for both Aβ(1-40) and Aβ(1-42). However, cholesterol-containing SLB tended to exhibited a more severe damaging. Since the presence of cholesterol molecules increased the amount of peptides adsorbed on the SLB, and the above-mentioned effects seemed related to the concentration of Aβ, the enhancement of the effects for cholesterol-containing SLB is not surprising. The results obtained are also in accordance with theories stating that Aβ can induce pore formation within the neuron membrane[244]. However, we observed these effects after the adsorption of initially unbound peptides rather than with peptides directly included within the membrane. In this aspect, our model seems closer to the events happening *in vivo*, despite the high concentration of Aβ. The effects observed in this thesis indicate that when Aβ interacts with the SLB, it promotes a concentration-dependent removal of lipids from the bilayer, eventually leading to a thinning or even a disruption of the membrane. In either case, such modification of the membrane integrity could drastically affect the metabolism of the neuron cells.

Apart from the integrity of the SLB, the mobility of the lipids within the bilayer is also an important feature of biological membranes. This aspect was also measurement during incubation with Aβ by extracting the lateral diffusion coefficient from FCS fitting of different areas within the SLB. Despite both peptides being able to influence the integrity of the SLB, the influence of the peptides over the diffusion of lipids was more specific. Under incubation with Aβ(1-40), the diffusion of lipids remained unchanged except around local defects such as lipid clusters and holes within the SLB. On the other hand, after incubation with Aβ(1-42), a peptide concentration of 25 µM was able to decrease the average mobility of lipids by around 30% even away from defects. The most probable explanation for this re-

sult is that the more massive peptides oligomers are the species hindering the diffusion of the lipids. Therefore, a general decrease of the diffusion of lipids is observed with Aβ(1-42) forming bigger aggregates (cfr. above), while the same decrease is only observed locally with Aβ(1-40) because its aggregates are more scarce and expected to be located near the damages in the SLB.

Calcium is known to be involved in the metabolism of neurons and possibly affecting or affected by Aβ. For example, Itkin et al. showed that calcium ions induced the formation of Aβ oligomers[198], which seemed to be the most toxic species in our previous experiment. Therefore, the fluorescence experiments measuring the affinity of Aβ for the SLB and its effect were reproduced in a buffer containing 2 mM of calcium ions. It was observed that at low peptide concentration (between 0.5 and 1-2 µM), the presence of $Ca^{2+}$ enhanced the adsorption of Aβ on the SLB. This was a direct observation of an effect predicted by computer simulation[232]. As it could be expected, an enhanced adsorption of Aβ also strengthened the removal of lipids from the SLB. However, $Ca^{2+}$ had no impact on the modified diffusion of lipids inside the SLB. This is probably because the range of peptide concentration affected by $Ca^{2+}$ was also unable to affect the mobility of the lipids either.

Finally, after the determination of the effects occurring when Aβ was incubated with SLB, the peptide conformation responsible for these effects was investigated. Supercritical angle Raman spectroscopy was the method used to characterize the secondary structure exhibited by the peptides situated close to the surface of the SLB. The use of Raman spectroscopy to study Aβ is common, but the targets vary drastically between research groups. Amyloid senile plaques[283], pre-formed oligomers[285, 286] or simply dissolved without lipids[287] have been characterize with Raman spectroscopy. But a basic model of interaction between initial monomers left to aggregate in the presence of lipids would be valuable.

The main drawback of the method was the low sensitivity of Raman for peptides and proteins, which was accentuated when combined with the supercritical angle technique. Therefore, the protocol used by Angelis et al.[259] was applied to SAR: the sample concentration was artificially increased by letting some of the peptide buffer evaporate and constantly recording the Raman scattering. Eventually, the spectrum of the peptides could be obtained. By comparison between the Raman spectra of supercritical angle (SAR) and classical Raman, a localization of different structures could be made and different for each peptide.

SAR spectra of Aβ(1-42) exhibited a dominant α-helix secondary structure, with a smaller contribution of β-sheet structure. Classical Raman spectra showed instead a clear dominance of β-sheet structure. These results were confirmed by the use of surface-enhanced Raman spectroscopy (SERS) combined with supercritical angle spectroscopy. The main advantage of the SERS experiment was to confirm the structures observed previously, while allowing to work without the need to increase the concentration in Aβ. Combining the two sets of data, the model of adsorption was detailed further, with an adsorption of α-helix-structured Aβ(1-42) prior to further aggregation of peptides which turned out to yield the β-sheet stacking often reported during the formation of amyloid fibrils. A check of the presence of these fibril structures with other analytical methods such as AFM or ThioflavinT fluorescence could be interesting to confirm the structure.
Raman spectra of Aβ(1-40) displayed a different layout, as the SAR spectra were mostly showing β-sheet and classical Raman spectra still exhibited a dominant β-sheet as well. The lack of α -helix structure was unexpected but somehow make sense with the results of the previous affinity experiments. Indeed, α-helix structure are reported to stabilize the peptide conformation when immersed in an hydrophobic environment, such as the SLB. The fact that Aβ (1-42) folded into such structure while Aβ(1-40) did not is a good explanation for the discrepancies in affinity between the two peptides. Aβ(1-42) exhibited a stronger interaction with the SLB because it folded into a structure favouring its insertion within the lipid bilayer. These results add details to the common hypothesis about the fibrillation process where the structure of adsorbed Aβ is totally converted into the fibril macrostructure (β-sheet stack)[212, 264, 266, 267]. A mixture of α-helix and β-sheet structures was also observed by Sahoo et al. for Aβ interacting with polymer encased lipid-nanodiscs[281]. In their work, slightly acidic pH conditions and a lower peptide-to-lipids molar ratio promoted an initial folding into helices, followed by a transition toward β-sheet. Our data suggest that the helical secondary structure adopted by Aβ remained as an "anchor-like" part even after the aggregation of additional peptides into another structure.

Combining all data of both supercritical angle fluorescence and supercritical angle Raman allowed to elaborate a precise model for the interaction of Aβ with lipid membrane and a possible cause for the death of neurons encountered in Alzheimer patients. The hypothetical model is as follows: while Aβ(1-40) remains quite harmless at low concentration due to its lower affinity for the membrane, the production of Aβ(1-42) is more critical. Aβ(1-42) is prone to fold into an α-helix structure upon interacting with the membrane, hence

strengthening its insertion within the lipids. Aβ which remain inserted for prolonged period of time can act as nuclei promoting the cooperative adsorption and aggregation of nearby peptides. When aggregates - or oligomers - reach a critical size and concentration, they somehow induce the desorption of some lipid molecules from the membrane bilayer. This effect alone can induce a thinning of the membrane and could easily perturb other processes taking place at the membrane of neurons (including the transfer of electrical potential). The desorption of lipids from the membrane due to the progressive accumulation of peptides could even promote the formation of holes via the disruption of the bilayer. Small-sized holes could be enough to perturb the ions homeostasis, while more important damage could easily lead to a leakage of metabolites outside of the cell.

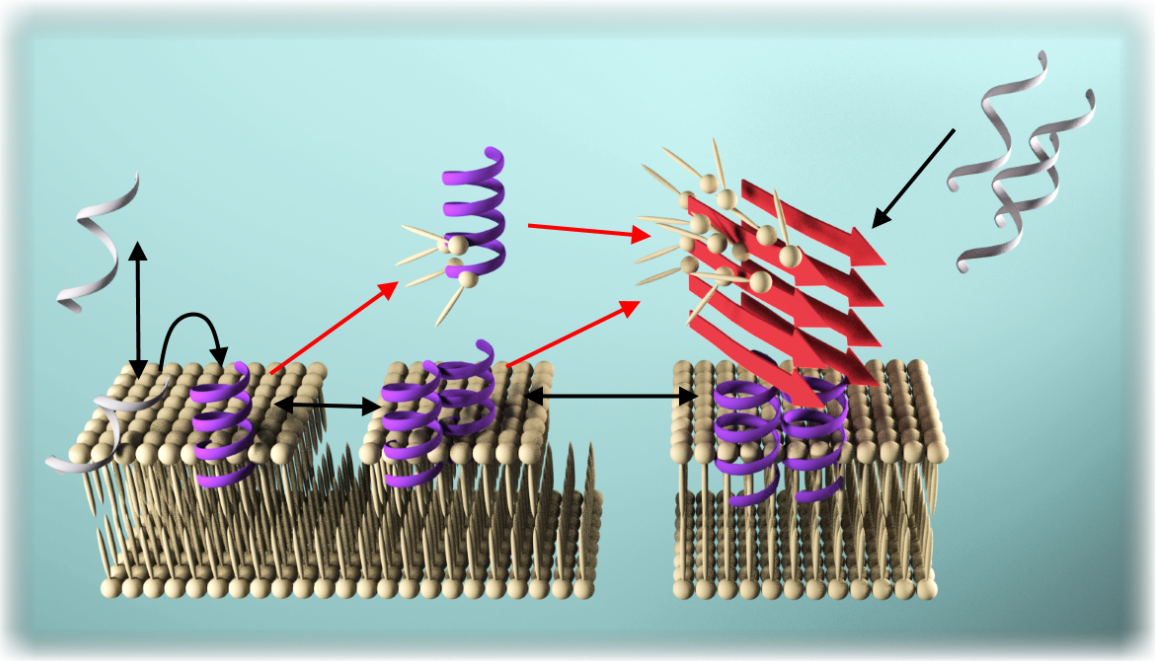

Figure 53: Hypothetical representation of the damaging process induced by Amyloid-β upon adsorption on a supported lipid bilayer. Peptides are represented exhibiting the secondary structures resolved with SAR/UAR experiments. "Toxic" damaging steps of the interaction pathway are indicated with red arrows.

# BIBLIOGRAPHY


[1] A. Alzheimer, M. Strassnig, M. Ganguli, "About a Peculiar Disease of the Cerebral Cortex: Alzheimer's Original Case Revisited," *Psychiatry* **2005**.

[2] S. Karantzoulis, J. E. Galvin, "Distinguishing Alzheimer's disease from other major forms of dementia," *Expert review of neurotherapeutics* **2011**, *11*, 1579–1591.

[3] B. L. Plassman et al., "Prevalence of dementia in the United States: the aging, demographics, and memory study," *Neuroepidemiology* **2007**, *29*, 125–132.

[4] C. Reitz, R. Mayeux, "Alzheimer disease: epidemiology, diagnostic criteria, risk factors and biomarkers," *Biochemical pharmacology* **2014**, *88*, 640–651.

[5] M. D. C. Kawas, P. S. Gray, P. R. Brookmeyer, P. J. Fozard, and A. Zonderman, "Age-specific incidence rates of Alzheimer's disease The Baltimore Longitudinal Study of Aging," *neurology* **2000**, *54*.

[6] D. M. Holtzman, J. C. Morris, A. M. Goate, "Alzheimer's Disease: The Challenge of the Second Century," *Science Translational Medecine* **2011**, *3*.

[7] Mann DM., "Pyramidal nerve cell loss in Alzheimer's disease.," *Neurodegeneration* **1996**.

[8] D. J. Selkoe, "Alzheimer's Disease Is a Synaptic Failure," *science* **2002**, *298*.

[9] Jack CR, Petersen RC, Xu YC, Waring SC, O'Brien PC, "Medial temporal atrophy on MRI in normal aging and very mild Alzheimer's disease," *neurology* **1997**.

[10] A. C. Bozoki, I. O. Korolev, N. C. Davis, L. A. Hoisington, K. L. Berger, "Disruption of limbic white matter pathways in mild cognitive impairment and Alzheimer's disease: a DTI/FDG-PET study," *Human brain mapping* **2012**, *33*, 1792–1802.

[11] J. F. Norfray, J. M. Provenzale, "Alzheimer's disease: neuropathologic findings and recent advances in imaging," *AJR. American journal of roentgenology* **2004**, *182*, 3–13.

[12] Haass C, Schlossmacher M, Hung A, Vigo-Pelfrey C, et al., "Amyloid b-peptide is produced by cultured cells during normal metabolism.," *Nature* **1992**, *359*.

[13] S. Hartmann, H. J. Möbius, "Tolerability of memantine in combination with cholinesterase inhibitors in dementia therapy," *International clinical psychopharmacology* **2003**, *18*, 81–85.

[14] M. S. Rafii, P. S. Aisen, "Recent developments in Alzheimer's disease therapeutics," *BMC medicine* **2009**, *7*, 7.

[15] Gowing E, Roher A, Woods A, Cotter R, Chaney M, Little S, Ball M, "Chemical characterization of Ab 17-42 peptide, a component of diffuse amyloid deposits of Alzheimer disease.," *Journal of Biological Chemistry* **1994**, 10987–10990.

[16] T. M. J. Allinson, E. T. Parkin, A. J. Turner, N. M. Hooper, "ADAMs family members as amyloid precursor protein alpha-secretases," *Journal of neuroscience research* **2003**, *74*, 342–352.

[17] S. Kitazume, Y. Tachida, R. Oka, K. Shirotani, T. C. Saido, Y. Hashimoto, "Alzheimer's beta-secretase, beta-site amyloid precursor protein-cleaving enzyme, is responsible for cleavage secretion of a Golgi-resident sialyltransferase," *Proceedings of the National Academy of Sciences of the United States of America* **2001**, *98*, 13554–13559.

[18] Abramov E, Dolev I, Fogel H, Ciccotosto G, Ruff E, Slutsky I, "Amyloid-b as a positive endogenous regulator of release probability at hippocampal synapses.," *Nature neuroscience* **2009**, *12*, 567–1576.

[19] J. Milano, J. McKay, C. Dagenais, L. Foster-Brown, F. Pognan, R. Gadient, R. T. Jacobs, A. Zacco, B. Greenberg, P. J. Ciaccio, "Modulation of notch processing by gamma-secretase inhibitors causes intestinal goblet cell metaplasia and induction of genes known to specify gut secretory lineage differentiation," *Toxicological sciences : an official journal of the Society of Toxicology* **2004**, *82*, 341–358.

[20] Serneels L, Van Biervliet J, Craessaerts K, "g-Secretase heterogeneity in the Aph1 subunit: relevance for Alzheimer's disease.," *science* **2009**, 639–642.

[21] Aisen P, Saumier D, Briand R, Laurin J, Gervais F, Tremblay P, Garceau D, "A phase II study targeting amyloid-b with 3APS in mild-to-moderate Alzheimer disease.," *neurology* **2006**, *67*, 1757–1763.

[22] Ritchie C, Bush A, Mackinnon A, Macfarlane S, Mastwyk M, MacGregor L, Kiers L, Cherny R, "Metal-protein attenuation with iodochlorhydroxyquin (clioquinol) targeting Ab amyloid deposition and toxicity in Alzheimer diseaseToxicity in Alzheimer DiseaseA Pilot Phase 2 Clinical Trial," *Arch. Neurol.* **2003**, *60*, 1685–1691.

[23] C. Holmes et al., "Long-term effects of Ab42 immunisation in Alzheimer's disease: follow-up of a randomised, placebo-controlled phase I trial," *The Lancet* **2008**, *372*, 216–223.

[24] D.-S. Wang, D. W. Dickson, J. S. Malter, "beta-Amyloid degradation and Alzheimer's disease," *Journal of biomedicine & biotechnology* **2006**, *2006*, 58406.

[25] F. M. Longo, S. M. Massa, "Neuroprotective strategies in Alzheimer's disease," *Neurotherapeutics* **2004**, *1*, 117–127.

[26] V. W. Rodwell, D. A. Bender, K . M. Botham, P. J. Kennely, P. A. Weil, *Harper's Illustrated Biochemistry, 30th edition*.

[27] Y. E. Kim, M. S. Hipp, A. Bracher, M. Hayer-Hartl, F. U. Hartl, "Molecular chaperone functions in protein folding and proteostasis," *Annual review of biochemistry* **2013**, *82*, 323–355.

[28] J. N. Onuchic, P. G. Wolynes, "Theory of protein folding," *Current opinion in structural biology* **2004**, *14*, 70–75.

[29] M. Sunde, L. C. Serpell, M. Bartlam, P. E. Fraser, M. B. Pepys, C. C. Blake, "Common core structure of amyloid fibrils by synchrotron X-ray diffraction," *Journal of molecular biology* **1997**, *273*, 729–739.

[30] T. R. Jahn, O. S. Makin, K. L. Morris, K. E. Marshall, P. Tian, P. Sikorski, L. C. Serpell, "The common architecture of cross-beta amyloid," *Journal of molecular biology* **2010**, *395*, 717–727.

[31] L. C. Serpell, M. Sunde, M. D. Benson, G. A. Tennent, M. B. Pepys, P. E. Fraser, "The protofilament substructure of amyloid fibrils," *Journal of molecular biology* **2000**, *300*, 1033–1039.

[32] Nelson R, Sawaya M, Balbirnie M, Madsen A, Riekel C Grothe R, Eisenberg D, "Structure of the cross-beta spine of amyloid-like fibrils.," *Nature* **2005**, 773–778.

[33] M. Fandrich, "The behaviour of polyamino acids reveals an inverse side chain effect in amyloid structure formation," *The EMBO Journal* **2002**, *21*, 5682–5690.

[34] Chiti F, Calamai N, Taddei N, Stefani M, Ramponi G, Dobson C, "Studies of the aggregation of mutant proteins in vitro provide insights into the genetics of amyloid diseases," *Proc. Natl. Acad. Sci. USA* **2002**, 16419–16426.

[35] Kelly J, "The alternative conformations of amyloidogenic proteins and their multi-step assembly pathways.," *Current opinion in structural biology* **1998**, 101–106.

[36] M. R. H. Krebs, G. L. Devlin, A. M. Donald, "Amyloid fibril-like structure underlies the aggregate structure across the pH range for beta-lactoglobulin," *Biophysical journal* **2009**, *96*, 5013–5019.

[37] S. Zhang, T. Holmes, C. Lockshin, A. Rich, "Spontaneous assembly of a self-complementary oligopeptide to form a stable macroscopic membrane," *Proceedings of the National Academy of Sciences* **1993**, *90*, 3334–3338.

[38] J. E. Straub, D. Thirumalai, "Toward a molecular theory of early and late events in monomer to amyloid fibril formation," *Annual review of physical chemistry* **2011**, *62*, 437–463.

[39] Lomakin A, Chung D, Benedek G, Kirschner D, Teplow D, "On the nucleation and growth of amyloid b-protein fibrils: detection of nuclei and quantitation of rate constants.," *Proc. Natl. Acad. Sci. USA* **1996**, 1125–1129.

[40] S. J. Massi F, "Energy landscape theory for Alzheimer's amyloid b-peptide fibril elongation.," *Proteins* **2001**, 217–229.

[41] W. P. Esler, E. R. Stimson, J. M. Jennings, H. V. Vinters, J. R. Ghilardi, J. P. Lee, P. W. Mantyh, J. E. Maggio, "Alzheimer's Disease Amyloid Propagation by a Template-Dependent Dock-Lock Mechanism †," *Biochemistry* **2000**, *39*, 6288–6295.

[42] B. Caughey, P. T. Lansbury, "Protofibrils, pores, fibrils, and neurodegeneration: Separating the responsible protein aggregates from the innocent bystanders," *Annual review of neuroscience* **2003**, *26*, 267–298.

[43] R. J. O'Brien, P. C. Wong, "Amyloid precursor protein processing and Alzheimer's disease," *Annual review of neuroscience* **2011**, *34*, 185–204.

[44] R. Baruch-Suchodolsky, B. Fischer, "Abeta40, either soluble or aggregated, is a remarkably potent antioxidant in cell-free oxidative systems," *Biochemistry* **2009**, *48*, 4354–4370.

[45] A. Kontush, "Amyloid-b: an antioxidant that becomes a pro-oxidant and critically contributes to Alzheimer's disease," *Free Radical Biology and Medicine* **2001**, *31*, 1120–1131.

[46] M. Tabaton, X. Zhu, G. Perry, M. A. Smith, L. Giliberto, "Signaling effect of amyloid-beta(42) on the processing of AbetaPP," *Experimental neurology* **2010**, *221*, 18–25.

[47] U. Igbavboa, G. Y. Sun, G. A. Weisman, Y. He, W. G. Wood, "Amyloid beta-protein stimulates trafficking of cholesterol and caveolin-1 from the plasma membrane to the Golgi complex in mouse primary astrocytes," *Neuroscience* **2009**, *162*, 328–338.

[48] Y. Ohyagi et al., "Intracellular Abeta42 activates p53 promoter: a pathway to neurodegeneration in Alzheimer's disease," *FASEB journal : official publication of the Federation of American Societies for Experimental Biology* **2005**, *19*, 255–257.

[49] M. Takami, Y. Nagashima, Y. Sano, S. Ishihara, M. Morishima-Kawashima, S. Funamoto, Y. Ihara, "gamma-Secretase: successive tripeptide and tetrapeptide release from the transmembrane domain of beta-carboxyl terminal fragment," *The Journal of neuroscience : the official journal of the Society for Neuroscience* **2009**, *29*, 13042–13052.

[50] Iwatsubo T, Saido T, Mann D, Lee V, Trojanowski J, "Full-length amyloid-b(1-42(43)) and amino-terminally modified and truncated amyloid-b42(43) deposit in diffuse plaques," *Am. J. of Pathology* **1996**, *34*, 11.

[51] H. Welander, J. Frånberg, C. Graff, E. Sundström, B. Winblad, L. O. Tjernberg, "Abeta43 is more frequent than Abeta40 in amyloid plaque cores from Alzheimer disease brains," *Journal of Neurochemistry* **2009**, *110*, 697–706.

[52] Joseph T. Jarrett, Elizabeth P. Berger, and Peter T. Lansbury, Jr., "The Carboxy Terminus of the Amyloid Protein Is Critical for the Seeding of Amyloid Formation: Implications for the Pathogenesis of Alzheimer's Disease," *Biochemistry* **1993**, *32*, 4693–4697.

[53] Y. Yoshiike, D.-H. Chui, T. Akagi, N. Tanaka, A. Takashima, "Specific compositions of amyloid-beta peptides as the determinant of toxic beta-aggregation," *The Journal of biological chemistry* **2003**, *278*, 23648–23655.

[54] A. Jan, O. Gokce, R. Luthi-Carter, H. A. Lashuel, "The ratio of monomeric to aggregated forms of Abeta40 and Abeta42 is an important determinant of amyloid-beta aggregation, fibrillogenesis, and toxicity," *The Journal of biological chemistry* **2008**, *283*, 28176–28189.

[55] J. Kim, L. Onstead, S. Randle, R. Price, L. Smithson, C. Zwizinski, D. W. Dickson, T. Golde, E. McGowan, "Abeta40 inhibits amyloid deposition in vivo," *The Journal of neuroscience : the official journal of the Society for Neuroscience* **2007**, *27*, 627–633.

[56] J. J. Balbach, A. T. Petkova, N. A. Oyler, O. N. Antzutkin, D. J. Gordon, S. C. Meredith, R. Tycko, "Supramolecular Structure in Full-Length Alzheimer's b -Amyloid Fibrils: Evidence for a Parallel b -Sheet Organization from Solid-State Nuclear Magnetic Resonance," *Biophysical journal* **2002**, *83*, 1205–1216.

[57] Luhrs T, Ritter C, Adrian M, Riek-Loher D, Bohrmann B, Döbeli H, Schubert D, Riek R, "3D Structure of Alzheimer's amyloid-b(1-42) fibrils.," *Proc. Natl. Acad. Sci. USA* **2005**, 17342–17347.

[58] A. T. Petkova, Y. Ishii, J. J. Balbach, O. N. Antzutkin, R. D. Leapman, F. Delaglio, R. Tycko, "A structural model for Alzheimer's beta -amyloid fibrils based on experimental constraints from solid state NMR," *Proceedings of the National Academy of Sciences of the United States of America* **2002**, *99*, 16742–16747.

[59] R. D. Terry, E. Masliah, D. P. Salmon, N. Butters, R. DeTeresa, R. Hill, L. A. Hansen, R. Katzman, "Physical basis of cognitive alterations in Alzheimer's disease: synapse loss is the major correlate of cognitive impairment," *Annals of neurology* **1991**, *30*, 572–580.

[60] C. J. Pike, A. J. Walencewicz, C. G. Glabe, C. W. Cotman, "In vitro aging of ß-amyloid protein causes peptide aggregation and neurotoxicity," *Brain Research* **1991**, *563*, 311–314.

[61] C. A. McLean, R. A. Cherny, F. W. Fraser, S. J. Fuller, M. J. Smith, K. Vbeyreuther, A. I. Bush, C. L. Masters, "Soluble pool of A? amyloid as a determinant of severity of neurodegeneration in Alzheimer's disease," *Annals of Neurology* **1999**, *46*, 860–866.

[62] P. F. Chapman et al., "Impaired synaptic plasticity and learning in aged amyloid precursor protein transgenic mice," *Nature neuroscience* **1999**, *2*, 271–276.

[63] J.-C. Dodart et al., "Immunization reverses memory deficits without reducing brain Abeta burden in Alzheimer's disease model," *Nature neuroscience* **2002**, *5*, 452–457.

[64] Walsh D, Lomakin A, Benedek G, Condron M, Teplow D, "Amyloid b-protein fibrillogenesis. Detection of a protofibrillar intermediate.," *Journal of Biological Chemistry* **1997**, 22364–22373.

[65] M. P. Lambert et al., "Diffusible, nonfibrillar ligands derived from A 1-42 are potent central nervous system neurotoxins," *Proceedings of the National Academy of Sciences* **1998**, *95*, 6448–6453.

[66] S. Lesné, M. T. Koh, L. Kotilinek, R. Kayed, C. G. Glabe, A. Yang, M. Gallagher, K. H. Ashe, "A specific amyloid-beta protein assembly in the brain impairs memory," *Nature* **2006**, *440*, 352–357.

[67] M. Hoshi, M. Sato, S. Matsumoto, A. Noguchi, K. Yasutake, N. Yoshida, K. Sato, "Spherical aggregates of beta-amyloid (amylospheroid) show high neurotoxicity and activate tau protein kinase I/glycogen synthase kinase-3beta," *Proceedings of the National Academy of Sciences of the United States of America* **2003**, *100*, 6370–6375.

[68] Kayed R, Head E, Thompson J, McIntire T, Milton S, Cotman C, Glabe C, "Common structure of soluble amyloid oligomers implies common mechanism of pathogenesis," *Science (New York N.Y.)* **2003**, *300*, 486–489.

[69] Alberts B, Johnson A, Lewis J, et al., *Molecular Biology of the Cell. The Compartmentalization of Cells*, 4th edition, New York, **2002**.

[70] R. B. Gennis, *Biomembranes. Molecular Structure and Function*, Springer Verlag, New York, **1989**.

[71] R. O. Calderon, B. Attema, G. H. DeVries, "Lipid Composition of Neuronal Cell Bodies and Neurites from Cultured Dorsal Root Ganglia," *Journal of Neurochemistry* **1995**, *64*, 424–429.

[72] D. Marsh, "Lateral pressure profile, spontaneous curvature frustration, and the incorporation and conformation of proteins in membranes," *Biophysical journal* **2007**, *93*, 3884–3899.

[73] J. Huang, G. W. Feigenson, "A Microscopic Interaction Model of Maximum Solubility of Cholesterol in Lipid Bilayers," *Biophysical journal* **1999**, *76*, 2142–2157.

[74] S. J. Singer, G. L. Nicolson, "The Fluid Mosaic Model of the Structure of Cell Membranes," *science* **1972**.

[75] G. L. Nicolson, "The Fluid-Mosaic Model of Membrane Structure: still relevant to understanding the structure, function and dynamics of biological membranes after more than 40 years," *Biochimica et biophysica acta* **2014**, *1838*, 1451–1466.

[76] D. Lingwood, J. Ries, P. Schwille, K. Simons, "Plasma membranes are poised for activation of raft phase coalescence at physiological temperature," *Proceedings of the National Academy of Sciences of the United States of America* **2008**, *105*, 10005–10010.

[77] G.L. Nicolson, S. J. Singer, "The distribution and asymmetry of saccharides on mammalian cell membrane surfaces utilizing ferritin-conjugated plant agglutinins as specific saccharide stains," *J. Cell Biol.* **1974**, *60*, 236–248.

[78] J. L. J.E. Rothman, "Membrane asymmetry," *science* **1977**, *195*, 743–753.

[79] D. L. Daleke, "Regulation of transbilayer plasma membrane phospholipid asymmetry," *Journal of lipid research* **2003**, *44*, 233–242.

[80] H. T. McMahon, J. L. Gallop, "Membrane curvature and mechanisms of dynamic cell membrane remodelling," *Nature* **2005**, *438*, 590–596.

[81] K. G. J. Zimmerberg, "The physical chemistry of biological membranes," *Nat. Chem Biol.* **2006**, *11*, 564–567.

[82] F. J. Sharom, "Flipping and flopping–lipids on the move," *IUBMB life* **2011**, *63*, 736–746.

[83] G. Lindblom, G. Orädd, "Lipid lateral diffusion and membrane heterogeneity," *Biochimica et biophysica acta* **2009**, *1788*, 234–244.

[84] Y.-K. Shin, J. H. Freed, "Thermodynamics of phosphatidylcholine-cholesterol mixed model membranes in the liquid crystalline state studied by the orientational order parameter," *Biophysical journal* **1989**, *56*, 1093–1100.

[85] M. Bretscher, S. Munro, "Cholesterol and the Golgi apparatus," *science* **1993**, *261*, 1280–1281.

[86] J. Aittoniemi, P. S. Niemelä, M. T. Hyvönen, M. Karttunen, I. Vattulainen, "Insight into the putative specific interactions between cholesterol, sphingomyelin, and palmitoyl-oleoyl phosphatidylcholine," *Biophysical journal* **2007**, *92*, 1125–1137.

[87] K. Simons, J. L. Sampaio, "Membrane organization and lipid rafts," *Cold Spring Harbor perspectives in biology* **2011**, *3*, a004697.

[88] K. S. D. Lingwood, "Lipid rafts as a membrane-organizing principle.," *science* **2010**, *327*, 46–50.

[89] A. P, Smith, H. H, Loh, "Architecture of the nerve ending membrane," *Life Sciences* **1979**, *24*, 1–20.

[90] W. Dowhan, M. Bogdanov, E. Mileykovskaya, *Biochemistry of Lipids: Lipoproteins and Membranes 4th Ed*, Elsevier, San Diego.

[91] B. A. Tsui-Pierchala, M. Encinas, J. Milbrandt, E. M. Johnson, "Lipid rafts in neuronal signaling and function," *Trends in Neurosciences* **2002**, *25*, 412–417.

[92] F. S. Walsh, P. Doherty, "Neural cell adhesion molecules of the immunoglobulin superfamily: role in axon growth and guidance," *Annual review of cell and developmental biology* **1997**, *13*, 425–456.

[93] J. R. Martens, R. Navarro-Polanco, E. A. Coppock, A. Nishiyama, L. Parshley, T. D. Grobaski, M. M. Tamkun, "Differential Targeting of Shaker-like Potassium Channels to Lipid Rafts," *Journal of Biological Chemistry* **2000**, *275*, 7443–7446.

[94] Geula C, Wu CK, Saroff D, Lorenzo A, Yuan M, Yankner BA., "Aging renders the brain vulnerable to amyloid beta-protein neurotoxicity.," *Nature methods* **1998**, *4*, 827–831.

[95] V. FOLKIS, A. STUPINA, O. MARTINENKO, S. TOTH, A. TIMCHENKO, "Aging of neurons in the mollusc Lymnaea stagnalis. Structure, function and sensitivity to transmitters," *Mechanisms of Ageing and Development* **1984**, *25*, 91–102.

[96] Svennerholm L, Bostrom K, Jungbjer B, Olsson L., "Membrane lipids of adult human brain: lipid composition of frontal and temporal lobe in subjects of age 20–100 years.," *Journal of Neurochemistry* **1994**, *63*, 1802–1811.

[97] S. Sonnino, V. Chigorno, "Ganglioside molecular species containing C18- and C20-sphingosine in mammalian nervous tissues and neuronal cell cultures," *Biochimica et Biophysica Acta (BBA) - Reviews on Biomembranes* **2000**, *1469*, 63–77.

[98] Angelie E, Bonmartin A, Boudraa A, Gonnaud PM, Mallet JJ, Sappey-Marinier D., "Regional differences and metabolic changes in normal aging of the human brain: proton MR spectroscopic imaging study.," *Ajnr* **2001**, *22(1)*, 119–127.

[99] Soderberg M, Edlund C, Kristensson K, Dallner G., "Lipid compositions of different regions of the human brain during aging.," *Journal of Neurochemistry* **1990**, 415–423.

[100] Igbavboa U, Avdulov NA, Schroeder F, Wood WG., "Increasing age alters transbilayer fluidity and cholesterol asymmetry in synaptic plasma membranes of mice.," *Journal of Neurochemistry* **1996**, 1717–1725.

[101] N. M. Giusto, M. E. Roque, M. G. Ilincheta de Boschero, "Effects of aging on the content, composition and synthesis of sphingomyelin in the central nervous system," *Lipids* **1992**, *27*, 835–839.

[102] E. Posse de Chaves, S. Sipione, "Sphingolipids and gangliosides of the nervous system in membrane function and dysfunction," *FEBS Letters* **2010**, *584*, 1748–1759.

[103] Favrelere S, Stadelmann-Ingrand S, Huguet F, De Javel D, Piriou A, Tallineau C, "Age-related changes in ethanolamine glycerophospholipid fatty acid levels in rat frontal cortex and hippocampus.," *Neurobiology of Aging* **2000**, *21*, 653–660.

[104] Lopez GH, Ilincheta de Boschero MG, Castagnet PI, Giusto NM., "Age-associated changes in the content and fatty acid composition of brain glycerophospholipids.," *Biochem Mol Biol* **1995**, 331–343.

[105] W. E. Hazel JR, "The role of alterations in membrane lipid composition in enabling physiological adaptation of organisms to their physical environment.," *Prog Lipid Res* **1990**, *29*, 167–227.

[106] E. S. Rosenzweig, C. A. Barnes, "Impact of aging on hippocampal function: plasticity, network dynamics, and cognition," *Progress in Neurobiology* **2003**, *69*, 143–179.

[107] S. T. Jahn R, "Membrane fusion and exocytosis.," *Annual review of biochemistry* **1999**, *68*, 863–911.

[108] Z. Chen, R. P. Rand, "The influence of cholesterol on phospholipid membrane curvature and bending elasticity," *Biophysical journal* **1997**, *73*, 267–276.

[109] M. A. Churchward, T. Rogasevskaia, J. Höfgen, J. Bau, J. R. Coorssen, "Cholesterol facilitates the native mechanism of Ca2+-triggered membrane fusion," *Journal of cell science* **2005**, *118*, 4833–4848.

[110] C. Frank, A. M. Giammarioli, R. Pepponi, C. Fiorentini, S. Rufini, "Cholesterol perturbing agents inhibit NMDA-dependent calcium influx in rat hippocampal primary culture," *FEBS Letters* **2004**, *566*, 25–29.

[111] T. Rogasevskaia, J. R. Coorssen, "Sphingomyelin-enriched microdomains define the efficiency of native Ca(2+)-triggered membrane fusion," *Journal of cell science* **2006**, *119*, 2688–2694.

[112] H.-T. Cheng, E. London, "Preparation and properties of asymmetric large unilamellar vesicles: interleaflet coupling in asymmetric vesicles is dependent on temperature but not curvature," *Biophysical journal* **2011**, *100*, 2671–2678.

[113] S. Sonnino, L. Mauri, V. Chigorno, A. Prinetti, "Gangliosides as components of lipid membrane domains," *Glycobiology* **2007**, *17*, 1R–13R.

[114] N. Yamamoto, U. Igbabvoa, Y. Shimada, Y. Ohno-Iwashita, M. Kobayashi, W. G. Wood, S. C. Fujita, K. Yanagisawa, "Accelerated Abeta aggregation in the presence of GM1-ganglioside-accumulated synaptosomes of aged apoE4-knock-in mouse brain," *FEBS Letters* **2004**, *569*, 135–139.

[115] C. J. Pei B, "More ordered, convex ganglioside-enriched membrane domains: the effects of GM1 on sphingomyelin bilayers containing a low level of cholesterol.," *J. Biochem* **2003**, 575–581.

[116] A. A. Cole, A. Dosemeci, T. S. Reese, "Co-segregation of AMPA receptors with G(M1) ganglioside in synaptosomal membrane subfractions," *The Biochemical journal* **2010**, *427*, 535–540.

[117] H. P. Morrison JH, "Life and death of neurons in the aging brain.," *science* **1997**, *278*, 412–419.

[118] B. S. McEwen, "Physiology and neurobiology of stress and adaptation: central role of the brain," *Physiological reviews* **2007**, *87*, 873–904.

[119] I. C. Paratcha G, "Lipid rafts and the control of neurotrophic factor signaling in the nervous system: variations on a theme.," *Current opinion Neurobiol* **2002**, *12*, 542–549.

[120] F. Iannilli, A. O. Sodero, M. D. Ledesma, C. G. Dotti, "Oxidative stress activates the pro-survival TrkA pathway through membrane cholesterol loss," *Neurobiology of Aging* **2011**, *32*, 1033–1042.

[121] V. Jain, M. C. Langham, F. W. Wehrli, "MRI estimation of global brain oxygen consumption rate," *Journal of cerebral blood flow and metabolism : official journal of the International Society of Cerebral Blood Flow and Metabolism* **2010**, *30*, 1598–1607.

[122] C. Rice-Evans, R. Burdon, "Free radical-lipid interactions and their pathological consequences," *Progress in Lipid Research* **1993**, *32*, 71–110.

[123] A. Reis, C. M. Spickett, "Chemistry of phospholipid oxidation," *Biochimica et biophysica acta* **2012**, *1818*, 2374–2387.

[124] L. I. Barsukov, A. V. Victorov, I. A. Vasilenko, R. P. Evstigneeva, L. D. Bergelson, "Investigation of the inside-outside distribution, intermembrane exchange and transbilayer movement of phospholipids in sonicated vesicles by shift reagent NMR," *Biochimica et Biophysica Acta (BBA) - Biomembranes* **1980**, *598*, 153–168.

[125] Ho L, Pieroni C, Winger D, Purohit DP, Aisen PS, Pasinetti GM., "Regional distribution of cyclooxygenase-2 in the hippocampal formation in Alzheimer's disease," *J Neurosci Res* **1999**, *57*, 295–303.

[126] F. Magni, C. Galbusera, L. Tremolada, C. Ferrarese, M. G. Kienle, "Characterisation of adducts of the lipid peroxidation product 4-hydroxy-2-nonenal and amyloid beta-peptides by liquid chromatography/electrospray ionisation mass spectrometry," *Rapid communications in mass spectrometry : RCM* **2002**, *16*, 1485–1493.

[127] Uz T, Pesold C, Longone P, Manev H, "Aging-associated up-regulation of neuronal 5-lipoxygenase expression: putative role in neuronal vulnerability," *FASEB journal : official publication of the Federation of American Societies for Experimental Biology* **1998**, *12*, 439–449.

[128] J. L. Kanter, S. Narayana, P. P. Ho, I. Catz, K. G. Warren, R. A. Sobel, L. Steinman, W. H. Robinson, "Lipid microarrays identify key mediators of autoimmune brain inflammation," *Nature medicine* **2006**, *12*, 138–143.

[129] P. Whitley, B. J. Reaves, M. Hashimoto, A. M. Riley, B. V. L. Potter, G. D. Holman, "Identification of mammalian Vps24p as an effector of phosphatidylinositol 3,5-bisphosphate-dependent endosome compartmentalization," *The Journal of biological chemistry* **2003**, *278*, 38786–38795.

[130] J. M. Kavran, D. E. Klein, A. Lee, M. Falasca, S. J. Isakoff, E. Y. Skolnik, M. A. Lemmon, "Specificity and Promiscuity in Phosphoinositide Binding by Pleckstrin Homology Domains," *Journal of Biological Chemistry* **1998**, *273*, 30497–30508.

[131] D. Marsh, "Lateral pressure in membranes," *Biochimica et Biophysica Acta (BBA) - Reviews on Biomembranes* **1996**, *1286*, 183–223.

[132] H. Brockman, "Lipid monolayers : why use half membrane to characterize protein–membrane interactions?" *Current opinion in structural biology* **1999**, *9*, 438–443.

[133] J. Sarkis, J.-F. Hubert, B. Legrand, E. Robert, A. Chéron, J. Jardin, E. Hitti, E. Le Rumeur, V. Vié, "Spectrin-like repeats 11-15 of human dystrophin show adaptations to a lipidic environment," *The Journal of biological chemistry* **2011**, *286*, 30481–30491.

[134] C. W. Meuse, G. Niaura, M. L. Lewis, A. L. Plant, "Assessing the Molecular Structure of Alkanethiol Monolayers in Hybrid Bilayer Membranes with Vibrational Spectroscopies," *Langmuir* **1998**, *14*, 1604–1611.

[135] E. T. Castellana, P. S. Cremer, "Solid supported lipid bilayers: From biophysical studies to sensor design," *Surface Science Reports* **2006**, *61*, 429–444.

[136] V. Kiessling, L. K. Tamm, "Measuring Distances in Supported Bilayers by Fluorescence Interference-Contrast Microscopy: Polymer Supports and SNARE Proteins," *Biophysical journal* **2003**, *84*, 408–418.

[137] S. Morandat, S. Azouzi, E. Beauvais, A. Mastouri, K. El Kirat, "Atomic force microscopy of model lipid membranes," *Analytical and bioanalytical chemistry* **2013**, *405*, 1445–1461.

[138] C. B. Fox, J. R. Wayment, G. A. Myers, S. K. Endicott, J. M. Harris, "Single-molecule fluorescence imaging of peptide binding to supported lipid bilayers," *Analytical chemistry* **2009**, *81*, 5130–5138.

[139] Q. Hong et al., "Two-step membrane binding by Equinatoxin II, a pore-forming toxin from the sea anemone, involves an exposed aromatic cluster and a flexible helix," *The Journal of biological chemistry* **2002**, *277*, 41916–41924.

[140] M. Besenicar, P. Macek, J. H. Lakey, G. Anderluh, "Surface plasmon resonance in protein-membrane interactions," *Chemistry and physics of lipids* **2006**, *141*, 169–178.

[141] A. L. Lai, H. Park, J. M. White, L. K. Tamm, "Fusion peptide of influenza hemagglutinin requires a fixed angle boomerang structure for activity," *The Journal of biological chemistry* **2006**, *281*, 5760–5770.

[142] Y. Li, L. K. Tamm, "Structure and plasticity of the human immunodeficiency virus gp41 fusion domain in lipid micelles and bilayers," *Biophysical journal* **2007**, *93*, 876–885.

[143] M. M. Baksh, M. Jaros, J. T. Groves, "Detection of molecular interactions at membrane surfaces through colloid phase transitions," *Nature* **2004**, *427*, 139–141.

[144] B. Kolesinska et al., "Permeation through phospholipid bilayers, skin-cell penetration, plasma stability, and CD spectra of a- and b-oligoproline derivatives," *Chemistry & biodiversity* **2013**, *10*, 1–38.

[145] Thor D. Osborn, Paul Yager, "Formation of Planar Solvent-Free Phospholipid Bilayers by Langmuir-Blodgett Transfer of Monolayers to Micromachined Apertures in Silicon," *Langmuir* **1995**, *11*, 8–12.

[146] A. Honigmann, C. Walter, F. Erdmann, C. Eggeling, R. Wagner, "Characterization of horizontal lipid bilayers as a model system to study lipid phase separation," *Biophysical journal* **2010**, *98*, 2886–2894.

[147] A. Samad, Y. Sultana, M. Aqil, "Liposomal Drug Delivery Systems: An Update Review," *Current Drug Delivery* **2007**, *4*, 297–305.

[148] N. S. Hatzakis, V. K. Bhatia, J. Larsen, K. L. Madsen, P.-Y. Bolinger, A. H. Kunding, J. Castillo, U. Gether, P. Hedegård, D. Stamou, "How curved membranes recruit amphipathic helices and protein anchoring motifs," *Nature chemical biology* **2009**, *5*, 835–841.

[149] A. H. Kunding, M. W. Mortensen, S. M. Christensen, D. Stamou, "A fluorescence-based technique to construct size distributions from single-object measurements: application to the extrusion of lipid vesicles," *Biophysical journal* **2008**, *95*, 1176–1188.

[150] F. Heinemann, V. Betaneli, F. A. Thomas, P. Schwille, "Quantifying lipid diffusion by fluorescence correlation spectroscopy: a critical treatise," *Langmuir : the ACS journal of surfaces and colloids* **2012**, *28*, 13395–13404.

[151] D. D. M.I. Angelova, "Liposome electroformation," *Faraday Discuss. Chem. Soc.* **1986**, *81*, 303–311.

[152] K. Carvalho, L. Ramos, C. Roy, C. Picart, "Giant unilamellar vesicles containing phosphatidylinositol(4,5)bisphosphate: characterization and functionality," *Biophysical journal* **2008**, *95*, 4348–4360.

[153] O. L. Baron, D. Pauron, S. Antipolis, "Protein-lipid interaction analysis by surface plasmon resonance (SPR).," *Bio-protocol* **2014**, *4*, 1–8.

[154] J. Homola, S. S. Yee, G. Gauglitz, "Surface plasmon resonance sensors: review," *Sensors and Actuators B: Chemical* **1999**, *54*, 3–15.

[155] M. Geitmann, U. H. Danielson, "Studies of substrate-induced conformational changes in human cytomegalovirus protease using optical biosensor technology," *Analytical biochemistry* **2004**, *332*, 203–214.

[156] G. Sauerbrey, "Verwendung von Schwingquarzen zur Wgung dnner Schichten und zur Mikrowgung," *Zeitschrift fr Physik* **1959**, *155*, 206–222.

[157] K. Keiji Kanazawa, J. G. Gordon, "The oscillation frequency of a quartz resonator in contact with liquid.," *Anal. Chim. Acta* **1985**, 99–105.

[158] J. A. Kotarek, K. C. Johnson, M. A. Moss, "Quartz crystal microbalance analysis of growth kinetics for aggregation intermediates of the amyloid-beta protein," *Analytical biochemistry* **2008**, *378*, 15–24.

[159] E. Chason, T. M. Mayer, "Thin film and surface characterization by specular X-ray reflectivity," *Critical Reviews in Solid State and Materials Sciences* **1997**, *22*, 1–67.

[160] H. Hähl, I. Möller, I. Kiesel, S. Campioni, R. Riek, D. Verdes, S. Seeger, "a-Synuclein insertion into supported lipid bilayers as seen by in situ X-ray reflectivity," *ACS chemical neuroscience* **2015**, *6*, 374–379.

[161] X.-L. Zhou, S.-H. Chen, "Theoretical foundation of X-ray and neutron reflectometry," *Physics Reports* **1995**, *257*, 223–348.

[162] Basso M, Giarre L, Dahleh M, Mezic I., "Numerical analysis of complex dynamics in atomic force microscopes.," *Proc. IEEE conf Control Appl. Trieste* **1998**, 1026–1030.

[163] Sebastian A, Salapaka M, Chen D, Cleveland J., "Harmonic analysis based modeling of tapping-mode AFM," *Proc Am Control Conf. San Diego CA* **1999**, 232–236.

[164] E. Drolle, F. Hane, B. Lee, Z. Leonenko, "Atomic force microscopy to study molecular mechanisms of amyloid fibril formation and toxicity in Alzheimer's disease," *Drug metabolism reviews* **2014**, *46*, 207–223.

[165] G. Binnig, C. F. Quate, and Ch. Gerber, "Atomic Force Microscope," *Physical review letters* **1986**, *56*.

[166] Thomas E. Fisher, Andres F. Oberhauser, "The study of protein mechanics with the atomic force microscope," *TIBS* **1999**, *24*.

[167] Robert W. Woody, "Circular Dichroism: Methods in enzymology," **1995**, *246*.

[168] P. Wittung-Stafshede, "A stable, molten-globule-like cytochrome c," *Biochimica et Biophysica Acta (BBA) - Protein Structure and Molecular Enzymology* **1998**, *1382*, 324–332.

[169] J. Walker, *The Protein Protocols Handbook.* Humana Press, **2002**.

[170] I. Wittig, H.-P. Braun, H. Schägger, "Blue native PAGE," *Nature protocols* **2006**, *1*, 418–428.

[171] R. Pujol-Pina, S. Vilaprinyó-Pascual, R. Mazzucato, A. Arcella, M. Vilaseca, M. Orozco, N. Carulla, "SDS-PAGE analysis of Ab oligomers is disserving research into Alzheimer´s disease: appealing for ESI-IM-MS," *Scientific reports* **2015**, *5*, 14809.

[172] A. J. Edwards, D. Reid, "Introduction to NMR of proteins," *Current protocols in protein science* **2001**, *Chapter 17*, Unit 17.5.

[173] E.R. Andrew, A. Bradbury, R.G. Eades, "Nuclear magnetic resonance spectra from a crystal rotated at high speed," *Nature* **1958**, *182*, 1659.

[174] C. Kim, J. Spano, E.-K. Park, S. Wi, "Evidence of pores and thinned lipid bilayers induced in oriented lipid membranes interacting with the antimicrobial peptides, magainin-2 and aurein-3.3," *Biochimica et biophysica acta* **2009**, *1788*, 1482–1496.

[175] M. Sauer, J. Hofkens, and J. Enderlein, *Handbook of Fluorescence Spectroscopy and Imaging*, WILEY-VCH Verlag GmbH & Co, Weinheim, **2011**.

[176] Y. Xing, E. Borguet, "Specificity and sensitivity of fluorescence labeling of surface species," *Langmuir : the ACS journal of surfaces and colloids* **2007**, *23*, 684–688.

[177] Schermelleh L, Carlton PM, Haase S, Shao L, Winoto L, et al., "Subdiffraction multicolor imaging of the nuclear periphery with 3D structured illumination microscopy.," *science* **2008**, *320*, 1332–133.

[178] V. Westphal, S. W. Hell, "Nanoscale resolution in the focal plane of an optical microscope," *Physical review letters* **2005**, *94*, 143903.

[179] M. G. L. Gustafsson, "Nonlinear structured-illumination microscopy: wide-field fluorescence imaging with theoretically unlimited resolution," *Proceedings of the National Academy of Sciences of the United States of America* **2005**, *102*, 13081–13086.

[180] M. J. Rust, M. Bates, X. Zhuang, "Sub-diffraction-limit imaging by stochastic optical reconstruction microscopy (STORM)," *Nature methods* **2006**, *3*, 793–795.

[181] K. N. Fish, "Total internal reflection fluorescence (TIRF) microscopy," *Current protocols in cytometry* **2009**, *Chapter 12*, Unit12.18.

[182] D. Axelrod, "Cell-substrate contacts illuminated by total internal reflection fluorescence," *The Journal of Cell Biology* **1981**, *89*, 141–145.

[183] D. Verdes, T. Ruckstuhl, S. Seeger, "Parallel two-channel near- and far-field fluorescence microscopy," *J. Biomed. Opt. 12(3)* **2007**.

[184] L. Stryer, "Fluorescence energy transfer as a spectroscopic ruler," *Annual review of biochemistry* **1978**, *47*, 819–846.

[185] G. Kang, I. López-Peña, V. Oklejas, C. S. Gary, W. Cao, J. E. Kim, "Förster resonance energy transfer as a probe of membrane protein folding," *Biochimica et biophysica acta* **2012**, *1818*, 154–161.

[186] M. Rabe, A. Soragni, N. P. Reynolds, D. Verdes, E. Liverani, R. Riek, S. Seeger, "On-surface aggregation of a-synuclein at nanomolar concentrations results in two distinct growth mechanisms," *ACS chemical neuroscience* **2013**, *4*, 408–417.

[187] E. L. Elson, "Fluorescence correlation spectroscopy: past, present, future," *Biophysical journal* **2011**, *101*, 2855–2870.

[188] J. Sýkora, K. Kaiser, I. Gregor, W. Bönigk, G. Schmalzing, J. Enderlein, "Exploring fluorescence antibunching in solution to determine the stoichiometry of molecular complexes," *Analytical chemistry* **2007**, *79*, 4040–4049.

[189] J. M. Tsay, S. Doose, S. Weiss, "Rotational and translational diffusion of peptide-coated CdSe/CdS/ZnS nanorods studied by fluorescence correlation spectroscopy," *Journal of the American Chemical Society* **2006**, *128*, 1639–1647.

[190] G. D. E. Smith, "Modern Raman Spectroscopy – A Practical Approach," *Wiley* **2005**.

[191] A. Rygula, K. Majzner, K. M. Marzec, A. Kaczor, M. Pilarczyk, M. Baranska, "Raman spectroscopy of proteins: A review," *Journal of Raman Spectroscopy* **2013**, *44*, 1061–1076.

[192] E. V. Efremov, F. Ariese, C. Gooijer, "Achievements in resonance Raman spectroscopy review of a technique with a distinct analytical chemistry potential," *Analytica chimica acta* **2008**, *606*, 119–134.

[193] A. C. Benniston, P. Matousek, I. E. McCulloch, A. W. Parker, M. Towrie, "Detailed Picosecond Kerr-Gated Time-Resolved Resonance Raman Spectroscopy and Time-Resolved Emission Studies of Merocyanine 540 in Various Solvents," *The Journal of Physical Chemistry A* **2003**, *107*, 4347−4353.

[194] David L. Jeanmaire, Richard P. Van Duyne, "Surface raman spectroelectrochemistry. Part I. Heterocyclic, aromatic, and aliphatic amines adsorbed on the anodized silver electrode," *Journal of Electroanalytical Chemistry* **1977**, *84*, 1–20.

[195] C. L. Haynes, R. P. van Duyne, "Nanosphere Lithography: A Versatile Nanofabrication Tool for Studies of Size-Dependent Nanoparticle Optics," *The Journal of Physical Chemistry B* **2001**, *105*, 5599–5611.

[196] H. Xu, J. Aizpurua, M. Käll, P. Apell, "Electromagnetic contributions to single-molecule sensitivity in surface-enhanced Raman scattering," *Physical Review E* **2000**, *62*, 4318–4324.

[197] D. Serrano, S. Seeger, "Supercritical angle Raman microscopy: A surface-sensitive nanoscale technique without field enhancement," *Light: Science & Applications* **2017**, *6*, e17066.

[198] A. Itkin, V. Dupres, Y. F. Dufrêne, B. Bechinger, J.-M. Ruysschaert, V. Raussens, "Calcium ions promote formation of amyloid b-peptide (1-40) oligomers causally implicated in neuronal toxicity of Alzheimer's disease," *PloS one* **2011**, *6*, e18250.

[199] R. P. Richter, R. Berat, A. R. Brisson, "Formation of solid-supported lipid bilayers: An integrated view," *Langmuir : the ACS journal of surfaces and colloids* **2006**, *22*, 3497–3505.

[200] P. Schwille, J. Korlach, W. W. Webb, "Fluorescence correlation spectroscopy with single-molecule sensitivity on cell and model membranes," *Cytometry* **1999**, *36*, 176–182.

[201] E. L. Elson, D. Magde, "Fluorescence correlation spectroscopy. I. Conceptual basis and theory," *Biopolymers* **1974**, *13*, 1–27.

[202] J. Ries, T. Ruckstuhl, D. Verdes, P. Schwille, "Supercritical angle fluorescence correlation spectroscopy," *Biophysical journal* **2008**, *94*, 221–229.

[203] T. Cordes, A. Maiser, C. Steinhauer, L. Schermelleh, P. Tinnefeld, "Mechanisms and advancement of antifading agents for fluorescence microscopy and single-molecule spectroscopy," *Physical chemistry chemical physics : PCCP* **2011**, *13*, 6699–6709.

[204] G. T. Dempsey, J. C. Vaughan, K. H. Chen, M. Bates, X. Zhuang, "Evaluation of fluorophores for optimal performance in localization-based super-resolution imaging," *Nature methods* **2011**, *8*, 1027–1036.

[205] *Molecular Probes Handbook - A Guide to Fluorescent Probes and Labeling Technologies 11th Edition (2010).*

[206] E. K. Esbjörner, F. Chan, E. Rees, M. Erdelyi, L. M. Luheshi, C. W. Bertoncini, C. F. Kaminski, C. M. Dobson, G. S. Kaminski Schierle, "Direct observations of amyloid b self-assembly in live cells provide insights into differences in the kinetics of Ab(1-40) and Ab(1-42) aggregation," *Chemistry & biology* **2014**, *21*, 732–742.

[207] L.-P. Choo-Smith, W. K. Surewicz, "The interaction between Alzheimer amyloid b(1-40) peptide and ganglioside G M1 -containing membranes," *FEBS Letters* **1997**, *402*, 95–98.

[208] H. Hayashi et al., "A seed for Alzheimer amyloid in the brain," *The Journal of neuroscience : the official journal of the Society for Neuroscience* **2004**, *24*, 4894–4902.

[209] L. Qiu, A. Lewis, J. Como, M. W. Vaughn, J. Huang, P. Somerharju, J. Virtanen, K. H. Cheng, "Cholesterol modulates the interaction of beta-amyloid peptide with lipid bilayers," *Biophysical journal* **2009**, *96*, 4299–4307.

[210] X. Yu, J. Zheng, "Cholesterol promotes the interaction of Alzheimer b-amyloid monomer with lipid bilayer," *Journal of molecular biology* **2012**, *421*, 561–571.

[211] K. Sasahara, K. Morigaki, K. Shinya, "Effects of membrane interaction and aggregation of amyloid b-peptide on lipid mobility and membrane domain structure," *Physical chemistry chemical physics : PCCP* **2013**, *15*, 8929–8939.

[212] K. Matsuzaki, "Physicochemical interactions of amyloid beta-peptide with lipid bilayers," *Biochimica et biophysica acta* **2007**, *1768*, 1935–1942.

[213] J. McLaurin, T. Franklin, P. E. Fraser, A. Chakrabartty, "Structural Transitions Associated with the Interaction of Alzheimer b-Amyloid Peptides with Gangliosides," *Journal of Biological Chemistry* **1998**, *273*, 4506–4515.

[214] C. F. Wertz, M. M. Santore, "Adsorption and Reorientation Kinetics of Lysozyme on Hydrophobic Surfaces," *Langmuir* **2002**, *18*, 1190–1199.

[215] S. M. Daly, T. M. Przybycien, R. D. Tilton, "Coverage-Dependent Orientation of Lysozyme Adsorbed on Silica," *Langmuir* **2003**, *19*, 3848–3857.

[216] M. Rabe, D. Verdes, J. Zimmermann, S. Seeger, "Surface organization and cooperativity during nonspecific protein adsorption events," *The journal of physical chemistry. B* **2008**, *112*, 13971–13980.

[217] B. Soreghan, J. Kosmoski, C. Glabe, "Surfactant Properties of Alzheimer's ABeta-Peptides and the Mechanism of Amyloid Aggregation," *The Journal of biological chemistry* **1994**, *269*.

[218] Y.-R. Chen, C. G. Glabe, "Distinct early folding and aggregation properties of Alzheimer amyloid-beta peptides Abeta40 and Abeta42: stable trimer or tetramer formation by Abeta42," *The Journal of biological chemistry* **2006**, *281*, 24414–24422.

[219] Y. Liu, L. Shen, "From Langmuir kinetics to first- and second-order rate equations for adsorption," *Langmuir : the ACS journal of surfaces and colloids* **2008**, *24*, 11625–11630.

[220] T. Ariga, K. Kobayashi, A. Hasegawa, M. Kiso, H. Ishida, T. Miyatake, "Characterization of high-affinity binding between gangliosides and amyloid beta-protein," *Archives of biochemistry and biophysics* **2001**, *388*, 225–230.

[221] D. L. Miller, I. A. Papayannopoulos, J. Styles, "Peptide Composition of the Cerebrovascular and Senile Plaque Core Amyloid Deposits of Alzheimer disease," *Archives of biochemistry and biophysics* **1993**, *301*.

[222] T. Iwatsubo, A. Odaka, N. Suzuki, "Visualization of AB42(43) and AB40 in Senile Plaques with End-Specific AB Monoclonals: Evidence that an Initially Deposited Species Is AB42(43)," *Neuron* **1994**, *13*, 45–53.

[223] J. B. V. Hlady, "Protein adsorption on solid surfaces," *Curr Opin Biotechnol* **1996**, 72–75.

[224] M. Rabe, D. Verdes, S. Seeger, "Surface-induced spreading phenomenon of protein clusters," *Soft Matter* **2009**, *5*, 1039.

[225] Z. S. Khachaturian, "Hypothesis on the Regulation of Cytosol Calcium Concentration and the Aging Brain," *Neurobiology of Aging* **1987**, *8*, 345–346.

[226] M. P. Mattson, B. Cheng, D. Davis, K. Bryant, I. Lieberburg, and R. E. Rydel, "B-Amyloid Peptides Destabilize Calcium Homeostasis and Render Human Cortical Neurons Vulnerable to Excitotoxicity," *the journal of neuroscience* **1992**, 376–389.

[227] M. Kawahara,N. Arispe, Y. Kuroda, and E. Rojas, "Alzheimer's Disease Amyloid (8-Protein Forms Zn2+ Sensitive, Cation-Selective Channels Across Excised Membrane Patches from Hypothalamic Neurons," *Biophysical journal* **1997**, *73*, 67–75.

[228] B. L. Kagan, R. Azimov, R. Azimova, "Amyloid peptide channels," *The Journal of membrane biology* **2004**, *202*, 1–10.

[229] H. W. Querfurth, D. J. Selkoe, "Calcium Ionophore Increases Amyloid .beta. Peptide Production by Cultured Cells," *Biochemistry* **1994**, *33*, 4550–4561.

[230] A. Yarlagadda, S. Kaushik, A. H. Clayton, "Blood Brain Barrier: The Role of Calcium Homeostasis," *Psychiatry* **2007**.

[231] P. Hortschansky, V. Schroeckh, T. Christopeit, G. Zandomeneghi, M. Fändrich, "The aggregation kinetics of Alzheimer's beta-amyloid peptide is controlled by stochastic nucleation," *Protein science : a publication of the Protein Society* **2005**, *14*, 1753–1759.

[232] C. Lockhart, D. K. Klimov, "Calcium enhances binding of Ab monomer to DMPC lipid bilayer," *Biophysical journal* **2015**, *108*, 1807–1818.

[233] J. Näslund, "Correlation Between Elevated Levels of Amyloid b-Peptide in the Brain and Cognitive Decline," *JAMA* **2000**, *283*, 1571.

[234] M. Novo, S. Freire, W. Al-Soufi, "Critical aggregation concentration for the formation of early Amyloid-b (1-42) oligomers," *Scientific reports* **2018**, *8*, 1783.

[235] N. P. Reynolds, A. Soragni, M. Rabe, D. Verdes, E. Liverani, S. Handschin, R. Riek, S. Seeger, "Mechanism of membrane interaction and disruption by a-synuclein," *Journal of the American Chemical Society* **2011**, *133*, 19366–19375.

[236] Harma Ellens, Joe Bentz, and Francis C. Szoka, "Proton- and calcium-induced fusion and destabilization of liposomes," *Biochemistry* **1985**.

[237] Isabelle Möller, "Interaction of alpha-Synuclein with Membranes - from Function to Malfunction: PhD thesis."

[238] R. Richter, A. Mukhopadhyay, A. Brisson, "Pathways of Lipid Vesicle Deposition on Solid Surfaces: A Combined QCM-D and AFM Study," *Biophysical journal* **2003**, *85*, 3035–3047.

[239] R. Schroeder, E. London, D. Brown, "Interactions between saturated acyl chains confer detergent resistance on lipids and glycosylphosphatidylinositol (GPI)-anchored proteins: GPI-anchored proteins in liposomes and cells show similar behavior," *Biochemistry* **1994**, *91*, 12130–12134.

[240] A. Kusumi, I. Koyama-Honda, K. Suzuki, "Molecular dynamics and interactions for creation of stimulation-induced stabilized rafts from small unstable steady-state rafts," *Traffic (Copenhagen Denmark)* **2004**, *5*, 213–230.

[241] A. K. Neumann, M. S. Itano, K. Jacobson, "Understanding lipid rafts and other related membrane domains," *F1000 biology reports* **2010**, *2*, 31.

[242] J. R. Cirrito et al., "In Vivo Assessment of Brain Interstitial Fluid with Microdialysis Reveals Plaque-Associated Changes in Amyloid-b Metabolism and Half-Life," *The Journal of Neuroscience* **2003**, *23*, 8844–8853.

[243] E. Karran, M. Mercken, B. de Strooper, "The amyloid cascade hypothesis for Alzheimer's disease: an appraisal for the development of therapeutics," *Nature reviews. Drug discovery* **2011**, *10*, 698–712.

[244] A. Quist, I. Doudevski, H. Lin, R. Azimova, "Amyloid ion channels: A common structural link for protein-misfolding disease," *PNAS* **2005**, *102*, 10427–10432.

[245] Daniel Axelrod, "Lateral Motion of Membrane Proteins and Biological Function," *Membrane Biology* **1983**, *75*, 1–10.

[246] E. Terzi, G. Hölzemann, J. Seelig, "Interaction of Alzheimer beta-amyloid peptide(1-40) with lipid membranes," *Biochemistry* **1997**, *36*, 14845–14852.

[247] T.-L. Lau, E. E. Ambroggio, D. J. Tew, R. Cappai, C. L. Masters, G. D. Fidelio, K. J. Barnham, F. Separovic, "Amyloid-beta peptide disruption of lipid membranes and the effect of metal ions," *Journal of molecular biology* **2006**, *356*, 759–770.

[248] C. S. Sweetenham, I. Notingher, "Raman spectroscopy methods for detecting and imaging supported lipid bilayers," *Spectroscopy* **2010**, *24*, 113–117.

[249] C. Lee, C. D. Bain, "Raman spectra of planar supported lipid bilayers," *Biochimica et biophysica acta* **2005**, *1711*, 59–71.

[250] A. J. Wright, J. L. Richens, J. P. Bramble, N. Cathcart, V. Kitaev, P. O'Shea, A. J. Hudson, "Surface-enhanced Raman scattering measurement from a lipid bilayer encapsulating a single decahedral nanoparticle mediated by an optical trap," *Nanoscale* **2016**, *8*, 16395–16404.

[251] K. Czamara, K. Majzner, M. Z. Pacia, K. Kochan, A. Kaczor, M. Baranska, "Raman spectroscopy of lipids: A review," *Journal of Raman Spectroscopy* **2015**, *46*, 4–20.

[252] Frank D. Gunstone, John L. Harwood, Albert J. Dijkstra, *The Lipid Handbook 3rd Edition*, CRC press, Boca Raton (Florida), **2007**.

[253] P. D. Enlow, M. Buncick, R. J. Warmack, T. Vo-Dinh, "Detection of nitro-polynuclear aromatic compounds by surface-enhanced Raman spectrometry," *Analytical chemistry* **1986**, *58*.

[254] V. G. Ivanov, N. D. Todorov, L. S. Petrov, T. Ritacco, M. Giocondo, E. S. Vlakhov, "Strong surface enhanced Raman scattering from gold nanoarrays obtained by direct laser writing," *Journal of Physics: Conference Series* **2016**, *764*, 012023.

[255] A. R. Mhashal, S. Roy, "Effect of gold nanoparticle on structure and fluidity of lipid membrane," *PloS one* **2014**, *9*, e114152.

[256] C. Weeraman, A. K. Yatawara, A. N. Bordenyuk, A. V. Benderskii, "Effect of nanoscale geometry on molecular conformation: vibrational sum-frequency generation of alkanethiols on gold nanoparticles," *Journal of the American Chemical Society* **2006**, *128*, 14244–14245.

[257] Penney CM, Goldman LM, Lapp M., "Raman scattering cross sections.," *Nat Phys Sci* **1972**, 110–112.

[258] J. P. Biscar, N. Kollias, "Pseudo-Raman behavior of the scattering broad band of BSA," *Journal of Polymer Science: Polymer Letters Edition* **1973**, *11*, 725–729.

[259] F. de Angelis et al., "Breaking the diffusion limit with super-hydrophobic delivery of molecules to plasmonic nanofocusing SERS structures," *Nature Photonics* **2011**, *5*, 682–687.

[260] L. B. Capeletti, I. M. Baibich, I. S. Butler, J. H. Z. dos Santos, "Infrared and Raman spectroscopic characterization of some organic substituted hybrid silicas," *Spectrochimica acta. Part A Molecular and biomolecular spectroscopy* **2014**, *133*, 619–625.

[261] N. Majoul, S. Aouida, B. Bessaïs, "Progress of porous silicon APTES-functionalization by FTIR investigations," *Applied Surface Science* **2015**, *331*, 388–391.

[262] L. D. Barron, Z. Q. Wen, and L. Hecht, "Vibrational Raman optical activity of proteins," *J. Am. Chem. Soc.* **1992**, *114*, 784.

[263] B. C. Galarreta, P. R. Norton, F. Lagugné-Labarthet, "SERS detection of streptavidin/biotin monolayer assemblies," *Langmuir : the ACS journal of surfaces and colloids* **2011**, *27*, 1494–1498.

[264] S. Tomaselli, V. Esposito, P. Vangone, N. A. J. van Nuland, A. M. J. J. Bonvin, R. Guerrini, T. Tancredi, P. A. Temussi, D. Picone, "The alpha-to-beta conformational transition of Alzheimer's Abeta-(1-42) peptide in aqueous media is reversible: A step by step conformational analysis suggests the location of beta conformation seeding," *Chembiochem : a European journal of chemical biology* **2006**, *7*, 257–267.

[265] K. Ikeda, T. Yamaguchi, S. Fukunaga, M. Hoshino, K. Matsuzaki, "Mechanism of amyloid b-protein aggregation mediated by GM1 ganglioside clusters," *Biochemistry* **2011**, *50*, 6433–6440.

[266] S. A. Kotler, P. Walsh, J. R. Brender, A. Ramamoorthy, "Differences between amyloid-b aggregation in solution and on the membrane: insights into elucidation of the mechanistic details of Alzheimer's disease," *Chemical Society reviews* **2014**, *43*, 6692–6700.

[267] S. M. Butterfield, H. A. Lashuel, "Amyloidogenic protein-membrane interactions: mechanistic insight from model systems," *Angewandte Chemie (International ed. in English)* **2010**, *49*, 5628–5654.

[268] Talafous J, Marcinowski KJ, Klopman G, Zagorski MG., "Solution structure of residues-1-28 of the Amyloid beta-peptide.," *Biochemistry* **1994**, *33*.

[269] S. Zhang, K. Iwata, M. J. Lachenmann, J. W. Peng, S. Li, E. R. Stimson, Y. Lu, A. M. Felix, J. E. Maggio, J. P. Lee, "The Alzheimer's peptide a beta adopts a collapsed coil structure in water," *Journal of structural biology* **2000**, *130*, 130–141.

[270] S. Vivekanandan, J. R. Brender, S. Y. Lee, A. Ramamoorthy, "A partially folded structure of amyloid-beta(1-40) in an aqueous environment," *Biochemical and biophysical research communications* **2011**, *411*, 312–316.

[271] I. Ashikawa, K. Itoh, "Raman spectra of polypeptides containingL-histidine residues and tautomerism of imidazole side chain," *Biopolymers* **1979**, *18*, 1859–1876.

[272] P. Lagant. G. Vergoten, G. FLeury, M.H. Loucheux-Lefebre, "Raman spectroscopy and normal vibrations of peptides," *Eur. J. Biochem* **1984**, *139*, 137–148.

[273] D. F. Clayton, J. M. George, "The synucleins: a family of proteins involved in synaptic function, plasticity, neurodegeneration and disease," *Trends Neurosci.* **1998**, *21*, 249–254.

[274] T. Bartels, J. G. Choi, D. J. Selkoe, "alpha-Synuclein occurs physiologically as a helically folded tetramer that resists aggregation," *Nature* **2011**, *477*, 107–110.

[275] R. Bussell, JR, T. F. Ramlall, D. Eliezer, "Helix periodicity, topology, and dynamics of membrane-associated alpha-synuclein," *Protein science : a publication of the Protein Society* **2005**, *14*, 862–872.

[276] B. Winner et al., "In vivo demonstration that alpha-synuclein oligomers are toxic," *Proceedings of the National Academy of Sciences of the United States of America* **2011**, *108*, 4194–4199.

[277] W. Wang et al., "A soluble a-synuclein construct forms a dynamic tetramer," *Proceedings of the National Academy of Sciences of the United States of America* **2011**, *108*, 17797–17802.

[278] H.-T. Li, H.-N. Du, L. Tang, J. Hu, H.-Y. Hu, "Structural transformation and aggregation of human alpha-synuclein in trifluoroethanol: non-amyloid component sequence is essential and beta-sheet formation is prerequisite to aggregation," *Biopolymers* **2002**, *64*, 221–226.

[279] F. Tofoleanu, N.-V. Buchete, "Alzheimer Ab peptide interactions with lipid membranes: fibrils, oligomers and polymorphic amyloid channels," *Prion* **2012**, *6*, 339–345.

[280] I. H. K. Dias, J. Mistry, S. Fell, A. Reis, C. M. Spickett, M. C. Polidori, G. Y. H. Lip, H. R. Griffiths, "Oxidized LDL lipids increase b-amyloid production by SH-SY5Y cells through glutathione depletion and lipid raft formation," *Free radical biology & medicine* **2014**, *75*, 48–59.

[281] B. R. Sahoo, T. Genjo, M. Bekier, S. J. Cox, A. K. Stoddard, M. Ivanova, K. Yasuhara, C. A. Fierke, Y. Wang, A. Ramamoorthy, "Alzheimer's amyloid-beta intermediates generated using polymer-nanodiscs," *Chemical communications (Cambridge England)* **2018**, *54*, 12883–12886.

[282] J. P. Lee, E. R. Stimson, J. R. Ghilardi, P. W. Mantyh, Y.-A. Lu, A. M. Felix, W. Llanos, A. Behbin, M. Cummings, "1H NMR of A.beta. Amyloid Peptide Congeners in Water Solution. Conformational Changes Correlate with Plaque Competence," *Biochemistry* **1995**, *34*, 5191–5200.

[283] J. Dong, C. S. Atwood, V. E. Anderson, S. L. Siedlak, M. A. Smith, G. Perry, P. R. Carey, "Metal binding and oxidation of amyloid-beta within isolated senile plaque cores: Raman microscopic evidence," *Biochemistry* **2003**, *42*, 2768–2773.

[284] M. Thomaier, L. Gremer, C. Dammers, J. Fabig, P. Neudecker, D. Willbold, "High-Affinity Binding of Monomeric but Not Oligomeric Amyloid-b to Ganglioside GM1 Containing Nanodiscs," *Biochemistry* **2016**, *55*, 6662–6672.

[285] V. Voiciuk, G. Valincius, R. Budvytytė, A. Matijoška, I. Matulaitienė, G. Niaura, "Surface-enhanced Raman spectroscopy for detection of toxic amyloid b oligomers adsorbed on self-assembled monolayers," *Spectrochimica acta. Part A Molecular and biomolecular spectroscopy* **2012**, *95*, 526–532.

[286] I. Choi, Y. S. Huh, D. Erickson, "Ultra-sensitive, label-free probing of the conformational characteristics of amyloid beta aggregates with a SERS active nanofluidic device," *Microfluidics and Nanofluidics* **2012**, *12*, 663–669.

[287] I.-H. Chou, M. Benford, H. T. Beier, G. L. Coté, M. Wang, N. Jing, J. Kameoka, T. A. Good, "Nanofluidic biosensing for beta-amyloid detection using surface enhanced Raman spectroscopy," *Nano letters* **2008**, *8*, 1729–1735.